University of Kentucky
UKnowledge

Masters Theses | Graduate School

2008

DETERMINATION OF THE EXTRAVASCULAR BURDEN OF CARBON MONOXIDE (CO) ON HUMAN HEART

Kinnera Erupaka
University of Kentucky, kinnerarey@uky.edu

Recommended Citation
Erupaka, Kinnera, "DETERMINATION OF THE EXTRAVASCULAR BURDEN OF CARBON MONOXIDE (CO) ON HUMAN HEART" (2008). *Masters Theses.* Paper 501.
http://uknowledge.uky.edu/gradschool_theses/501

This Thesis is brought to you for free and open access by the Graduate School at UKnowledge. It has been accepted for inclusion in Masters Theses by an authorized administrator of UKnowledge. For more information, please contact UKnowledge@lsv.uky.edu.

ABSTRACT OF THE THESIS

DETERMINATION OF THE EXTRAVASCULAR BURDEN OF CARBON MONOXIDE (CO) ON HUMAN HEART

Noninvasive measurements of myocardial carboxymyoglobin levels (%*MbCO*) and oxygen tensions (PtO_2) are difficult to obtain experimentally. We have developed a compartmental model which allows prediction of myocardial %*MbCO* levels and PtO_2 for varied carbon monoxide (*CO)* exposures. The cardiac compartment in the model consists of vascular subcompartments which contain two tissue subcompartments varying in capillary density. Mass-balance equations for oxygen (O_2) and *CO* are applied for all compartments. Myocardial oxygen consumption and blood flow are quantified from predictive formulas based on heart rate. Model predictions are validated with experimental data at normoxia, hypoxia, exercise and hyperoxia. CO exposures of varying concentration and time (short-high, long-low), CO rebreathing during 100% O2, and exposure during exercise is simulated. Results of the simulations demonstrate that during *CO* exposures and subsequent therapies, the temporal changes of *%MbCO* in the heart differ from those of carboxyhemoglobin levels (*%HbCO*). Analysis of correlation between *%HbCO*, %*MbCO* and PtO_2 was done to understand myocardial injury due to *CO* hypoxia. This thesis demonstrates that the model is able to anticipate the uptake and distribution of *CO* in the human myocardium and thus can be used to estimate the extravascular burden (*MbCO*, PtO_2) of *CO* on the human heart.

Key words: Myocardial Oxygen Tension, CO Hypoxia, Exercise, Tissue Oxygenation, Cardiac Muscle

Kinnera Erupaka

01 – 09- 2008

DETERMINATION OF THE EXTRAVASCULAR BURDEN OF CARBON MONOXIDE (CO) ON HUMAN HEART

By
KINNERA ERUPAKA

Dr.EugeneBruce
Director of Thesis

Dr. Abhijit Patwardhan
Director of Graduate Studies

01-09-2008
Date

RULES FOR THE USE OF THESES

Unpublished theses submitted for the Master's degree and deposited in the University of Kentucky Library are as a rule open for inspection, but are to be used only with due regard to the rights of the authors. Bibliographical references may be noted, but quotations or summaries of parts may be published only with the permission of the author, and with the usual scholarly acknowledgments.

Extensive copying or publication of the thesis in whole or in part also requires the consent of the Dean of the Graduate School of the University of Kentucky.

A library that borrows this thesis for use by its patrons is expected to secure the signature of each user.

Name	Date

“Thesis”

Kinnera Erupaka

The Graduate School
University of Kentucky
2008

DETERMINATION OF THE EXTRAVASCULAR BURDEN OF CARBON MONOXIDE (CO) ON HUMAN HEART

THESIS

A thesis submitted in partial fulfillment of the
requirements for the degree of
Master of Science
College of Engineering
Center for Biomedical Engineering
at the University of Kentucky

By
Kinnera Erupaka
Lexington, Kentucky
Director: Dr. Eugene N. Bruce, Professor of Biomedical Engineering
Lexington, Kentucky
2008
Copyright © Kinnera Erupaka 2008

ACKNOWLEDGEMENTS

I am very thankful to my advisor Dr. Eugene Bruce for giving me this opportunity to work on this project. His constant support, guidance, encouragement and daily involvement helped in successful completion of my work.

I would like to thank my committee members Dr. Abhijit Patwardhan, Dr. Bruce Walcott and Dr. Michael Reid for their valuable suggestions, patience and time.

I am thankful to Dr. Peggy Bruce for helping me in estimating parameters for the model and proof reading my thesis.

I also wish to thank my best friends Prasad and Jagan for helping me with formatting my thesis and for the moral support and confidence they have been extending.

Last but not the least; I would like to thank NIH for providing me funding to work on this project.

TABLE OF CONTENTS

LIST OF TABLES

LIST OF FIGURES

LIST OF FILES

CHAPTER 1
Introduction

Chapter 1 explains the importance of the need for developing a model for predicting the extravascular burden of *CO* on the human heart. The chapter gives a basic introduction to carbon monoxide (*CO*) toxicity, and details the sources of *CO*, reactions of *CO* with the heme pigments in the body and the effects of *CO* exposure on oxygen (O_2) delivery to tissues. This chapter discusses the symptoms, effects and treatment strategies of *CO* poisoning cases. Finally, the chapter highlights the hypothesis made and goals to be achieved in the following thesis.

1.1 Carbon Monoxide (CO) Toxicity

Carbon Monoxide (*CO*) is a byproduct of incomplete combustion of carbon-based fossil fuels. *CO* is generated in toxic amounts by internal-combustion engines, faulty fossil-fuel heating systems, fire accidents, and emissions from modern automobiles in poorly ventilated spaces. The body produces *CO* as a by-product of hemoglobin degradation, but the gas does not reach toxic concentrations in vivo unless it is inhaled from exogenous sources (like faulty heaters, indoor charcoal grills, cigarette smoke, swimming behind a motorboat or under a houseboat, etc.). Carbon monoxide, which is a colorless, tasteless and odorless gas, is often referred to as an invisible killer as it is difficult to detect. Exposure to *CO* concentrations exceeding permissible exposure levels (PEL) of 50 ppm over an average of 8 hrs (1, 2) is a significant environmental and occupational health concern. There are approximately 4000 deaths per year occurring in United States due to *CO* poisoning (3, 4, and 5). *CO* exposures and poisonings occur more often during the fall and winter, when people are more likely to use gas furnaces, heaters and generators in their homes (4, 6).

CO produces tissue toxicity by impairing oxygen (O_2) delivery to the tissues. *CO* is absorbed by the respiratory tract and diffuses through the alveolar-capillary membrane and enters the blood, following a path similar to that of O_2. The rate of absorption of *CO* decreases when the partial pressures of *CO* in blood of the

pulmonary capillaries and the alveolar air reach a state of equilibrium. After being absorbed and diffusing through the respiratory tract, *CO* combines reversibly with the heme pigments of the body, namely: (i) Hemoglobin (*Hb*) present in blood (ii) Myoglobin (*Mb*) present in muscle tissues, and (iii) other membrane bound heme-containing compounds (e.g., cytochromes). Hemoglobin (*Hb*) is a tetrameric heme protein present in red blood cells whose main function is oxygen (O_2) transport (Figure 1.1.1). O_2 is stored in the lungs as a gas and in the blood. In the blood it is present in two (7) forms: (i) dissolved in plasma (normally 1.5% or 3 ml in 1 liter blood) and (ii) reversibly combined with hemoglobin (normally 98.5% or 197 ml in 1 liter blood). Each hemoglobin molecule can bind to four oxygen molecules forming fully-saturated oxyhemoglobin (O_2Hb), (Figure 1.1.2). *Hb* binds *CO* ~220 times more strongly than it binds O_2, to form carboxyhemoglobin (*HbCO*) (Figure 1.3.1).

Myoglobin (*Mb*) is a monomeric heme protein present in muscle tissue (Figure 1.2.2) and each myoglobin molecule can bind to one oxygen molecule forming oxymyoglobin (O_2Mb) (Figure 1.2.1). It is an oxygen store and also binds to CO to form carboxymyoglobin (*MbCO*) (Figure 1.2.3). *Mb* binds *CO* ~36 times more strongly than it binds O_2.

Thus *CO* toxicity causes mortality primarily due to the effects of severe hypoxia by attaching itself to Hb and Mb and reducing the oxygen carrying capacity of these heme proteins. *CO* usually replaces only two of the four O_2 molecules bound to the heme groups of hemoglobin. In cases of high *CO* concentrations it is possible that *CO* may replace the third O_2 molecule by binding to the third heme group (Figure 1.3.2). Thus *CO* toxic hypoxemia causes changes in the circulatory, respiratory and metabolic demands of the tissue (8-18).

Groups especially susceptible to the hypoxic stress of carbon monoxide exposure would potentially be individuals with cardiovascular and obstructive lung diseases, individuals with cerebrovascular and peripheral vascular diseases, and individuals with anemia. In addition, hospitalized individuals suffering from tissue hypoxia (e.g. shock) or those undergoing operations may be at increased risk. Individuals with undetected or undiagnosed coronary artery disease as well as the fetus, the newborn or, even pregnant women may be assumed to be at increased risk

because of the anticipated reduced capacity to accommodate hypoxic stress or some inherent sensitivity to hypoxia. Furthermore, other populations such as those living at high altitudes, young children, or older adults may also be at increased risk (2).

1.2 Symptoms, Diagnosis and Treatments of CO Poisoning

Symptoms and effects of *CO* poisoning are greatly dependent on the concentration and duration of exposure. *CO* poisoning could be acute (exposure to *CO* occurs and lasts no longer than 24 hrs) or chronic (exposure to *CO* that occurs more than once and lasts longer than 24 hrs). Generally, chronic exposures involve lower *HbCO* saturations due to lower *CO* exposures. Diagnosis of *CO* poisoning is difficult unless the event of toxicity occurs at site of high *CO* concentration like a house on fire or a blast in a coal mine. *CO* poisoning can be difficult to diagnose because *CO* poisoning symptoms are similar to those of flu. Specific information regarding the CO exposure duration and the concentration of CO inhaled is often unavailable. In addition valid blood *HbCO* level measurements are readily obtained but are an unreliable predictor of injury, and there are no clinical tests that can determine the extra vascular burden of *CO* (e.g., a noninvasive measurement of *MbCO* levels or tissue PO_2 in humans). Although *CO* poisoning does not cause a fever, other symptoms are similar to those of the flu (including nausea, severe headache, vomiting) and also include neurological sequellae (memory loss, personality and behavior changes, brain damage etc), cardiac abnormalities in ECG, abnormal ventricular function and elevated cardiac biomarkers diagnostic of myocardial injury depending on the type of *CO* exposure. Treatment for *CO* poisoned victims involves administering supplemental O_2. The treatment is with either normobaric hyperoxia, where 100% Oxygen (O_2) is administered if the victim is conscious and *HbCO* levels in the blood are less than 25%, or hyperbaric hyperoxia where 100% Oxygen (O_2) is administered, at 1-3 ATA (1 atmosphere = 760 mm of Hg) pressure, if the victim is unconscious or the *HbCO* level exceeds 25%. However, there are some problems with the treatment strategies for *CO* poisoning victims. Decision of the treatment protocol is based on the measured *HbCO* levels in the

venous blood. Blood *%HbCO* is readily measurable but is thought to be an unreliable measure of poisoning severity. Carboxymyoglobin (*MbCO*) levels and tissue partial pressures of oxygen (PO_2) which are more reliable indicators of *CO* toxicity in the tissue are difficult to measure through any clinical procedures. Treatment strategy is often debatable and it may not be very clear whether hyperbaric hyperoxia rather than normobaric hyperoxia treatment is necessary (19, 20, 21, 22, 23). Despite treatment after CO poisoning, neurological and cardiac sequellae often occur.

1.3 Motivation for the Thesis

CO hypoxia results in impaired O_2 delivery causing a decrease in O_2 uptake by the cells. This diminished O_2 utilization causes alterations in biochemical (cardiac troponin I, phosphocreatine (PCr), lactate) and physiological (cardiac output, rate pressure product, metabolic rate) activities. Elevated cardiac biomarkers (cardiac troponin I $\geq$ 0.7ng/ml, CK-MB (Creatine kinase MB isoenzyme) mass $\geq$5.0ng/ml) and diagnostic EKG (electrocardiogram) changes (like ST segment elevation, T-wave changes), abnormal left ventricular (LV) function (like alternations in left ventricular ejection fractions) and regional wall motion abnormality are observed in moderate to severely *CO* poisoned patients (24). In a population of 230 *CO* poisoned patients, 44% of deaths were reported to be due to cardiovascular causes such as cardiac arrest, myocardial infarction, congestive heart failure, fatal arrhythmia (24).

Also, there is evidence that workers who are exposed to high *CO* concentrations have an increased risk for cardiovascular morbidity and mortality (25, 26). The effect of high *CO* exposures would pose a greater risk for injury during exercise, as there would be increased demand for O_2 in the tissue accompanied with O_2 impairment due to *CO* binding to hemoglobin and myoglobin. Exercise also increases ventilation which, in turn, increases the amount of *CO* inhaled and thus the dose of *CO*.

Coronary circulation is very sensitive to O_2 deprivation as the myocardium has a very high O_2 extraction fraction (Measure of quantity of O_2delivered to the tissue and is defined as ratio of arterial and venous (A- V) O_2 concentration difference and arterial (A) O_2 concentration) to causing profound effects of *CO* in the myocardium. Each molecule of myoglobin in the heart is capable of binding to one *CO* molecule by

means of the heme group to form carboxymyoglobin (*MbCO*), which would further increase the *CO* content in the heart tissue causing a decrease in O_2 availability. Also, the contribution of myoglobin diffusion during *CO* hypoxia is unclear (27, 28, 29). All the above recent reports on cardiac impairment, occurring with *CO* poisoning motivated scientists to understand the causes of cardiovascular abnormalities in *CO* poisoning victims (30, 31, 32). Therefore, keeping these facts in mind, the following hypothesis was made for the thesis:

Hypothesis: "During CO exposures and subsequent therapies, the temporal changes of %MbCO in the heart differ from those of %HbCO; in particular, there are times during the therapy %MbCO can sometimes increase when %HbCO is decreasing".

The importance of this hypothesis is that *CO* load delivered to the heart impairs oxygen delivery, further affecting the tissue oxygen tension (PtO_2) and O_2 pressure gradients. This *CO* load is related to both *%HbCO* in arterial blood perfusing the heart and *%MbCO* in cardiac tissue. If *%MbCO* and *%HbCO* change in opposite directions, then the currently-used clinical indicator of potential injury (i. e., *%HbCO*) will be inaccurate and possibly misleading. Thus, determining the total *CO* load on the cardiac cells (or its effect on tissue PO_2) might be a better predictor of injury.

1.4 The Need for our Model

Determination of the burden of *CO* (vascular - *%HbCO* and extra vascular - *%MbCO*) and its effects on tissue PO_2 during uptake and washout would provide a better assessment of risk associated with a range of exposure conditions in *CO* toxicology. This specific task can be accomplished in two ways:

1. Conduct experiments involving *CO* exposures

2. Estimate *CO* burden from a "Mathematical Model"

Conducting experiments involving low *CO* exposures can be accomplished in human subjects, but it would be unethical to expose subjects to high *CO* exposures to understand causes of injury due to *CO* and predict clinical outcomes. Also, these

experiments are difficult to conduct and require detailed care, great expertise and are also expensive. Even if these experiments are conducted, non-invasive measurements of *MbCO* are not possible. Also, invasive or non-invasive reliable measurements of tissue oxygenation in healthy human hearts are difficult to make. Experimental measurements of human myocardial *O2* tension have been reported in patient populations with cardiovascular abnormalities (33, 34). Thus, the best option would be to build a model to predict the burden (vascular-*HbCO*; extra vascular- *MbCO*) of *CO* on the human heart by doing simulations for a range of *CO* exposures. If one can implement O_2 interaction equations, the model can also help to predict oxygen tension in the heart. Further, the model can be used to anticipate levels of *CO* that may be lethal to the heart or to assess the risk of cardiac injury when exercise is accompanied with *CO* exposure. This information would be helpful to design treatment protocols for people exposed to *CO* while at work. Thus the approach I decided to take to test the hypothesis is as follows:

Approach: "Since O_2 and CO levels in heart are not measurable non-invasively in humans, a plan to estimate these values from a model was made."

After formulating a hypothesis, the next task was to assess the literature for the availability of an appropriate model for predicting uptake and washout of *CO*. After making a diligent search, the model developed in our lab by the authors of reference 35 seemed most suitable. The process from setting an objective to reaching a solution is summarized in Figure 1.4.

The reasons for selecting this model are explained in detail in section 2.1 of chapter 2. This model consisted of lumped compartments for lungs, blood (arterial and venous), skeletal tissue and non-muscle tissue. Mass balance equations for *CO* were used to represent the compartments (35). However, this model also had some limitations and so the model was further modified in our lab resulting in a better and more efficient model (Bruce, Bruce, and Erupaka, in preparation) which, however, was still inadequate for the present purposes because it did not include a compartment for the heart. Figure 1.5 shows the different stages of model development. Thus, the next task was to accomplish the following goals of the thesis to test the hypothesis made.

The major goals of the thesis are:

(1) Introduce a two compartment cardiac block into the model.

(2) Implement mass balance equations for O_2 and CO.

(3) Test and validate the model with experimental data for conditions of rest, exercise, CO exposure and hypoxic hypoxia and hyperoxia.

(4) Use the developed and validated model to predict extravascular burden of CO and O_2 tension in the cardiac tissue during short-high concentration CO exposures, CO rebreathing studies in 100% O_2, long-low concentration CO exposure, exercise in the absence and presence of CO, and to determine CO concentrations injurious to the heart.

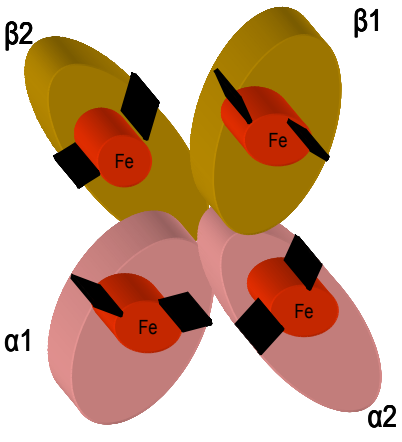

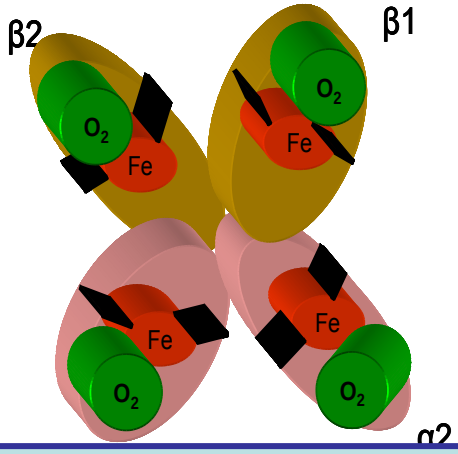

Figure1.1.1 Hemoglobin Figure 1.1.2 Oxyhemoglobin

Figure 1.1: Hemoglobin (Hb) and Oxyhemoglobin (HbO_2). Hemoglobin (Figure 1.1.1) is a tetrameric heme protein present in red blood cells. O_2 binds to the heme (Fe) protein present in hemoglobin to form oxyhemoglobin (Figure 1.1.2).

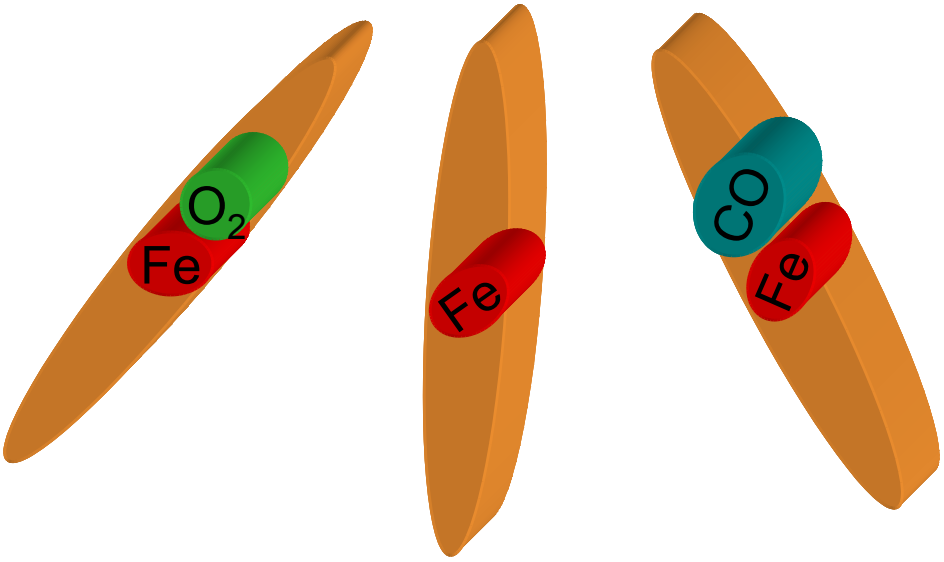

Figure1.2.1	Figure 1.2.2	Figure 1.2.3
Oxymyoglobin	Myoglobin	Carboxymyoglobin

Figure 1.2: Oxymyoglobin (*MbO2*), Myoglobin (*Mb*), Carboxymyoglobin (*MbCO*). Myoglobin (Figure 1.2.2) is a monomeric heme protein present in muscle tissue. O_2 binds to the heme (Fe) protein present in myoglobin to form oxymyoglobin (Figure 1.2.2).*CO* also binds to the heme protein to form carboxymyoglobin (Figure 1.2.3)

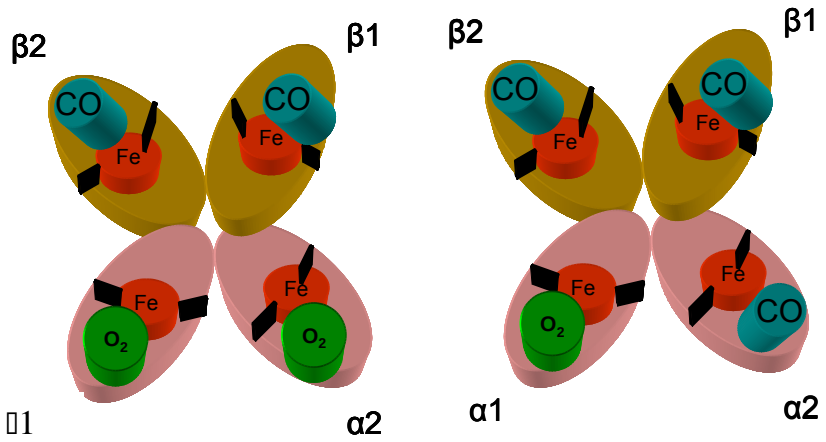

Figure1.3.1 Carboxyhemoglobin	Figure 1.3.2 Carboxyhemoglobin

Figure 1.3: Carboxyhemoglobin (*MbCO*). *CO* binds to the heme (*Fe*) protein present in hemoglobin to form carboxyhemoglobin.

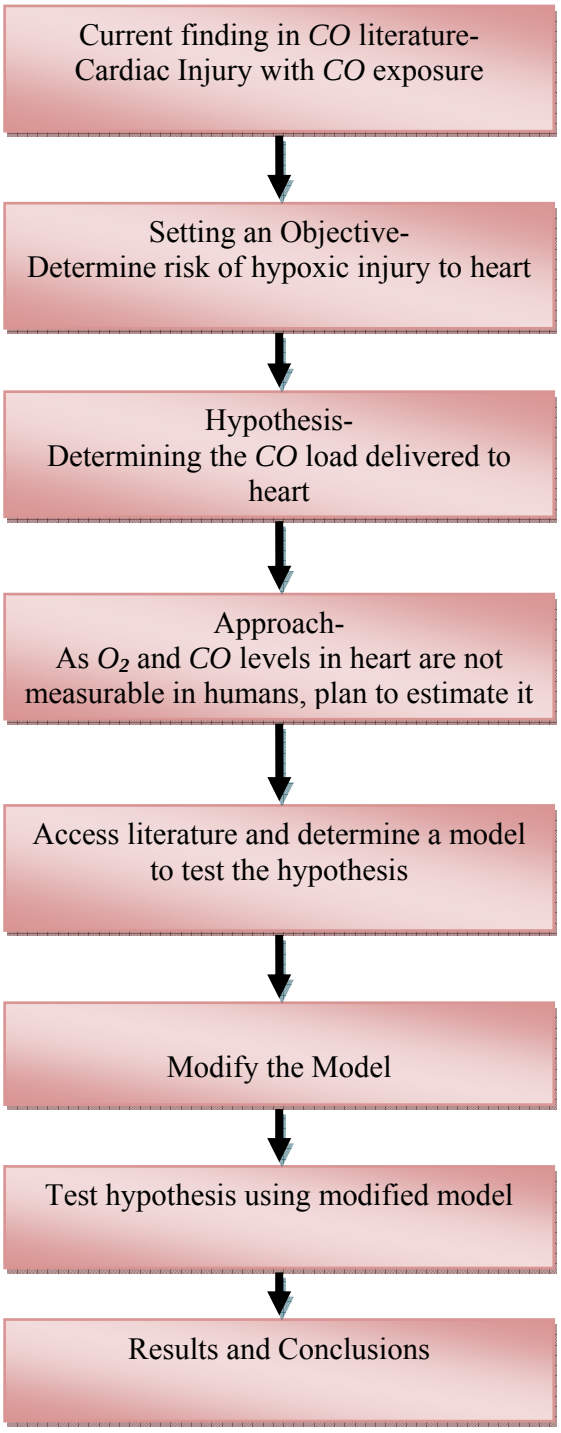

Figure 1.4: Overview of the Thesis

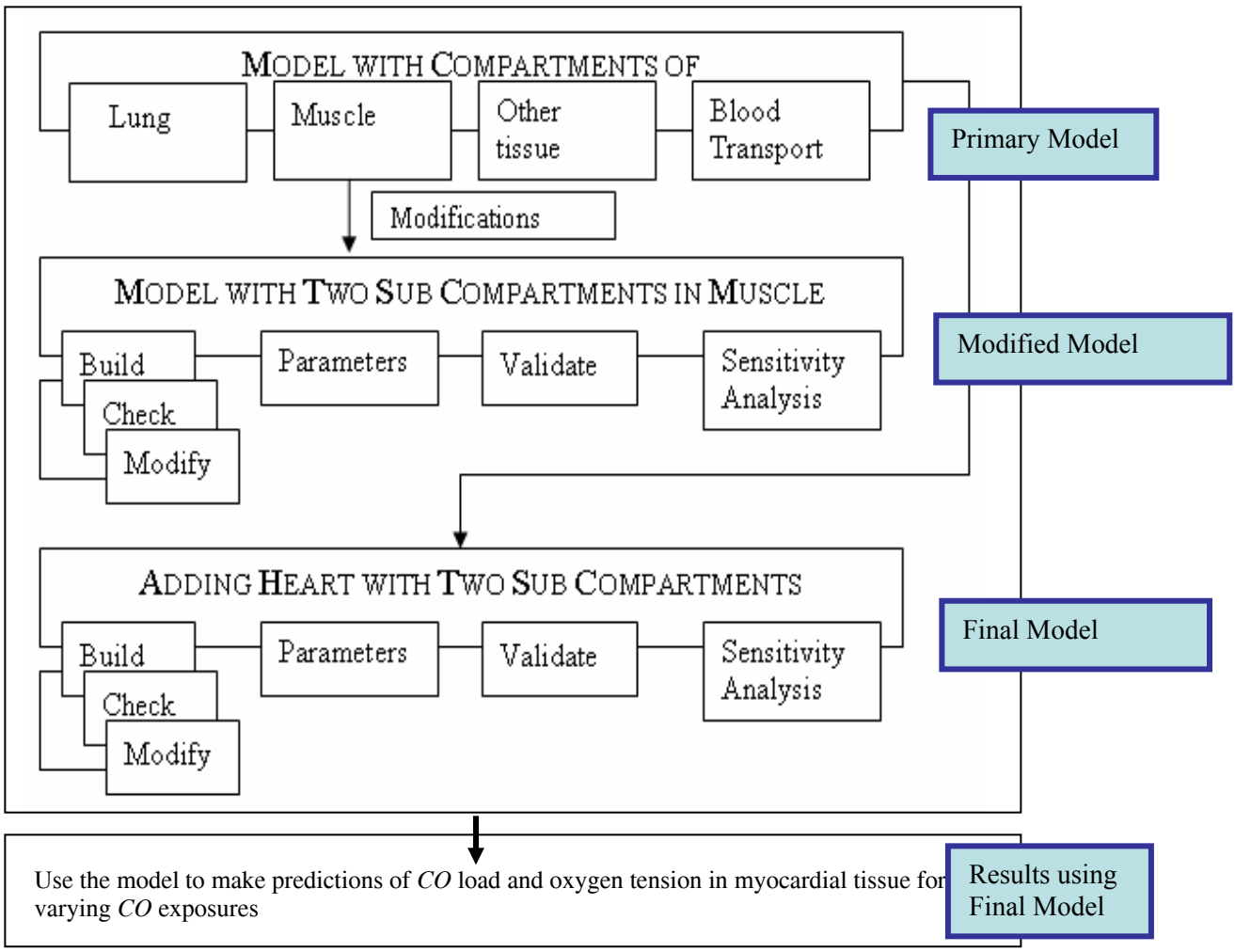

Figure 1.5: Stages of Model Development

CHAPTER 2
Background

Chapter 2 provides information on models present in the scientific literature that predict *CO* uptake and the limitations of these models. This chapter discusses the basis for selecting a specific model for the thesis from the models present in the literature and the necessity to modify the selected model to test the hypothesis made. This chapter also gives a basic introduction to the concepts, simulation software used and an overview of all the compartments present in the model. As it is difficult to measure (non-invasively) carboxymyoglobin levels (*MbCO*) and tissue O_2 tension (PtO_2) in the human heart, building a model for estimating these parameters seemed the best approach. Modification may include implementing desired features to cater to the needs of the desired model and to overcome the limitations of the available models.

2.1 Previous Models

The CFK (Coburn Forster Kane) model often discussed in the carbon monoxide level (*CO*) literature predicts carboxyhemoglobin (*COHb)* levels for acute and chronic *CO* exposures (Coburn et al. 1965). The CFK equation establishes a relation between the blood *COHb* levels, rate of endogenous *CO* production, and *CO* exchange rate due to respiration. However, this model has certain limitations. For example, the model lumps the total blood volume into a single homogeneous, well mixed compartment and also excludes the dissolved *CO* or oxygen *(*O_2) in the blood while determining the *COHb* levels in the blood. The CFK model analytically solves the linearized CFK equation by assuming a constant O_2Hb concentration in the blood.

The model predictions agree well with experimental values under normal conditions but disagree with experimental values involving transient *CO* exposures (154), involving fast reactions of *CO* with *Hb* (Forster (1970), Holland (1970), Roughton (1964), Waller et.al (1988)). Later Peterson & Stewart (1975), Bernad & Duker (1981), Tyuma et. al (1981) and Collier & Goldsmith (1983) solved the CFK

equation by accounting for the variation of O_2Hb using iterative methods, analytical solutions etc.

More recently, a mathematical model was developed (36) to predict alveolar partial pressure of *CO* and blood *HbCO* as a function of exposure time and *CO* concentration. *CO* uptake by blood was predicted taking into account the diffusion based transport mechanisms of *CO* and the replacement reaction of *CO* with O_2Hb. Benignus et al. (1995) developed a model to predict blood *COHb* levels considering variations in inhaled O_2, CO_2 and *CO* concentrations. But the drawback of these models was that they limited their *CO* uptake predictions to the vascular compartments. They did not include diffusion of gases from vascular compartments to the surrounding tissue. This results in exclusion of extravascular storage sites of *CO* like myoglobin present in muscle tissue and cytochrome oxidase in mitochondria. Also, the concept of lumping blood into one single compartment results in loss of physiological relevance related to variability in O_2 concentrations (O_2 content is greater at the arterial side compared to venous side) and partial pressures present in different blood subcompartments, which affects the predicted *CO* load.

Bruce (2003) developed a model that predicted distribution of *CO* in the body by considering *CO* diffusion between the vascular and extravascular compartments. The model (Figure 2.1) had a lung compartment, blood (arterial and venous) compartments, muscle and non-muscle tissue with vascular and extravascular compartments. Herein this model will be referred to as the primary model in this thesis. Mass balance equations for *CO* were written for all the compartments of the model and are described in detail in (35). An example of the mass balance equation for *CO* for the alveolar compartment from the above model is as follows:

$$V_L \frac{dC_ACO(t)}{dt} = [P_iCO(t) - P_ACO(t)]\frac{\dot{V}_A}{P_B} - COflux_{LB}(t)$$

where V_L is lung volume, C_ACO is the alveolar *CO* concentration, P_ACO is the alveolar partial pressure of *CO* (P_{CO}), P_iCO is inhaled partial pressure of *CO*, t is time, and $COflux_{LB}(t)$ is the *CO* flux from lungs to blood defined as

$$COflux_{LB}(t) = [P_ACO - ((1-K_v)P_{ec}CO(t) + K_vP_vCO(t-d_v))]D_LCO$$

where $P_{ec}CO$ is end-capillary PCO, d_v is the mean transport delay in mixed venous blood, P_vCO is mixed venous partial pressure of CO, and K_v is used to apportion the effective pulmonary capillary PCO between the mixed venous and end-capillary pressures. Vascular mixing in the pulmonary capillary compartment is ignored and $C_{ec}CO$ is determined by adding $COflux_{LB}$ to the mixed venous blood, which enters the lungs after the mean transport delay (d_v) from venous blood compartments.

In the modified model (discussed in Section of 3.2 of chapter 3) and final model (discussed in Section 3.3 of chapter 3) the same CO mass balance equations are used for the alveolar compartment (as shown above) and the non-muscle tissue. For the skeletal muscle (tissue and blood subcompartments), CO mass balance equations in the final model (model developed for thesis) are described for two tissue subcompartments and three blood vascular subcompartments, unlike equations used for the single blood vascular and tissue compartments discussed in (35).

To determine the partial pressure of carbon monoxide (PCO) in each blood compartment of the primary model it was necessary to solve three simultaneous algebraic equations of O_2 (discussed in Reference 35):

1. Oxyhemoglobin Dissociation Curve (ODC).
2. Haldane's Equation.
3. Blood to Tissue Oxygen Flux Equations.

2.1.1 Oxyhemoglobin Dissociation Curve

The oxyhemoglobin dissociation curve gives the saturation of oxygen as a function of the partial pressure of oxygen. There are number of factors that affect the binding of oxygen to hemoglobin which change the shape of the curve. Factors that affect the ODC are variation of the hydrogen ion concentration (pH), effects of carbon dioxide, effects of 2,3-DPG (2,3-Diphosphoglycerate), temperature, carbon monoxide, effects of methemoglobinemia (a form of abnormal hemoglobin) and fetal hemoglobin (37). ODC is shifted to the right by an increase in temperature, 2, 3-DPG,

or PCO_2, or a decrease in pH. In this model, for the conditions that the authors intend to simulate the most important factor that may affect the curve is the carbon monoxide level. In the absence of *CO*, the sigmoidal shaped curve approaches a horizontal asymptote as the partial pressure of oxygen exceeds approximately 70 mmHg and declines with a steep slope toward a point of inflexion when the partial pressure of oxygen falls approximately below 60 mmHg. Carbon monoxide also has the effect of shifting the curve to the left. Thus, a set of equations were derived to represent the O_2 dissociation relationship in the presence of *CO* by determining the dependence of the Hill parameters on the *HbCO* level and then applying a correction to the Hill equation at low O_2 pressures. The method for the derivation is detailed in the paper (35). When the inspired *CO* levels are zero, the ODC retains its shape. Except at low PO_2 values, a reasonable approximation to this curve for any given level of *HbCO* is the Hill equation given below

$$Co_2 = \frac{Co_{2(\max)} \cdot \left(\frac{PO_2}{P_{50}}\right)^n}{1 + \left(\frac{PO_2}{P_{50}}\right)^n}.$$

Where $P_{50} = ap_1\left[1 + \exp\left(ap_2 \cdot \%COHb\right)\right] - 1$ and

$n = an_1 + an_2 \cdot \exp(-0.025 \cdot \%COHb)$

ap_1,ap_2,an_1, an_2 are constants resulting from curve fitting for various concentrations of *CO*. P_{50} is the PO_2 necessary to half-saturate the *Hb*.

The *ODC* for *Mb* (Figure 5 of reference 38) is also represented by a Hill equation, but it is assumed that its parameters are independent of the carboxymyoglobin (*MbCO*) level except for that of the maximum O_2-binding capacity. At each time step of the simulation, the dissociation curve for *Mb* and the Haldane equation for *Mb* are satisfied simultaneously via an implicit solution using an iterative procedure.

The Hill equation for myoglobin is

$$PO_2 = \frac{[O_2Mb] \cdot P_{50}}{1 - [O_2Mb]}.$$

where PO_2 is the oxygen tension and $[O_2Mb]$ is the fractional O_2 saturation of myoglobin. P_{50} is the PO_2 at which myoglobin is half-saturated with oxygen and is dependent on temperature and pH.

2.1.2 Haldane's Equation

PCO was determined by first solving for the other variables, assuming that *PCO* is constant across an integration step, and then updating its value via the Haldane equation as shown below.

$$\frac{M_{Hb}P_{CO}}{COHb} = \frac{P_{O2}}{O_2Hb}$$

M_{Hb} is the Haldane affinity ratio for hemoglobin and has a value of 218. The volumetric carrying capacity of *Hb* for O_2 or *CO* is calculated as the product of *Hb* concentration and the nominal maximum O_2 content, 1.38 ml O_2/g *Hb*. The Haldane equation for myoglobin is

$$\frac{M_{Mb}P_{CO}}{COMb} = \frac{PO_2}{O_2Mb}$$

M_{Mb} is the Haldane affinity ratio for myoglobin and has a value of 36. At each time step of the simulation, the dissociation curve for *Mb* and the Haldane equation for *Mb* were satisfied simultaneously via an implicit solution using an iterative procedure.

2.1.3 Blood to Tissue Oxygen Flux Equations

The blood to tissue oxygen flux equations are described in (35). It was assumed that O_2 diffuses from the vascular to the extravascular subcompartments of the tissues

at rates just sufficient to meet the metabolic demand of the tissue. Endogenous *CO* production was included by assuming that all endogenous *CO* is delivered to the mixed venous compartment.

2.2 Chosen Model and Proposed Modifications

The model (primary model) developed by Bruce (2003) fit the criteria of the model needed for the thesis as the model accounted for transport of *CO* in the pulmonary compartment, *CO* bound to Hb and dissolved in plasma, and transport of *CO* from the blood flow to surrounding tissue. This model consists of five major compartments: 1.The arterial blood, 2. The Lungs, 3. Skeletal Muscle, 4. Non-muscle tissue and 5. Mixed venous blood compartments (Figure 2.1). Herein this model will be referred to as the primary model in this thesis. However, O_2 parameters were assumed to be constant in this model and were passed as arguments.

Thus the primary model was chosen and certain modifications were proposed to test the hypothesis made. The proposed modifications are as follows:

Tissue O_2 tension which is an important predictor of the oxygenation state of the tissue can also be anticipated by adding equations for O_2 mass balances. This would also aid in accounting for the nonlinearities in an efficient way.

The model predictions would be more physiologically relevant if the single muscle compartment was divided into subcompartments. This would allow diffusion of gases within the tissue resulting in better solution estimates for O_2 tensions and *CO* load. Therefore, in our lab we intended to replace the single lumped muscle compartment with two subcompartments. Regional heterogeneity of blood flow and O_2 consumption in skeletal muscle demanded development of predictive equations to calculate the arm, the trunk and the leg skeletal mass distributions. Also, a formula was developed to predict an increase in cardiac output with increased *COHb* level in blood. A paper on the updated model is in preparation (Bruce, Bruce, and Erupaka).

Though heart is a muscle tissue, it has a different morphology from skeletal muscle tissue. Cardiac muscle has a different capillary density (39), resting blood flow (Table 2.1) and metabolic rate (Table 2.2) from that of skeletal muscle (Table 2.3 and Table 2.4). Lumping the skeletal muscle and cardiac muscle into a single

compartment would not be a good assumption to make. Thus, it would be important to add a heart compartment to the model in order to model *CO* uptake and PO_2 in the myocardium and relate them to cardiac injury.

Another objective was to develop better and more efficient algorithms to determine PO_2 and *PCO* in the compartments. The algorithms used in the primary model had convergence issues while solving the O_2 dissociation curves of *Hb* and *Mb* (especially solving for PO_2 and *PCO* when certain conditions caused ODC to be flat) and resulted in numerical errors. It was also important to modify the blood to tissue oxygen flux equations by evaluating them as a function of pressure gradients and diffusion coefficients of O_2 instead of making an assumption of equality between O_2 flux and metabolic demand of the compartment.

2.3 Basic Concepts of the Model

The basic concept used in developing the model is the continuum theory of conservation of mass. Figure 2.2 gives a summary of basic concepts needed to build a model. Mass balance equations are written for *CO* and O_2 for all compartments. Mass balance equations state that for any substance Q in a compartment,

$$dQ/dt = (\text{rate of inflow} + \text{rate of creation}) - (\text{rate of outflow} + \text{rate of destruction})$$

The model diagram and dynamic equations are described in detail in chapter 3. The simulation tool or software used to apply principles of physiology and engineering to a model is ACSL (Advanced Continuous Simulation Language). This tool has been exclusively developed for the purpose of modeling systems described by time dependent, non-linear differential equations or transfer functions. ACSL application areas include control system design, missile and aircraft simulation, power plant dynamics, biomedical systems, vehicle handling, heat transfer analysis, etc. Most of its basic elements are defined from FORTRAN, however the latest version is a fusion of various other languages like C++, JAVA, etc., which supports enhanced graphical user interface (GUI) and displays. The algorithm used for integration is the Runge-Kutta-Fehlberg algorithm with fixed order and variable step. The algorithm evaluates the derivative three times per step and makes a second order advance. If any error in a state is larger than that allowed, the step size is reduced

until the error criteria are satisfied for all the states. Apart from the integration algorithm which is built-in in ACSL, other algorithms are developed as macros and called to solve certain simultaneous algebraic equations which are discussed in section 3.8 of chapter 3.

In general models have several parameters to be estimated and the values for these parameters are either taken from the literature available or they are estimated. When available, subject-specific values of model parameters were obtained from the literature or directly from the investigators. Usually, the age, weight, and height of a subject were available, and often one or more additional parameters, such as *Hb* concentration, total blood volume, cardiac output ($Q^{\cdot}$), or ventilation, were provided by the investigators. In some cases, average values for a group of subjects were used. Predictive formulas were used to estimate $Q^{\cdot}$ (when it was not measured) and tissue volume of skeletal muscle (V_m) as functions of body weight (*BW*), age (*A*), height (*HT*), and gender (*G*; has a value of 1 for a male and 0 for a female subject). Predictive formulas were used from published papers,

$$\mathrm{Q}^{\cdot} = (54.1 + 7.9G)BW + 1400 - 200G \quad (40)$$

Cardiac output was calculated in ml/min

$$V_m = 1000(0.244BW + 7.80HT + 6.6G - 0.098A - 3.3)/1.04 \quad (41)$$

Tissue volume of skeletal muscle was calculated in ml.

2.4 Anatomy of the Heart

The heart is the mechanical pump that circulates blood through the blood vessels involuntarily maintaining the homeostasis of blood to tissue exchange. The heart has several surfaces (anterior, inferior) and membranes that surround and protect the heart without interrupting the contraction and vigorous movement of heart. The heart wall consists of three layers namely the epicardium which is the external layer, the myocardium which is the middle layer of the wall and the endocardium, the inner layer of the heart wall. The myocardium is an involuntary cardiac muscle tissue which makes up the bulk of the heart and is responsible for the pumping action of the

heart. There exists oxygen supply and consumption heterogeneity in theses layers of the heart wall corresponding to variable oxygen tensions (Table 2.5).

The heart has four chambers. The right and left atria which receive blood from the great veins (superior vena cava, inferior vena cava, coronary sinus) and from the lungs through the pulmonary veins, respectively. The right and left ventricles perform the pumping action of blood. However, these chambers also vary in thickness according to their function. The left ventricle pumps blood to vasculature at greater distances with large blood flow resistance resulting in higher pressures compared to the right ventricle. Thus the left ventricle has a thicker wall as it works harder. The left heart is generally considered the energy source of the system. The greater work load in the left ventricle results in higher blood flow through the cardiac muscle and greater oxygen consumption compared to other chambers of the heart, as the tissues match their vascular function to their metabolic needs. During resting conditions, the myocardial oxygen extraction fraction is 60-70% (42).

It is a known fact that the heart requires energy to maintain ionic balance and synchronous contractions. This energy is supplied by the ATP (Adenosine Tri Phosphate), which needs oxygen for aerobic metabolism to take place. In cases of increased myocardial stress, conditions of hypoxia, hypoxemia or *CO* poisoning, the energy metabolism cycles are disrupted (43-47) and an increase in coronary supply should occur to prevent tissue hypoxia. Thus, modeling O_2 delivery and demand is needed to estimate the burden of hypoxia on the cardiac tissue. As *CO* impairs oxygen delivery, causing discrepancies in the tissue-blood PO_2 gradients, the objective was to develop a model to estimate the oxygen tension in the cardiac tissue and also predict the burden of the CO load delivered to the heart.

Table 2.1: Myocardial Blood Flow

Species	Condition	Region	Value (ml/min/g)	Technique	Reference
Baboons	Awake, Sitting	Left ventricle	2.41 ± 0.90 ml/min/g (80%)	15 um Microspheres	55
		Right ventricle	1.74 ± 0.73 ml/min/g (16%)		
Dogs	Sedated - Responsive	Left ventricle	0.96 ± 0.11 ml/min/g	Microspheres	56
		Right ventricle	0.77 ± 0.07 ml/min/g		
		Interventricular septum	0.91 ± 0.10 ml/min/g		
Dogs	Anesthetized	Left ventricle	1.14 ± 0.38 ml/min/g	Microspheres	57
		Right ventricle	0.72 ± 0.28 ml/min/g		
Dogs	anesthetized	Left ventricle	0.86 ml/min/g	Microspheres	58
		Right ventricle	0.48 ml/min/g		
Dog-closed chest	anesthetized	Left ventricle	1.0 ml/min/g	Microspheres	59
Humans 25 ± 3 yr	[LV=196 ± 38 g]	Left ventricle	0.79 ml/min/g	PET - semi-supine	60
Humans 46±12 yr	[LV=193 ± 20 g]	Left ventricle	0.88 ± 0.19 ml/min/g	PET	61

(Table also referred in Section 3.4)

Table 2.2: Myocardial Oxygen Consumption

Species	Region	Value (ml/min/100g)	Technique	Reference
Awake Dog	Right ventricle	4.7 ± 0.5	BNII nephelometer	51
Dog	Right atrium	4	,,	52
Dog	Left ventricle	8.6	,,	52
Dog	Left atrium	0.8	,,	52
Dog	Whole heart	8.2 ± 2.1	PET	53
Dog	Whole heart	7.0 ± 1.5	PET	
Dog	Left ventricle	8.8 ± 1.5	PET	54
Human	Heart	8.2+/-2.1 ml/min/100g	11C-acetate and PET	53

(Table also referred in Section 3.4)

Table 2.3: Skeletal Muscle Blood Flow

Values(ml/min/100ml tissue)	Species	Region	Method	Reference
1.4±0.6	Human	Gastrocnemius	133Xe clearance technique	62
1.6±0.4	Human	Brachioradialis	133Xe clearance technique	"
1.8±0.7	Human	Flexor digitorum superficialis	133Xe clearance technique	"
1.5±0.6	Human	Biceps	133Xe clearance technique	"
1.6±0.4	Human	Triceps	133Xe clearance technique	"
1.4±0.6	Human	Tibialis	133Xe clearance technique	"
1.6±0.6	Human	Quadriceps	133Xe clearance technique	"
2± 0.5	Human	Leg proximal	auto radiographic	50

Table 2.3 Skeletal Muscle Blood Flow (Continued)				
Values(ml/min/100ml tissue)	**Species**	**Region**	**Method**	**Reference**
3.1±1.7	Human	Muscle	emission tomography and 15 O labelled water	63
1.9± 0.5	Human	Leg proximal	auto radiographic method	50
1.9± 0.5	Human	Leg middle	auto radiographic method	"
1.6± 0.4	Human	Leg distal	auto radiographic method	"
1.4± 0.3	Human	Leg distal	auto radiographic method	
1.4± 0.64	Human	Brachiradialis	NIRS technique after venous occlusion	49
0.81± 0.47	Human	Flexor digitorum superficialis	NIRS IO50	64
0.72± 0.32	Human	Flexor digitorum superficialis	NIRS IO36	"

Table 2.3 Skeletal Muscle Blood Flow (Continued)				
Values(ml/min/100ml tissue)	**Species**	**Region**	**Method**	**Reference**
1.42± 1.04	Human	Brachioradialis	Fick/plethysmography	64
2.06± 0.7	Human	Forearm	"	"
2.6± 1.2	Human	Calf-profound flexors	"	"
3.1± 0.27	Human	Forearm	venous occlusion and strain gauge plethysmography	65
3.12±1.55	Human	Femoral	(15O)H2O and PET	"
3±2	Human	Skeletal muscle	(15O)H2O,(15O)CO and PET	66

(Table also referred in Section 3.1, Section 3.2.2)

Table 2.4: Skeletal Muscle Oxygen Consumption

Species	Region	MRO_2 Value (ml/min/100g)	Technique	Reference
Human	Forearm	0.15 ± 0.01	NIRS -arterial occlusion	**48**
Human	Forearm	0.114 ± 0.03	NIRS -venous occlusion	**49**
Human	Quadriceps femoris	0.21 ± 0.04	PET	**50**
Human	Quadriceps femoris	0.21 ± 0.03 mid	PET	50
Human	Quadriceps femoris	0.17 ± 0.02 most distal	PET	50

(Table also referred in Section 3.2, Section 3.2.2)

Table 2.5: Myocardial Tissue Oxygen Tension in Various Species

Species	Region	Mean PO2 Value	Arterial PO2	Method	Reference
Mice(N=5)	Left ventricle mid-myocardium	Mean PO2 = ~15.5 mm Hg		OxySpin - EPR	145
Cat(N=6)	Surface of beating heart (histogram) (~ 5 - 60 Torr)	Median PO2 = 31 mm Hg	"Steady state" (normoxia)	Platinum electrode 8 mm	146
Cat(N=6)	Surface of beating heart (histogram) (~ 5 - 125 Torr)	42 mm Hg	464.7 mm Hg	Platinum electrode 8 mm	146
Cat(N=6)	Surface of beating heart (histogram) (~ 10 - 115 Torr)	35 mm Hg	259.3 mm Hg	Platinum electrode 8 mm	146
Cat(N=6)	Surface of beating heart (histogram) (~ 0 - 15 Torr)	4 mm Hg (79% = 0-5 Torr)	18.7 mm Hg	Platinum electrode 8 mm	146
Mouse (N=7)	Mid-myocardium	16.4 ± 0.7 mm Hg	(normoxia)	LiPc crystals - EPR	147
Dog (N=24)	Left ventricle 6 mm deep	42±7 mm Hg	143 ± 23	Paratrend probe	147
Dog (N=5)	Anterior wall of left ventricle	36±8 mm Hg		Polarographic Clark type	148
Dog (N=12)	Left epicardium (2 mm deep) "coronary stenosis"	52±7 mm Hg	Ventilated with 100% O2 to maintain normocapnia	Monopolar Polarographic needle	149
Dog (N=9)	Left ventricular myocardium: shallow - before bypass	17.1 mm Hg	65 mm Hg	Mass spec	150

Table 2.5 Myocardial tissue Oxygen tension in various species (Continued)					
Species	**Region**	**Mean PO2 Value**	**Arterial PO2**	**Method**	**Reference**
Dog (N=9)	Left ventricular myocardium: deep - before bypass	14.5 mm Hg	65 mm Hg	Mass spec	150
Dog (N=9)	Left ventricular myocardium: shallow - after bypass	28.3 mm Hg	65 mm Hg	Mass spec	150
Dog (N=12)	Left ventricular myocardium: 3 mm deep - subepicardium	29.5 ± 2.5 mm Hg	Coronary blood flow in LAD=29.7 ± 3.9 ml/min	polarography	151
Pig (N=13)	Left ventricle (surface of epicardium)	49 ± 2 mm Hg	23 ± 1 mm Hg	Clark-type electrodes	151
Human M 38yr	Right ventricular myocardium: 6 mm deep	39.73 mm Hg; (median=28)	168-210 mm Hg	Platinum needle electrode	152
Human M 42yr	Left ventricular myocardium: 6 mm deep	19.4 mm Hg; (median=17)	78-126 mm Hg	Platinum needle electrode	152
Human F 8yr	Left ventricular myocardium: 6 mm deep	27.4 mm Hg; (median=24)	48-51	Platinum needle electrode	152
Human (N=13)	Left ventricle - mid-myocardium	42 mm Hg (n=15)	93 to 470 mm Hg	mass spec	153
Piglets	Epicardial surface of left ventricle	16.8 ± 4.2 mm Hg	106 ± 5.5 on room air	phosphorescent O2	153

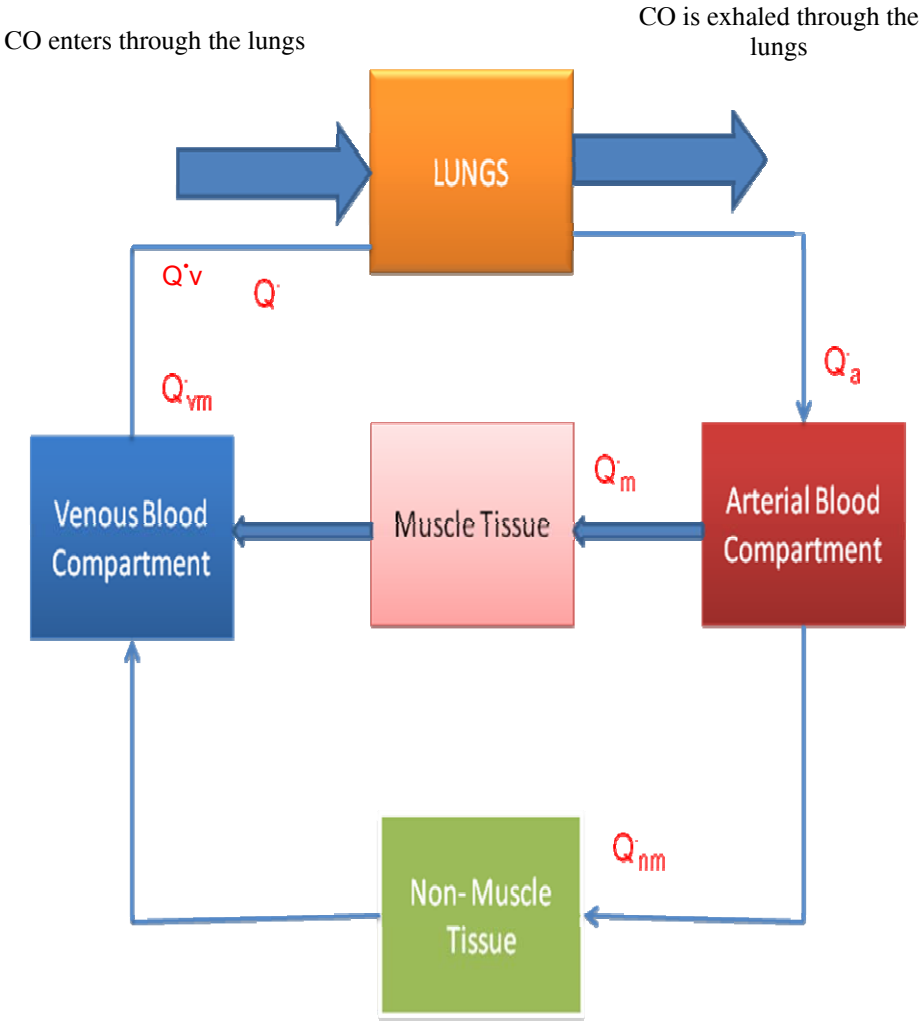

Figure 2.1: Primary Model. The model consists of five major compartments. Mass balance equations were written for *CO*. *CO* enters through the lungs and diffuses to the muscle tissue and non-muscle tissue compartments via the arterial blood compartment. *CO* then enters the venous blood compartments after a time delay. For the detailed figure refer to 35

(Figure also referred in Section 3.1)

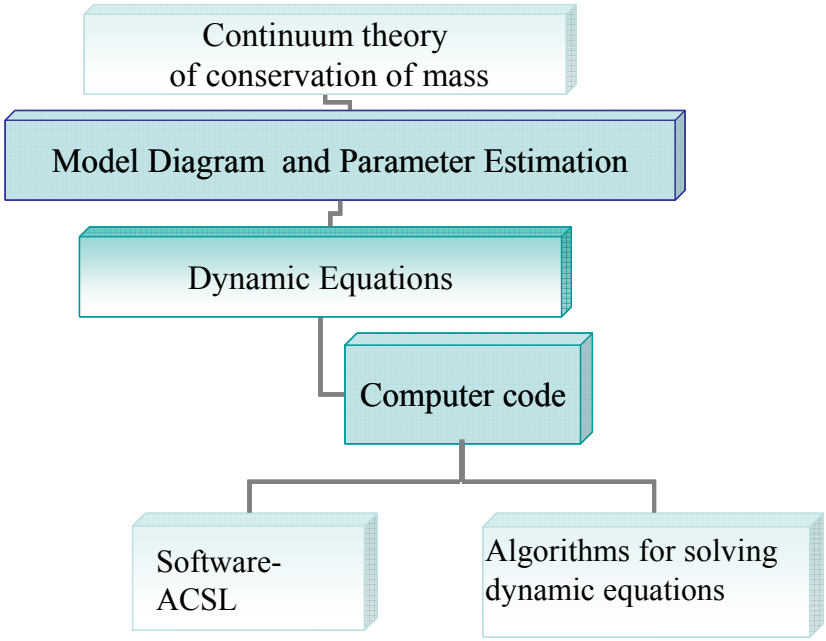

Figure 2.2: Basic Concepts of Building a Model. The basic concepts for building a model are determining the principle for the model (conservation of mass), sketching the model diagram, determining the parameters, and choosing suitable software to build the model.

CHAPTER 3
Model Description

Chapter 3 discusses a brief overview of the modifications to the primary model. The chapter explains the general form of the mass balance equations for O_2 and CO for a model with two subcompartments. After a brief description of the cardiac compartment of the model, the mass balance equations written for O_2 and CO for each blood and cardiac tissue subcompartment are explained in detail. Parameter estimation for the cardiac compartment and development of predictive equations are also discussed in this chapter. Predictive equations are developed for: (i) estimating the volumes of muscular regions (arms, legs and trunk) for males and females (ii) percent increase in cardiac output and heart rate as functions of increased $HbCO$ levels in the blood, (iii) cardiac output and heart rate as functions of total body oxygen consumption, (iv) percent increase in heart rate as a function of increased $HbCO$ levels in the blood. Estimation equations were also developed for: (v) myocardial oxygen consumption, and (vi) myocardial blood flow, both as functions of heart rate. Sensitivity analysis is performed and parameters that influence the oxygen tension in the myocardial tissue and vascular PO_2 are determined. This chapter also explains the validation protocol for the cardiac compartment of the whole body model where predicted data are compared with experimental values (from humans and animals during conditions of normoxia, hypoxia, exercise and hyperoxia).

3.1 Overview of Desired Model

In our lab, the initial model (referred to as the primary model in this thesis, Figure 2.1) developed by Dr. Bruce (2003) was modified to produce a second model (referred to as the modified model in this thesis, Figure 3.1), which accounts for mass balance of oxygen (Bruce, Bruce, and Erupaka, manuscript in preparation). Additions in this model include O_2 mass balance equations, an algorithm to calculate PO_2 corresponding to the concentration of oxygen halfway between the inlet and outlet of the vascular subcompartment of a tissue, and a regression equation to predict

the associated increase in cardiac output due to an increase in *COHb* level in the blood. Also, skeletal muscle mass was distributed into volumes of muscular regions (arms, legs and trunk) for males and females to account for regional heterogeneities in muscle blood flow (Table 2.3) and O_2 consumption (Table 2.4). The physiological phenomenon of arterio-venous shunting was implemented in the lungs. Later, in an enhancement of the modified model, a two subcompartment cardiac compartment was added (referred to as the final model in this thesis, Figure 3.2). Development of this cardiac compartment in the model is the first main goal of this thesis.

The skeletal and cardiac muscles exhibit major differences in morphology, blood flow and O_2 demand. Also, cardiac muscle works constantly to pump blood unlike the skeletal muscle, and it would be inappropriate to lump the cardiac muscle with the resting skeletal muscle. In the process of building the cardiac compartment various other prediction equations were developed to estimate parameters needed for the model. Parameters like myocardial O_2 consumption and myocardial blood flow were predicted as functions of heart rate; cardiac output and heart rate were calculated from body oxygen consumption when values for heart rate and cardiac output were not available. Also, increase in heart rate was predicted as a function of increased *COHb* levels in blood.

3.2 Modified Model

The modified model consists of five major compartments: 1.The arterial blood, 2. The Lungs, 3. Skeletal Muscle with two subcompartments, 4. Non-muscle tissue and 5. Mixed venous blood compartments (Figure 3.1). Mass balance equations are written for oxygen (O_2) and carbon monoxide (*CO*) for each of these compartments to model whole body uptake of, and distribution of, *CO* and O_2. Section 3.2.1, explains the mass balance equation of O2 for the alveolar compartment, and Sections 3.2.2 and 3.2.3 introduce the general form of mass balance equations of O_2 and *CO* for the vascular and tissue compartments of the modified model.

3.2.1 Mass Balance Equations for the Alveolar Compartment

The O_2 mass balance equation for the alveolar compartment was added to the model as follows,

$$V_L \frac{dC_AO_2(t)}{dt} = [P_iO_2(t) - P_AO_2(t)]\frac{\dot{V_A}}{P_B} - O_2\,flux_{LB}$$

where, V_L is lung volume, C_AO_2 is the alveolar O_2 concentration, P_AO_2 is the alveolar partial pressure of oxygen , P_iO_2 is inhaled PO_2, t is time, $\dot{V_A}$ is alveolar ventilation, P_B is barometric pressure, and $O_2\,flux_{LB}(t)$ is the oxygen flux from lungs to blood, defined as

$$O_2\,flux_{LB}(t) = \dot{Q}(1 - SF)[C_{ep}O_2(t) - C_{mx}O_2(t)].$$

Where $\dot{Q}$ is the cardiac output and SF is the shunt fraction, the percentage of pulmonary blood flow that passes from the right to left heart without undergoing oxygenation by the lung. $C_{ep}O_2\ (t)$ is the end pulmonary oxygen concentration and $C_{mx}O_2\ (t)$ is the oxygen concentration in the mixed venous compartment. It is assumed that the end pulmonary partial pressure of oxygen ($P_{ep}O_2$) equals alveolar partial pressure of oxygen (P_AO_2). CO mass balance equations for the alveolar compartment are used from the primary model which was discussed in Section 2.1 of chapter 2.

3.2.2 Mass Balance Equations for Blood Compartments

The mass balance equations for O_2 in the arterial, mixed venous and vascular subcompartments of the skeletal muscle tissue are each described by an equation of the general form

$$V_i \frac{dC_iO_2(t)}{dt} = [C_i^{in}(t) - C_iO_2(t)].\dot{Q_i} - O_2Flux_i(t)$$

where i is the index representing the arterial (ar), mixed venous (mx), skeletal muscle (subcompartment m1 or m2), or venous (v) compartments. V_i is volume of the compartment i, C_i^{in} is the concentration of O_2 in blood entering the compartment

i, $C_i O_2$ is the total concentration of O_2 in the blood compartment *i*, and $Flux_i$ is the rate of diffusion of O_2 out of the vascular compartment i. (Mass balance equations of O_2 and *CO* for individual cardiac compartments are discussed in Section 3.3 of this chapter.)

The flux is zero for the arterial and venous blood compartments. For the non-muscle (other) - tissues (ot) blood compartment, the $Flux_{ot}(t)$ is defined as

$$O_2 Flux_{ot}(t) = [Pb_{ot}O_2(t) - P_{ot}O_2(t)].D_{ot}O_2$$

where, $Pb_{ot}O_2(t)$ is the mean partial pressure of O_2 in the arterial inflow and venous outflow of the non-muscle vascular compartment. $P_{ot}O_2(t)$ is the partial pressure of O_2 in the non-muscle tissue compartment. $D_{ot}O_2$, is the blood to tissue diffusion coefficient of oxygen. The non-muscle soft tissue in the model is a single compartment. Because it does not contain Mb, its uptake of *CO* is very small.

For the skeletal muscle (m) blood subcompartments, the general form of the equation for $Flux_{mj}(t)$ is as follows:

$$O_2 Flux_{m(j=1,2,3)}(t) = G_{sf}(P_{bmj}O_2) \cdot \left[D_{bmj}O_2 \cdot \left(P_{bmj}O_2(t) - P_{m1(or)m2}O_2(t)\right)\right]$$

$$G_{sf}(P) = 1 - \left[\frac{\left(\frac{P}{1500}\right)^3}{1+\left(\frac{P}{1500}\right)^3}\right] \text{ and } D_{bmj}O_2 = \frac{PS_m * SO_2 * V_{m1(or)m2}}{1.04}$$

where *j* is the index of the blood vascular subcompartments j =1,2,3 for blood subcompartments 1 ,2 and 3, respectively. $D_{bmj}O_2$ is the blood to muscle tissue diffusion coefficient. $P_{bmj}O_2(t)$ is the partial pressure of O_2 corresponding to the concentration of oxygen halfway between the inlet and outlet of the vascular subcompartment of the skeletal muscle. $P_{m1}O_2(t)$ and $P_{m2}O_2(t)$ are the two subcompartment (m1, m2) tissue O_2 tensions. V_{m1} and V_{m2} are the volumes of the muscle tissue subcompartment 1 and 2, respectively. SO_2 is the solubility of oxygen in plasma and PS_m is the permeability surface area product of the skeletal muscle.

Gsf(P) is a heuristic "gain" whose only purpose is to reduce the diffusion coefficient in hyperbaric O_2 (which is not considered in this thesis). During hyperbaric O_2, hemoglobin is completely saturated with O_2 and dissolved O_2 concentrations increase, thereby resulting in a decrease of the effective diffusion coefficient of O_2. Gsf = 1 for all simulations herein. The diffusion coefficient of O_2 is directly proportional to permeability surface area product. Greater permeability of the membrane for O_2 means that the diffusion coefficient of O_2 from blood is greater and efficiency of O_2 transport from blood to tissue is greater. O_2 flux depends on the pressure gradient and the diffusion coefficient, $D_{bm(j=1,2,3)}O_2$.

The total concentration of O_2 in the blood compartment, $C_{(j=1,2,3)}O_2(t)$, is calculated from dissolved and Hb-bound O_2 concentration components so that

$$C_{(j=1,2,3)}O_2(t) = O_2Hb_j(t) + SO_2.P_jO_2(t),$$

where O_2Hb is the oxygen bound to hemoglobin, $P_{(j=1,2,3)}O_2(t)$ is the partial pressure of O_2 in the muscle blood subcompartment *j*.

Mass balance equations for *CO* in the arterial, mixed venous and non-muscle tissue are described in reference 35. *CO* mass balance equations for vascular subcompartments of the skeletal muscle are each described by an equation of the form

$$V_i \frac{dC_iCO(t)}{dt} = [C_i^{in}CO(t) - C_iCO(t)]Q_i - Flux_iCO(t)$$

where *i=m1 or m2*, the index representing skeletal muscle subcompartment 1 (m1), or muscle subcompartment 2 (m2). $C_i^{in}CO(t)$ is the concentration of *CO* in blood entering the compartment i, $C_i\,CO$ is the total concentration of *CO* in the blood compartment *i*,

$$C_iCO(t) = COHb_i(t) + SCO.P_iCO(t)$$

$COFlux_i$ is the rate of diffusion of *CO* out of the vascular compartment.

$$COFlux_{m(j=1,2,3)}(t) = \left[D_{bmj}CO \cdot \left(P_{bmj}CO(t) - P_{m1(or)m2}CO(t)\right)\right]$$

$D_{bmj}CO$ is the blood to muscle tissue diffusion coefficient and is estimated by fitting the model to experimental data (35). $P_{bmj}CO(t)$ is the average partial pressure of *CO* of the vascular subcompartment j of the tissue. $P_{m1}CO(t)$ and $P_{m2}CO(t)$ are the partial pressures of *CO* in the muscle tissue subcompartments 1 and 2, respectively. *CO* mass balance equations for non-muscle tissue are the same as those in the primary model.

3.2.3 Mass Balance Equations for the Tissue Compartments

The mass balance equations for O_2 for the first skeletal muscle subcompartment (m1) in the two subcompartment skeletal muscle model is

$$\frac{dC_{m1}O_2(t)}{dt} = \frac{Flux_{m1}O_2(t)}{V_{m1}} + \frac{D_mO_2\left[C_{m2}O_2(t) - C_{m1}O_2(t)\right]}{D_{xm}}$$

Second subcompartment m2:

$$\frac{dC_{m2}O_2(t)}{dt} = \frac{Flux_{m2}O_2(t)}{V_{m2}} + \frac{D_mO_2\left[C_{m1}O_2(t) - C_{m2}O_2(t)\right]}{D_{xm}}$$

where, D_mO_2 is the diffusion coefficient of O_2 between the two subcompartments (m1, m2) of the skeletal muscle tissue. $C_{m1}O_2(t)$ and $C_{m2}O_2(t)$ are the partial pressures of O_2 of the two muscle subcompartments 1 and 2. D_{xm} is the intercapillary distance. The $Flux_{m1}O_2(t)$ and $Flux_{m2}O_2(t)$ are defined as

$$Flux_{m1}O_2(t) = O_2Flux_{m1}(t) + O_2Flux_{m3}(t) - MRO_{2m1}$$

$$Flux_{m2}O_2(t) = O_2Flux_{m2}(t) - MRO_{2m2}$$

where,

$O_2Flux_{m1}(t)$, $O_2Flux_{m2}(t)$ and $O_2Flux_{m3}(t)$ are the O_2 diffusion rates of vascular blood compartments 1, 2 and 3, respectively. MRO_{2m1} and MRO_{2m2} are the O_2 metabolic rates of the tissue subcompartments 1 and 2, respectively. O_2 diffuses from the vascular to the extra vascular compartments based on the pressure gradient between the compartments and the blood-to-tissue diffusion coefficients.

The *CO* mass balance equation for the two compartment tissue model is

First subcompartment m_1:

$$\frac{dC_{m1}\mathrm{CO}(t)}{dt} = \frac{Flux_{m1}\mathrm{CO}(t)}{V_{m1}} + \frac{D_m\mathrm{CO}\left[C_{m2}\mathrm{CO}(t) - C_{m1}\mathrm{CO}(t)\right]}{D_{xm}}$$

Second subcompartment m_2:

$$\frac{dC_{m2}\mathrm{CO}(t)}{dt} = \frac{Flux_{m2}\mathrm{CO}(t)}{V_{m2}} + \frac{D_m\mathrm{CO}\left[C_{m1}\mathrm{CO}(t) - C_{m2}\mathrm{CO}(t)\right]}{D_{xm}}$$

where, the subscripts and parameters are the same as those above, except, $D_{\mathrm{m}}\mathrm{CO}$ is the diffusion coefficient of *CO* within the two subcompartments of the tissue. $C_{m1}\mathrm{CO}(t)$ and $C_{m2}\mathrm{CO}(t)$ are the *CO* concentrations of the two tissue subcompartments 1 and 2, respectively. $Flux_{m1}CO(t)$ and $Flux_{m2}CO(t)$ are defined as

$$Flux_{m1}CO(t) = COFlux_{m1}(t) + COFlux_{m3}(t)$$

$$Flux_{m2}CO(t) = COFlux_{m2}(t)$$

where $COFlux_{m1}(t)$, $COFlux_{m2}(t)$ and $COFlux_{m3}(t)$ are defined in the blood compartments. The only difference between the mass balance equations for *CO* and O_2 is that oxygen is metabolized to meet the tissue metabolic demand while *CO* is not metabolized.

3.2.4 Prediction equations in modified model:

Predictive equations were developed as part of this thesis and added into the model to account for the blood flow and metabolic O_2 demand heterogeneities in the skeletal muscle tissue. Also there is an observed increase in cardiac output during *CO* exposure (68,69,70). Regulation of cardiac output in response to blood *HbCO* levels has been implemented into the model.

Prediction equations to estimate the volumes of regions (arms, legs and trunk for males and females) of skeletal muscle model: Muscle metabolic rate ($MRO_{2\mathrm{m}}$) is reported to be 20% (88, 89) of the total body oxygen consumption (MRO_2) during

rest. The metabolic rates of O_2 for leg, arm and trunk muscles are different (Table 2.4). Also the blood flows to different regions of the skeletal muscle vary (Table 2.3). Thus, to incorporate these heterogeneities (different metabolic rates and blood flows) of muscle in various regions, the skeletal mass is distributed into three muscle volume compartments namely leg muscle volume, arm muscle volume, and trunk muscle volume. The derivation of the equation is detailed in the appendix. The equations (Table 3.1) for calculating the masses of trunk, leg and arm muscle are functions of total skeletal muscle mass, V_m (41).

Tabulated blood flows and O_2 consumptions for skeletal muscle tissues are shown in table (Table 2.3 and Table 2.4) of the chapter 2. So after estimating the volumes of the skeletal muscle regions, average values (Table 3.2) for blood flow and oxygen consumption were determined for the muscular regions (arms, legs and trunk). From the Table 2.2 and Table 2.3, blood flow and oxygen consumption heterogeneity within the submuscular regions of arm (biceps, triceps, brachioradialis etc) and leg (gastrocnemius, biceps femoris etc) muscular regions can be clearly seen. Thus to determine the blood flow (or oxygen consumption) for the muscular regions (arms, legs and trunk), an average of the blood flows (or oxygen consumption) from different submuscular regions of the arm was taken. For example, to estimate the blood flow for the arm muscular region an average of all reported blood flows (in ml/min/gm) for the biceps, the triceps and the brachioradialis muscles was considered. Data for blood flow and oxygen consumption for the trunk muscles in healthy humans has not yet been reported in the literature. Hence, blood flow and O_2 consumption for the trunk muscular region was assumed to be equal to that of the leg muscular region. Blood flow for muscles in the trunk region was reported in animals (71, 72), but these values could not be considered due to postural differences in humans (bipedalism) and animals (quadrupedalism). There are some constantly working muscles in the trunk region like diaphragm (aid in breathing) which implies that blood flow and myocardial O_2 consumption must be higher than the arm muscular region. Also the muscles in the leg region work constantly against gravity to maintain postural balance. Since the leg and trunk muscle regions are mildly working

skeletal muscle regions, an assumption of equal blood flow and O_2 consumption was made.

There is reported to be an increase in cardiac output and heart rate with increase in carboxyhemoglobin levels in blood (68, 69, 70). When simulating experiments, increased carboxyhemoglobin levels in the blood had to be taken into account. Data for cardiac output, heart rate and carboxyhemoglobin (up to 50%) were collected from reference 68 and 69. Linear or nonlinear regression was performed on data, and statistical significance of the equations was tested using SYSTAT 9.0 after outliers were eliminated. The resulting equation was tested with data (70) which were not used in the regression. Then the equation was implemented into the model. A detailed derivation of the equation below is discussed in appendix. Figure 3.3 shows the data points used to build the regression relation and the relation fit developed for predicting the increase in cardiac output as a function of blood *HbCO* levels, as shown below

$$\%\Delta\dot{Q} = 0.572(\%\Delta HbCO)$$

3.3 The Cardiac Compartment

The myocardial compartment comprises three vascular subcompartments; 1, 2, 3 as shown in the Figure 3.4 and two tissue subcompartments; 1 and 2. The arterial blood which has a partial pressure of O_2, $ParO_2$, flows into the first vascular compartment 1, which has a blood volume of Vbcm1. O_2 in blood is present in two forms: (1) dissolved in plasma and (2) reversibly combined with hemoglobin molecules forming oxyhemoglobin (O_2Hb). Oxygen continuously diffuses into the tissue compartment 1 as oxygen is being utilized by the tissue to meet metabolic demand (MRO_{2cm1}), causing tissue PO_2 to be lower than that of the PO_2 in the blood. It is assumed that O_2 diffuses from the vascular subcompartment 1 to the extravascular subcompartment 1 of the tissues at a rate O_2flux_{cm1} which is based on the oxygen diffusion coefficient $Db_{cm1}O_2$ and O_2 pressure gradients between the blood and tissue. This phenomenon establishes O_2 concentrations of $C_{cm1}O_2$ and $C_{cmv1}O_2$ in the first tissue and blood subcompartments, respectively. In all tissue compartments O_2 bound to myoglobin is considered in addition to the prevailing O_2

concentrations. The tissue compartment 1 which has a volume V_{cm1} is assumed to be perfused by small arterioles and small venules, as well as by capillaries (Figure 3.5). The permeability surface area product for O_2 in this tissue compartment is $PS_{cm1}O_2$. The oxygen tension prevailing in the blood exiting from compartment 1, $P_{cmv1}O_2$, is the source for the O_2 supply to the second blood compartment 2 which has a blood volume Vb_{cm2}. There is diffusion of O_2 from the blood compartment 2 to the tissue subcompartment 2 at rate of O2fluxcm2 with the diffusion coefficient being $Db_{cm2}O_2$. The metabolic demand of O_2 (MRO_{2cm2}), of this tissue compartment is met by diffusion of oxygen from the vascular compartment 2 and also by diffusion from the tissue compartment 1 with a diffusion coefficient of $D_{cm}O_2$. Approximately 15% of the metabolic rate of the tissue compartment 2 is met by diffusion of O_2 from its neighboring tissue compartment 1. The tissue compartment 2, which has a volume V_{cm2}, is perfused mostly by capillaries (Figure 3.5) and has a permeability surface area product of $PS_{cm2}O_2$. Diffusion of O_2 establishes O_2 concentrations of $C_{cm2}O_2$ and $C_{cmv2}O_2$ in the second tissue and blood subcompartments, respectively. Now the oxygen tension of blood exiting from the vascular subcompartment 2, $P_{cmv2}O_2$ is the O_2 source for the vascular compartment 3 which has a blood volume of Vb_{cm3}. Based on the pressure gradients established between tissue compartment 1 and the third blood compartment 3, there is flow of O_2 at a rate of O_2flux_{cm3} from the tissue compartment 1 into the blood compartment 3, resulting in an O_2 concentration of $C_{cmv3}O_2$ in the third blood subcompartment. The O_2 diffuses with a coefficient of $Db_{vcm1}O_2$. However, when the tissue PO_2 is lower than the PO_2 in the third blood compartment then O_2flux_{cm3} is positive, indicating that O_2 diffuses from the third blood compartment to the tissue compartment 1. Because O_2 diffusivity is similar in plasma and muscle tissue (77), the model assumes that O_2 diffusion coefficients from blood to tissue or vice versa are equal. The concept of the two compartment model was introduced to allow diffusion of oxygen within the tissue and also to implement indirect arterio-venous shunting. Description of cardiac variables are summarized in Table 3.3.

3.3.1 Mass Balance Equation of the Cardiac Vascular Blood Compartments:

The equations below are the mass balance equations for the three vascular blood compartments,

Cardiac vascular blood compartment 1:

Mass balance equations for O_2
$$V_{cm1}\frac{dC_{cmv1}O_2(t)}{dt} = [C_{ar}O_2(t) - C_{cmv1}O_2(t)]Q_{cm}^{\cdot} - O_2Flux_{cm1}(t)$$
$$O_2Flux_{cm1}(t) = G_{sf}\,(Paa_{cm}O_2)\cdot\left[Db_{cm1}O_2\cdot\left(Paa_{cm}O_2(t) - P_{cm1}O_2(t)\right)\right]$$
$$Db_{cm1}O_2 = \frac{PS_{cmav} * SO_2 * V_{cm1}}{1.04}$$
Mass balance equations for *CO*
$$V_{cm1}\frac{dC_{cmv1}CO(t)}{dt} = [C_{ar}CO(t) - C_{cmv1}CO(t)].Q_{cm}^{\cdot} - COFlux_{cm1}(t)$$
$$COFlux_{cm1}(t) = \left[Db_{cm1}CO\cdot\left(P_{bcm1}CO(t) - P_{cm1}CO(t)\right)\right]$$
$$P_{bcm1}CO(t) = 0.5(\mathrm{ParCO} + \mathrm{Pcmv1CO})$$
$$Db_{cm1}CO = \mathrm{D_MCO_1}.\left(\frac{\mathrm{Dbcm_1O_2}}{\mathrm{Db_{M1}O_2}}\right)$$
$$\mathrm{D_MCO_1} = D_M CO.\left(\frac{\mathrm{Db_{M\,1}O_2}}{\mathrm{Db_{M\,2}O_2}}\right)$$

where, Paa_{cm} is the partial pressure of O_2 corresponding to the concentration of oxygen halfway between the arterial (inlet) and vascular subcompartment 1 (outlet). P_{aacm} is determined by an algorithm using a gradient search technique, where the average O_2 concentration is calculated and then the PO_2 corresponding to the average O_2 concentration is determined using the oxyhemoglobin saturation curve. $P_{bcm1,}$ is the average partial pressure of *CO* in the blood vascular subcompartment 1. $Db_{cm1}CO$ is the blood to tissue *CO* diffusion coefficient, D_MCO_1 is the blood to muscle diffusion coefficient of *CO* in blood compartment 1 and $Dbcm_1O2$ is the blood to tissue oxygen diffusion coefficients of cardiac blood compartment 1. $Db_{M1}O2$, $Db_{M2}O2$ and D_MCO are blood to tissue O_2 and *CO* diffusion coefficients of muscle blood compartments described in Section 3.2. All other variables are defined

in Table 3.3.

Cardiac vascular blood compartment 2:

Mass balance equations for O_2
$V_{cm2}\frac{dC_{cmv2}O_2(t)}{dt} = [C_{cmv1}O_2(t) - C_{cmv2}O_2(t)].\dot{Q}_{cm} - O_2Flux_{cm2}(t)$
$O_2Flux_{cm2}(t) = G_{sf}(Pbb_{cm}O_2)\cdot[Db_{cm2}O_2\cdot(Pbb_{cm}O_2(t) - P_{cm2}O_2(t))]$
$Db_{cm2}O_2 = \frac{PS_{cmcap} * SO_2 * V_{cm2}}{1.04}$
Mass balance equations for *CO*
$V_{cm2}\frac{dC_{cmv2}CO(t)}{dt} = [C_{cmv1}CO(t) - C_{cmv2}CO(t)].Q_{cm} - COFlux_{cm2}(t)$
$COFlux_{cm2}(t) = [Db_{cm2}CO\cdot(P_{bcm2}CO(t) - P_{cm2}CO(t))]$
$P_{bcm2}CO(t) = 0.5(\mathrm{Pcmv1CO} + \mathrm{Pcmv2CO})$
$Db_{cm2}CO = \mathrm{D_MCO} * (\mathrm{Dbcm2O2}/\mathrm{Db_{M2}O_2})$

Where Pb_{bcm} is the partial pressure of O_2 corresponding to the concentration of oxygen halfway between the inlet ($\mathrm{P_{cmv1}}O_2$) and outlet ($P_{\mathrm{cmv2}}O_2$) of vascular subcompartment 2. $D_{\mathrm{bcm2}}O_2$ is the blood to tissue diffusion coefficient. P_{bcm2} is the average partial pressures of *CO* in the blood vascular subcompartment 2. $Db_{\mathrm{cm2}}CO$ is the blood to tissue diffusion coefficient, $\mathrm{D_M}$CO is the blood to muscle diffusion coefficient of *CO* in blood compartment 2 and $\mathrm{Dbcm2O_2}$ and $\mathrm{Dbm2O_2}$ are blood to tissue oxygen diffusion coefficients of cardiac and muscle blood compartment 2. All other variables are define in Table 3.3

Cardiac vascular blood compartment 3:

Mass balance equations for O_2
$V_{cm1}\frac{dC_{cmv3}O_2(t)}{dt} = [C_{cmv2}O_2(t) - C_{cmv3}O_2(t)].\dot{Q}_{cm} - O_2Flux_{cm3}(t)$

$$O_2Flux_{cm3}(t) = G_{sf}\,(Pcc_{cm}O_2)\cdot\left[Db_{vcm1}O_2\cdot\left(Pcc_{cm}O_2(t) - P_{cm1}O_2(t)\right)\right]$$

$$Db_{vcm1}O_2 = Db_{cm1}O_2 * D_{bvcm\_on}$$

Mass balance equations for CO

$$V_{cm1}\frac{dC_{cmv3}CO(t)}{dt} = [C_{cmv2}CO(t) - C_{cmv3}CO(t)]\dot{Q}_{cm} - COFlux_{cm3}(t)$$

$$COFlux_{cm3}(t) = \left[Db_{vcm1}CO\cdot\left(P_{bcm3}CO(t) - P_{cm1}CO(t)\right)\right]$$

$$P_{bcm2}CO(t) = 0.5(\text{Pcmv2CO} + \text{Pcmv2CO})$$

$$Db_{vcm1}CO = \text{DMCO3}.\left(\frac{\text{Dbvcm}_1\text{O2}}{\text{Dbv}_{M1}\text{O2}}\right)$$

$$\text{DMCO3} = D_M CO.\left(\frac{\text{Db}_{VM_1}\text{O2}}{\text{Db}_{M_2}\text{O2}}\right)$$

where P_{cccm} is the partial pressure of O_2 corresponding to the concentration of oxygen halfway between the inlet ($P_{cmv2}O_2$) and outlet ($P_{cmv3}O_2$) of vascular subcompartment 3. $Db_{vcm1}O_2$ is the tissue to blood diffusion coefficient, Db_{vcm_on} is the fraction of blood volume in cardiac vascular compartment 1 (Vbcm1) available for gas exchange with (venules) cardiac vascular compartment 3 (Vbcm3). P_{bcm3} is the average partial pressure of CO in the blood vascular subcompartment 3. $Db_{vcm1}CO$ is the blood to tissue diffusion coefficient. Dbvcm1O2 is the blood to tissue oxygen diffusion coefficient of cardiac blood compartment 3. $Dbv_{M1}O2$, $Db_{M2}O2$ and D_MCO_3 are blood to tissue O_2 and CO diffusion coefficients of muscle blood compartments described in Section 3.2. All other variables are defined in Table 3.3

The O_2 concentration at the input to the mixed venous compartment is determined by a flow-weighted summation of the concentrations of O_2 in the venous outflow from the tissue compartments. This input concentration then passes through the mixed venous compartment and returns to the lungs after a time delay. Thus the O_2 concentration at the input to the mixed venous compartment is

$$C_VO_2(t) = [C_{vot}\,O_2(t).(\frac{\dot{Q}_{ot}}{\dot{Q}})] + [C_{vm}O_2(t).(\frac{\dot{Q}_m}{\dot{Q}})] + [C_{vcm}O_2(t).(\frac{\dot{Q}_{cm}}{\dot{Q}})].$$

Where,

$C_{vot}O_2(t), C_mO_2(t), C_{cm}O_2(t)$ are the O_2 concentrations in the non-muscle, skeletal muscle, and cardiac muscle tissues, respectively. $Q_{ot}^{\cdot}, Q_m^{\cdot}, Q_{cm}^{\cdot}$ are the blood flows to the non-muscle, skeletal muscle, and cardiac muscle tissue compartments, respectively.

3.3.2 Mass balance equation of the cardiac tissue subcompartments :

First cardiac tissue subcompartment:

The mass balance equation for O_2 in the first tissue subcompartment is

$$\frac{dC_{cm1}O_2(t)}{dt} = \frac{Flux_{cm1}O_2(t)}{V_{cm1}} + \frac{D_{cm}O_2\left[C_{cm2}O_2(t) - C_{cm1}O_2(t)\right]}{D_{xcm}}$$

where $Flux_{cm1}O_2(t)$ is defined as

$$Flux_{cm1}O_2(t) = O_2Flux_{cm1}(t) + O_2Flux_{cm3}(t) - MRO_{2\,cm1}$$

$C_{cm1}O_2(t), C_{cm2}O_2(t)$ are the total O_2 concentrations in the first and second tissue compartments, $Pb_{cm1}O_2(t)$ and $Pb_{cm2}O_2(t)$ are the partial pressures of O_2 of the two tissue subcompartments. O_2Flux_{cm1} *and* O_2Flux_{cm3} are the blood O_2 fluxes of subcompartments 1 and 3 defined in Section 3.3. MRO_{2cm1} is the metabolic rate of O_2 in the tissue compartment 1.

The mass balance equation for *CO* in the first tissue subcompartment is

$$\frac{dC_{cm1}CO(t)}{dt} = \frac{Flux_{cm1}CO(t)}{V_{cm1}} + \frac{D_{cm}CO\left[C_{cm2}CO(t) - C_{cm1}CO(t)\right]}{D_{xcm}}$$

where $Flux_{cm1}CO(t)$ is defined as

$$Flux_{cm1}CO(t) = COFlux_{cm1}(t) + COFlux_{cm3}(t)$$

$C_{cm1}CO\ (t), C_{cm2}CO(t)$ are the *CO* concentrations in the first and second tissue compartments. $CO\,Flux_{cm1}$ *and* $CO\,Flux_{cm3}$ are the rates of *CO* fluxes of the blood subcompartments 1 and 3.

Second cardiac tissue subcompartment:

$$\frac{dC_{cm2}O_2(t)}{dt} = \frac{Flux_{cm2}O_2(t)}{V_{cm2}} - \frac{D_{cm}O_2.V_{cm1}.[C_{cm2}O_2(t) - C_{cm1}O_2(t)]}{V_{cm2}.D_{xcm}}$$

where $Flux_{cm2}O_2(t)$ is defined as

$$Flux_{cm2}O_2(t) = O_2Flux_{cm2}(t) - MRO_{2\,cm2}$$

$C_{cm1}O_2(t), C_{cm2}O_2(t)$ are the O_2 concentrations in the first and second tissue compartments, $Pb_{cm1}O_2(t)$ and $Pb_{cm2}O_2(t)$ are the partial pressures of O_2 of the two tissue subcompartments. O_2Flux_{cm2} is the blood O_2 flux of subcompartment 2 defined in Section 3.3. MRO_{2cm2} is the metabolic rate of O_2 in the tissue compartment 2.

$$\frac{dC_{cm2}CO(t)}{dt} = \frac{Flux_{cm2}CO(t)}{V_{cm2}} - \frac{D_{cm}CO.V_{cm1}.[C_{cm2}CO(t) - C_{cm1}CO(t)]}{V_{cm2}.D_{xcm}}$$

where $Flux_{cm2}CO(t)$ is defined as

$$Flux_{cm2}CO(t) = COFlux_{cm2}(t)$$

$C_{cm1}CO\ (t)$ and $C_{cm2}CO(t)$ are the CO concentrations in the first and second tissue compartments. $CO\,Flux_{cm2}$ is the CO flux of the blood subcompartment 2.

3.4 Parameters for the Model

Estimating parameters for a model is a crucial task. The heart muscle is similar to exercising skeletal muscle. Constant exercise results in the heart muscle parameters being different from the skeletal muscle. There are marked regional variations in flow and oxygen consumption (Table 2.1, Table 2.2). Blood flow, oxygen consumption and capillary density of per unit mass are greater in cardiac muscle than in resting skeletal muscle. Capillary density/gm is ~8 times greater in cardiac muscle than in skeletal muscle (39). Higher capillary density promotes efficient O_2 transport from blood to tissues and also within the tissue. Because blood flow and O_2 consumption increase with workload and as the heart is a vigorously working blood pump, it has a higher blood flow and a vasculature designed for efficient O_2 delivery to match the O_2 demand. There is parameter heterogeneity (blood flow, oxygen consumption, regional tissue oxygen tension, capillary density) within the various regions of the heart, the

epicardium, myocardium and endocardium (Table 2.5, 73, 74, 75). Also, the chambers of the heart (right atrium, left atrium, left ventricle and right ventricle) and the septa separating them have varied blood flow and oxygen consumption (Table 2.1,Table 2.2).The weight of the heart varies with age, gender and ethnicity of the subject (76). Keeping in mind the inhomogeneity of heart muscle, parameters were estimated from the available literature.

Nominal values for most of the parameters were obtained from the literature or directly from the investigators whose data we simulated e. g., total body metabolic rate, heart rate, cardiac output etc. In some cases parameters were estimated with average values from a group of subjects or published predictive formulas in literature e.g., volume of heart, blood volume, myocardial myoglobin concentration etc. Parameter values were also estimated from predictive formulas described previously in this thesis, e. g., myocardial O_2 consumption, myocardial blood flow etc. There are parameters like the permeability surface area product of the compartments, which have a value at resting conditions but linearly increase in proportion to the blood flow (90). There are some parameters like cardiac muscle volume fraction (Fvcm) and fraction (Dbvcm_on) of blood volume in the cardiac vascular compartment 1 (Vbcm1) available for gas exchange with (venules) cardiac vascular compartment 3 (Vbcm3) that represent quantities that are very difficult, or even impossible to measure. Values of such parameters are unknown and estimates are made for these values based on physiology. Parameters in this model are classified based on their estimation method:

1. Physiological parameters
2. Model-derived parameters
3. Simulation parameters

3.4.1 Physiological parameters

These parameters are constants whose values can be found from the literature or from experimental measurements available. Some physiological parameters are body weight (BW), solubility of O_2 in plasma (SO_2), blood flows to a specific compartment, etc. Most of these parameters are estimated by taking an average of

several published values like myoglobin concentration (Table 3.4), values present in literature like the volume of heart, fraction of blood etc or are directly obtained from the experimental database to be simulated. The physiological parameters are listed in Table 3.5

3.4.2 Model-derived parameters

These are the parameters whose values are estimated in the model from predictive equations, e.g., myocardial blood flow, myocardial O_2 consumption etc or from formulas like the diffusion coefficients for O_2 and CO or volumes of tissue compartments. The model-derived parameters are listed in Table 3.6

3.4.3 Simulation parameters

These parameters are intermediate values of the model which help to establish the simulation conditions. These parameters are used in accessory equations that are needed for evaluating the derivative functions for numerical integration; aid in simulating experimental conditions (e, g., TW, TZSS etc.). Simulation parameters specific to *ACSL* are the time step (*CINT*) of the algorithm, the integration algorithm used (*IALG*), TMAX etc**.** Simulation parameters are listed in the Table 3.7

3.5 Predictive Equations in the Model

Prediction equations for estimating model parameters were implemented into the model either from the literature (published journals) or were developed especially for the thesis. The following prediction equation for estimating blood volume in humans was reported in reference 78. Thus the prediction equation for estimating blood volume (when its value is not available) was added into the model:

$$\text{Volume of blood} = \frac{70}{\sqrt{BMI\_p/22(HT)^2}} \quad (78)$$

$$\text{BMI} = \frac{bw}{(HT)^2}$$

$$\text{delta\_IBW} = \left(\frac{BMI}{22}\right)100$$

$$\text{BMI\_p} = \left(\frac{delta\_IBW}{100} \right) 22 + 22 ,$$

where BMI is the body mass index, bw is the body weight and HT is the height of the subject.

Estimation equations were developed for myocardial oxygen consumption and myocardial blood flow as functions of heart rate, and for cardiac output and heart rate as functions of total body metabolic rate. Data to establish values for parameters of these equations were collected from various papers in the literature. Linear or nonlinear regression was performed on data (different model/order of equations were checked) and statistical significance of the equations was tested using SYSTAT 9.0 after outliers were eliminated. The resulting equation was validated with data which was not used in the regression. Then the equation was implemented into the model. The following prediction equations were developed as part of this thesis to estimate values for unknown parameters of the model.

3.5.1 Prediction Equations for Myocardial Oxygen Consumption and Blood Flow

Myocardial oxygen supply and oxygen demand balance are very important for the tissue to be viable. Data from various published papers (80-86) of myocardial oxygen consumption and myocardial blood flow were tabulated. The strategy followed for developing the prediction equation is shown in Figure 3.6. The data used to develop the prediction equation had values obtained during rest and exercise conditions. Most of the blood flow data for humans was from studies that used the nitrous oxide dilution method. But the nitrous oxide method is reported to have certain limitations (87) which tend to under-estimate the true blood flow; values based on this method resulted in oxygen supply and demand mismatch when implemented into the model. Thus, to predict the myocardial blood flows, data from a published experiment (79) was used to derive the predictive formulas. The steps described below were followed to establish the relations.

1. Constructed regression relation for myocardial blood flow as a function of heart rate. Data for regression relation was obtained from the reference 79. Myocardial blood flow in their study was measured by dynamic PET (Positron Emission Tomograph) accompanied by intravenous injection of labeled water ([^{15}O]H2O). Data used for deriving the relation and its fitted equation using linear regression is shown in Figure 3.7
2. The next step was to correct the myocardial oxygen consumption data which was calculated using FICK's method, where oxygen consumption is measured as a product of myocardial blood flow and Arterio –Venous oxygen differences. Myocardial oxygen consumption data had to be corrected as the papers from which (80-86) myocardial oxygen consumption data was available used blood flow measurements based on the nitrous oxide method to calculate oxygen consumption. The approach taken for correcting the myocardial oxygen consumption is as follows:

   (i) A-V difference was calculated as ratio of myocardial oxygen consumption and myocardial blood flow values obtained from studies using the nitrous oxide method.

   (ii) Corrected myocardial oxygen consumption = Product of blood flow calculated for heart rates in the nitrous oxide papers using regression relation developed in step 1 and A-V differences (calculated in step 2(i)).
3. After the myocardial oxygen consumption values were corrected for the differences in the methods, a non-linear curve fit was done using MATLAB to establish myocardial oxygen consumption as a function of heart rate. Data used to derive the relation and its fitted equation using nonlinear regression is shown in Figure 3.8 .The relation obtained is as follows:

$$\text{Myocardial Oxygen Consumption} = \frac{a-d}{1+(c/HR)^b} + d$$

where,

HR= heart rate,

a= 56.3217, asymptotic maximum,

b= 4.8485, defines the slope of the function,

c= 122.6617, *c* is the value of the independent variable *x* at the inflection point.

d= 9.7643, asymptotic minimum.

Thus, to determine the myocardial oxygen consumption (ml/min/100gm) and myocardial blood flow (ml/min/100gm), the following predictive formulas were developed:

$$\text{Myocardial Blood Flow } (\dot{Q}cm) = 2.18 * (HR) - 27.3$$

$$\text{Myocardial Oxygen Consumption (MRO2cm)} = \frac{56.3217 - 9.7643}{1 + (122.6617/HR)^{4.8485}} + 9.7643$$

3.5.2 Prediction Equations for Cardiac Output

Cardiac output (Q.) was previously estimated as a function of body weight and gender. This equation could be used only during conditions of basal rest. Since we wanted to simulate experimental conditions of exercise where the cardiac output increases, we developed equations to predict cardiac output as a function of total body oxygen consumption (MRO_2). Cardiac output and total body oxygen consumption values were collected from various papers in the literature (See the appendix.). The data were obtained at rest and various loads of exercise. The tabulated aggregated data were fit with a 2nd-order polynomial as shown in the appendix. Thus the equation developed is

$$\dot{Q} = 3.186 + 7.346 \times MRO_2 - 0.535 \times (MRO_2)^2$$

3.5.3 Prediction Equations for Heart Rate

Often for the experiments we simulated, the investigators provided heart rates of the subjects at rest. In simulation cases where heart rate data were not provided we estimated the heart rate as function of total body oxygen consumption from the equation below. The procedure for developing the equation is detailed in the appendix. The heart rate parameter is used for estimating the myocardial oxygen

consumption and myocardial blood flow which is discussed in Section 3.5.1 of this chapter.

$$\text{Heart Rate } (HR) = 42.819+68.884*(MRO_2)-8.26* (MRO_2)^2$$

Predicting percent increase in the heart rate (HR) as a function of percent change of carboxyhemoglobin (% ΔCOHb) levels in blood: There is reported to be an increase in cardiac output and heart rate with increases in carboxyhemoglobin levels in blood (68,69,70). While simulating experiments involving carbon monoxide (*CO*) exposures, increased heart rate due to increased carboxyhemoglobin levels in the blood had to be taken into account. These increases were implemented by introducing the following equation whose derivation is discussed in the appendix.

$$\%\Delta HR = 0.012(\%\Delta COHb)^2 + 0.26(\%\Delta COHb)$$

The heart rate (HR) was increased by $\%\Delta HR$ respectively, calculated from the above equations every 0.001 min of simulated time.

3.6 Sensitivity Analysis:

Sensitivity analysis is used to determine how "sensitive" a model is to changes in the value of the parameters of the model and to changes in the structure of the model. It surveys how a given model output depends upon its parameter values. It is an important method for checking the quality, robustness and reliability of analyses and for building confidence in the model by studying the uncertainties that are often associated with parameters in models. It helps to determine the level of accuracy needed for a parameter to make the model sufficiently useful and valid. The process involves varying model parameters (one at a time, keeping other parameters constant) over a reasonable range (especially when there is an uncertainty in values of the varied parameter) and observing the relative changes in model response. If the testing process reveals that the parameter varied has no significant effects on the model response, then it may be possible to use an estimate rather than a value with greater accuracy. But if the system behavior greatly changes with the varied parameter then an accurate value should be determined for that parameter. If the value of the

sensitive parameter is unknown in from the literature, then doing sensitivity analysis helps to estimate deviations in model predictions with the parameter variation. Thus sensitivity analysis was done to analyze the effect of model parameters on the model predictions of myocardial tissue PO_2 and coronary venous PO_2. It was found that the predicted myocardial tissue PO_2 and coronary venous PO_2 are most sensitive to variations in the myocardial blood flow ($\dot{Q}_{cm}$), myocardial oxygen consumption ($MRO2_{cm}$), permeability surface area product (PScm), and volume distribution fraction of the tissue (FVcm). Table 3.9 shows the values of predicted myocardial tissue PO_2 and coronary venous PO_2 with variations in the input parameters. In this table myocardial O_2 consumption (MRO_2cm), myocardial blood flow ($\dot{Q}cm$), PS product (Pscm), AV Shunt fraction (Dbvcm_on), volume distribution (Fvcm) and, inter capillary distance (Dxcm) were increased (and decreased) by 50% and the response of the model predictions - i.e. tissue and blood oxygen tensions - to variation of these parameters was tabulated (Table 3.8).

After doing the sensitivity analysis, a standard set of values for the following parameters (PScm, Fvcm,Dbvcm_on, Dxcm), whose values were difficult to estimate (due to unavailability of data) was determined. The values for these parameters are shown in table 3.7. This standard set of parameters was arrived at after analyzing the coronary physiology, vasculature density in myocardium and other experimental facts such as the extent of hypoxia, exercise or CO exposure which did not cause permanent injury or death of the subject. The volume of the cardiac compartment (Vcm) is divided into two subcompartments of volume Vcm1 and Vcm2 by means of the cardiac muscle volume fraction (Fvcm). The value for Fvcm was estimated to be 0.2 in order to make best estimates for tissue PO_2. The permeability surface area product of O2 for cardiac muscle model was reported to be 200 ml/min/Torr/gm by Beard and Bassinghwaite (90). When the above reported value for permeability surface area product was used, final model predicted myocardial tissue P*O2*'s were very low. The best estimates for tissue *PO2* predictions were obtained when the PS for the first and second cardiac subcompartments were 180 ml/min/Torr/gm and 450 ml/min/Torr/gm, respectively. There is reported to be capillary recruitment during

exercise in skeletal muscle (102). However, the extent of capillary recruitment in myocardium during exercise is unknown. Increase in capillary recruitment would increase the PS as the surface area available for oxygenation would increase. PS is reported to increase with blood flow (90), thus in the final model PS increases with increases in blood flow. The intercapillary distance in skeletal muscle in the modified model is 0.1 cm. The capillary density in cardiac muscle is approximately 8 times greater than that of the skeletal muscle (39), thus the intercapillary distance for cardiac compartment in the final model is 0.0353 cm ($0.1/\sqrt{8}$). Fraction (Dbvcm_on) of blood volume in cardiac vascular compartment 1 (Vbcm1) available for gas exchange with (venules) cardiac vascular compartment 3 (Vbcm3) was estimated by analyzing the coronary vasculature (103,104). Also from the sensitivity analysis, it can be seen that Dbvcm_on does not have a significant impact on the model predictions of myocardial tissue PO_2 and coronary venous PO_2. A value of 9.5% was chosen for Dbvcm_on as better estimates for coronary venous PO_2 and myocardial tissue PO_2 were obtained for that value.

3.7 Validation Schema for the Cardiac Compartment

The final model (Figure 3.4) was used for the simulations to test the validity of the predicted O_2 related variables of the cardiac compartment. Predictions from the model were compared with published observations on human subjects and animal data. The model was tested for conditions of normoxic rest (91,92,95,99,100), hypoxic rest (91,92,93,98), hypoxic exercise (91) and hyperoxia (93,94,96,97,98) with regard to its predictions of coronary venous PO_2 and tissue PO_2. For validation of human data, subject morphological data like body weight, age, etc., were used

The protocol for validation of the model was as follows:

1. Inspired levels of O_2 were set equal to the experimental values. Ventilation was adjusted to achieve the measured arterial PO_2 in the steady state.
2. Experimentally measured values for myocardial O_2 consumption and myocardial blood flow were used in the simulations.
3. Each simulation was allowed a stabilization time of 12 min (simulation time) and the model predictions were noted after reaching steady state.

4. The model predictions of cardiac oxygen tensions and coronary venous PO_2's for various conditions were compared to experimental data
5. Usually, experimental tissue PO_2 values were available as either mean values or as histograms. When a mean value was published, based on the size of the electrode used to measure PO_2, it was either classified as the average first compartment (large electrode, assuming it was close to an arteriole) or second compartment PO_2. In the case of histograms, the mean value was used to represent the average tissue PO_2. An average of the PO_2 in the histogram above the mean was considered as the first compartment oxygen tension and an average of the PO_2 in the histogram below the mean represented the second compartment oxygen tension.
6. Other variables validated were arterial hemoglobin saturations, venous hemoglobin saturations and capillary PO_2. But very scarce experimental data were available for validation of these variables.

The figures showing the validation of model predicted values to the experimental measured values for oxygen tension and coronary venous PO2 are shown in Figures 4.1- 4.3. It can be seen from the figures that the model is fairly capable of predicting the experimental values using a standard parameter set. This set shall be used for simulating various experimental strategies in the Results Section. For a human subject weighing 70 kg, 1.75 m tall and 30 years old, the predicted steady state cardiac tissue and blood oxygen tensions during normoxia (arterial PO_2 = 99 Torr) are tabulated in Table 3.10

3.8 Algorithms

In order to determine the partial pressure of oxygen (PO_2), partial pressure of carbon monoxide (P*CO*) and O_2 flux in each blood compartment of the model, it is necessary to solve three simultaneous algebraic equations

1. Oxyhemoglobin dissociation curve (Section 2.2, chapter 2).
2. Haldane's equation (Section 2.2, chapter 2).
3. Blood to Tissue oxygen flux equations (Section 3.1.2, chapter 3).

The solutions for these equations were obtained by using algorithms based on gradient search methods which were developed for the modified model. An additional algorithm is also developed (bisection halving) to determine the PO_2 corresponding to the average O_2 concentration in the blood compartment. The technique used is a closed domain bracketing method and the root is trapped in the interval using interval halving (bisection) method. In this algorithm, two estimates for the root (x= PO_2) are passed as arguments, which are generally the inlet (PO_2max) and outlet (PO_2min) variables (blood O_2 tension, tissue O_2 tension, total concentration of O_2, volume of blood or the tissue etc) of the blood vascular subcompartments. Now the root, x= PO_2 lies in the interval (PO_2max , PO_2min). The interval is systematically reduced based on the evaluate function decision and the error criterion, €. The algorithm for the search technique is shown in Figure 3.9.

Table 3.1: *Prediction Equation for Estimating Volumes of Muscular Regions (Arms, Legs and Trunk) for Males and Females*

Region	Volume in Men	Volume in Women
Leg	(46.63* V_m)/100	(49.53* V_m)/100
Arm	(15.64* V_m)/100	(13.96* V_m)/100
Trunk	(37.73* V_m)/100	(36.51* V_m)/100

Table 3.2: *Blood flow and Oxygen Consumption Values for Muscular Regions*

Muscular Region	Blood Flow (ml/min/g)	Oxygen consumption (ml/min/g)
Arm	0.021	0.0014
Leg	0.03	0.002
Trunk	0.03	0.002

Table 3.3 : Cardiac Compartment Variables and Description

Parameter	Description
$Q_{cm}^{\cdot}$	Blood flow to the myocardium
SO_2	Solubility of oxygen in plasma
$D_{cm}O_2$	Diffusion coefficient of O_2 between the two tissue subcompartments
D_{xcm}	Intercapillary distance
$D_{cm}CO$	Diffusion coefficient of CO between the two tissue subcompartments
Blood Subcompartment 1	
$C_{cmv1}O_2$	Concentration of O_2 in the blood compartment 1
$C_{ar}O_2$	O_2 concentration of arterial blood entering the blood compartment 1
O_2Flux_{cm1}	Rate of O_2 diffusion out of the blood compartment 1
$PScm_{av}$	Permeability surface area product for arterioles and venules
$Db_{cm1}O_2$	Blood to tissue diffusion coefficient
V_{cm1}	Volume of the cardiac tissue compartment 1
$C_{cmv1}CO$	Concentration of CO in the blood compartment
$C_{ar}CO$	CO concentration of arterial blood entering the blood compartment 1
$COFlux_{cm1}$	Rate of CO diffusion out of the blood compartment 1
ParCO	Partial pressures of CO in the arterial blood compartment
Pcmv1CO	Partial pressures of CO in the blood vascular subcompartment 1
Blood Subcompartment 2	
V_{cm2}	Volume of the cardiac tissue compartment 2
$C_{cmv2}O_2$	Concentration of O_2 in the blood compartment 2
O_2Flux_{cm2}	Rate of O_2 diffusion out of the blood compartment 2
$PScap$	Permeability surface area product of capillaries

Table 3.3: Cardiac Compartment Variables and Description (Continued)	
Parameter	**Description**
$C_{cmv2}CO$	Concentration of *CO* in the blood compartment 2
$COFlux_{cm2}$	Rate of *CO* diffusion out of the blood compartment 2
Pcmv2CO	Partial pressures of C*O* in the blood vascular subcompartment 2
Blood Subcompartment 3	
$C_{cmv3}O_2$	Concentration of O_2 in the blood compartment 3
O_2Flux_{cm3}	Rate of O_2 diffusion into the blood compartment 2
$C_{cmv3}CO$	Concentration of *CO* in the blood compartment 3
$COFlux_{cm3}$	Rate of *CO* diffusion into the blood compartment 2
Pcmv3CO	Partial pressures of C*O* in the blood vascular subcompartments 3

Table 3.4: Myoglobin Concentration of the Heart. Concentrations of myoglobin were measure by BNII nephelometer technique in various regions of the human heart. The values were reported by CJM Joost et al (Am J Clin pathol 2001:115:770-777)

Region	**Mb Value (g/gm wet wt)**
Right ventricle	1.9
Right atrium	1.0
Left ventricle	2.4
Left atrium	0.8
Left ventricle	2.4 (0.25-11.7)
Posterior wall	2.4 (0.78-4.05)
Lateral wall	2.5 (0.67-5.21)
Anterior wall	2.2 (0.38-11.7)
Septum	2.4 (0.25-3.69)

Table 3.5: Physiological Cardiac Parameters

Parameter	Description and references	Value
DBVcm_on	Fraction of blood that allows gas exchange with tissue compartment 1 (Section 3.6)	0.095
rho	Density of cardiac muscle (35)	1.04 (gm/cm^3)
KcmO2	Michales-Menton coefficient of cardiac muscle(35)	0.2
DXcm	Intercapillary distance in cardiac muscle (Section 3.6)	0.0353(cm)
PScm_cap	Permeability surface area product of O_2 for capillaries (Section 3.6)	450(ml/min/Torr/gm)
PScm_av	Permeability surface area product of O_2 for arterioles/venules (Section 3.6)	180(ml/min/Torr/gm)
ConcMgb	Concentration of myoglobin (Mb) (Table 3.4)	0.0023 (mg/g wet wt. muscle)
Vcm	Volume of heart (L Reiner, 1959)	254(M),180(F) (gm)
Vlv	Volume of left ventricle (75)	94(M), 67(F) (gm)
Vrv	Volume of right ventricle (75)	46(M), 33(F) (gm)
Va	Volume of atria (75)	49(M), 39(F) (gm)
Viv	Volume of intra ventricular septum (75)	64(M), 49(F) (gm)
Volfraccm	Distribution fraction of blood volume to the tissue (A Indermuhle,2006)	0.1161(ml/gm)
FVcm	Fraction of muscle volume in comp. around arteriole and venial blood comp.(Section 3.6)	0.2

Table 3.6: Model -Derived Parameters

Parameter	Description	Value
Vcm1	Volume of cardiac muscle in compartment 1 perfused by arterioles/venules	FVcm.Vcm
Vcm2	Volume of cardiacmuscle in compartment 2 perfused by capillaries	(1.-FVcm).Vcm
MRO2cm	Metabolic rate (MR) of O_2 of cardiac muscle tissue	Refer Section 3.5.1
MRO2_cm1	MR of O_2 of skeletal muscle tissue 1	MRO2cm.Vcm1/(Vcm1+Vcm2)
MRO2_cm1	MR of O_2 of skeletal muscle tissue 2	MRO2cm.Vcm2/(Vcm1+Vcm2)
Qdotcm	Blood flow to the cardiac muscle tissue	2.18 . (HR) – 27.3
DcmCO	Cardiac Muscle diffusion coefficient for CO	D_MCO.(Dbcm2O2/Db_MO_2)
Vbcm	Volume of blood in cardiac compartment	Volfraccm.Vcm
Vbcm1	Blood volume of cardiac blood compartment 1	(Fvcm.Vbcm) -Vbcm3
Vbcm2	Blood volume of cardiac blood compartment 2	(1.0-Fvcm).Vbcm
Vbcm3	Blood volume of cardiac blood compartment 3	Fvcm.Vbcm .Dbvcm_on
DcmO2	Inter-cardiac tissue diffusion coefficient of O_2	60.DO2.10.
DcmCO	Intercardiac tissue diffusion coefficient ofCO	fac.DcmO2
Dbcm1O2	Diffusion coefficient of O_2 from blood compartment 1 to cardiac tissue compartment 1;	PScm_av.SO2.Vtm1/rho
Dbcm2O2	Diffusion coefficient of O_2 from blood compartment 2 to cardiac tissue compartment 2;	PScm_cap.SO2.Vtm2/rho
DcmCO_1	Diffusion coefficient of O_2 from blood compartment 1 to cardiac tissue compartment 2	(Dbm1O_2/Dbm$_2O_2$).DcmCO
DcmCO_2	Diffusion coefficient of O_2 from blood compartment 2 to cardiac tissue compartment 2	DcmCO
DcmCO_3	Diffusion coefficient of O_2 from blood compartment 2 to cardiac tissue compartment 3	DMCO_3.(Dbvcm1o2/Dbvm1o2)
fac	Diffusion coefficient. for CO in tissues is 75% of O_2 diffusion coefficient	0.75

Table 3.7: Simulation Parameters

Parameter	Description	Value
PbO2wi	Atmospheric pressure during CO exposure	Simulation specific
Pbo2wo	Atmospheric pressure during treatment	Simulation specific
TW	Time by which the model reached steady state.	12 minutes
COcm0pc	Initial %CO in cardiac compartment(cpt)	Subject specific **(%)**
COcvm0pc	Initial %CO in cardiac venous cpt.	Subject specific **(%)**
Gmix_cm	O_2 mix gain of cardiac tissues	1
CINT	Time step of the integration algorithm	0.001
Tmax	Maximum time of the simulation	Simulation specific
IALG	Integration algorithm used	8(Runge kutta Fehlberg)
Tzss, Tco	Time at which CO exposure begins (or is present) in the simulation	Simulation specific
COppm	Concentration of CO in part per million	Simulation specific
VdotWI	Ventilation at the time of CO exposure	Subject specific
VdotWO	Ventilation at the time of treatment	Subject specific

Table 3.8: Sensitivity Analysis of the Parameters

Parameter	Variation	Tissue PO2_1	Tissue PO2_2	Venous PO2
O2 consumption	↑ 50%	↓	↓	↓
Mro2cm	↓ 50%	↑	↑	↑
Blood Flow	↑ 50%	↑	↑	↑
Q.cm	↓ 50%	↓	↓	↓
PS product	90	21.78	22.05	20.76
Pscm_av	270	44.7	20.98	20.74
PS product	225	37.97	12.711	20.86
Pscm_cap	675	39.38	24.47	20.73
AV Shunt fraction	0.0475	40.34	21.69	20.74
Dbvcm_on	0.1425	37.86	21.28	20.74
Volume distribution	0.1	49.52	23.25	20.74
fvcm	0.3	32.45	19.98	20.7

Table 3.9: Values for Standard Set of parameters

Parameter	Value
Pscm_av	180
Pscm_cap	450
Dbvcm_on	0.095
fvcm	0.2
Dxcm	0.0353

Table 3.10: Steady State Values in human

Parameter	Value(torr)
PCM1O2	39
PCM2O2	21.47
PCMV1O2	50.91
PCMV2O2	20.23
PCMV3O2	20.74

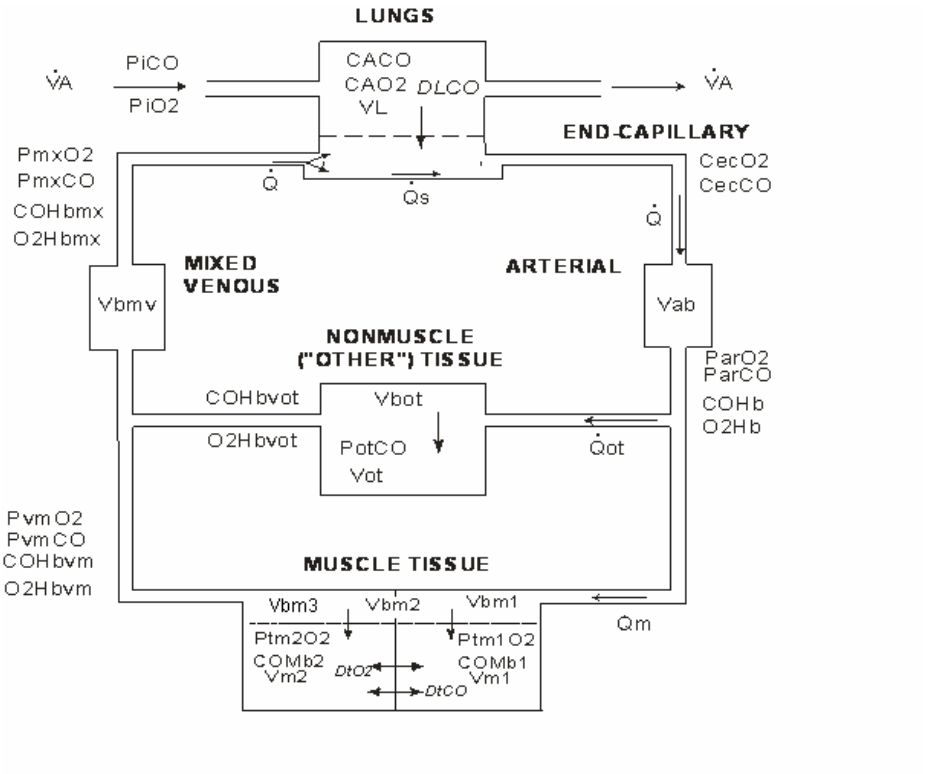

Figure 3.1: Modified Model. The model consists of lungs, arterial and mixed venous blood, non-muscle tissue and two subcompartments within the muscle tissue. (Bruce, Bruce, Erupaka)

(Figure also referred in Section 3.2)

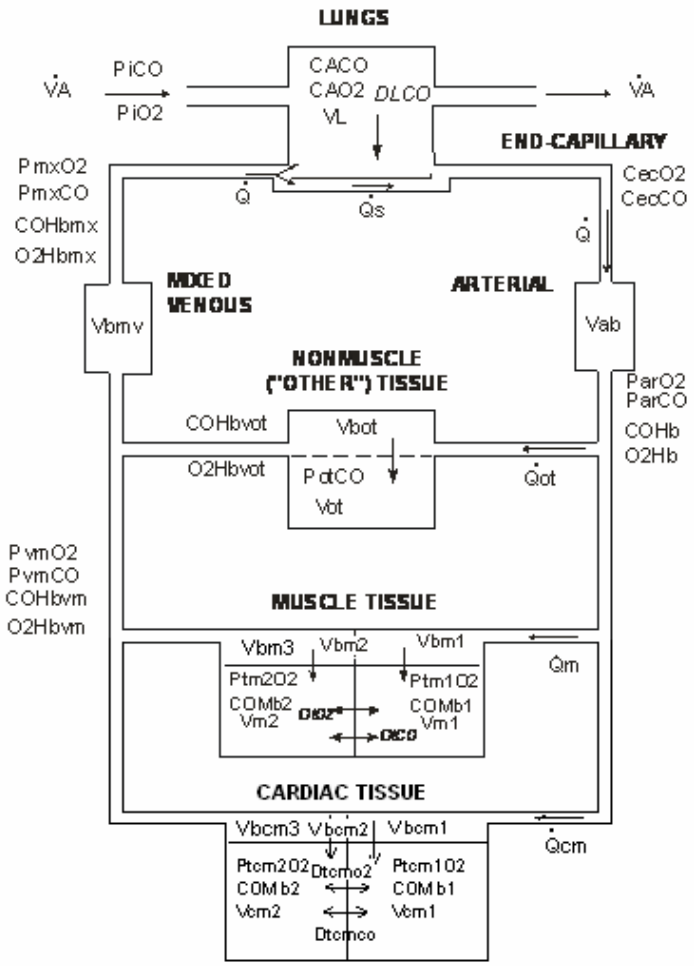

Figure 3.2: Final Model. The model consists of lungs, arterial and mixed venous blood, non-muscle tissue, two subcompartments within the muscle tissue and the cardiac compartment with two subcompartments.

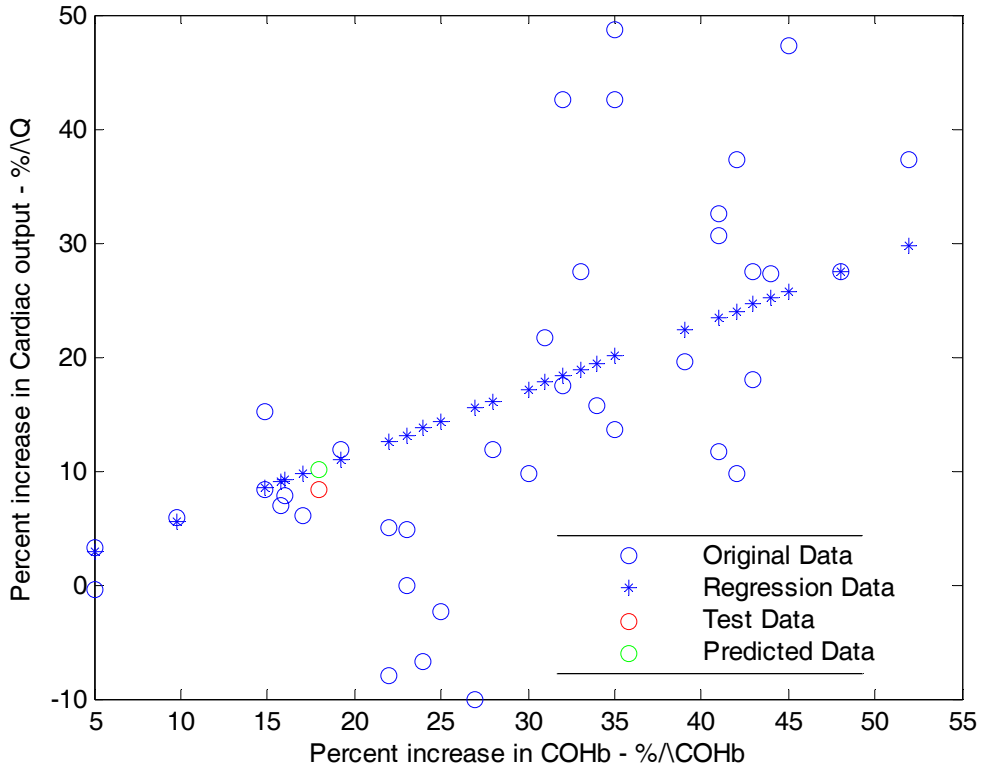

Figure 3.3: Cardiac Output and Carboxyhemoglobin. Figure shows the plot of the data (o) used (68,69,70) to build the relationship and the predicted data (*). The percent increase in carboxyhemoglobin levels of blood, %ΔCOHb is plotted on the x-axis and the percent increase in cardiac output, %ΔQ˙ on the Y-axis. Test data points (o) were considered from experiments whose data were not included in building the relation to check with the values (o) obtained from the predictor equation.

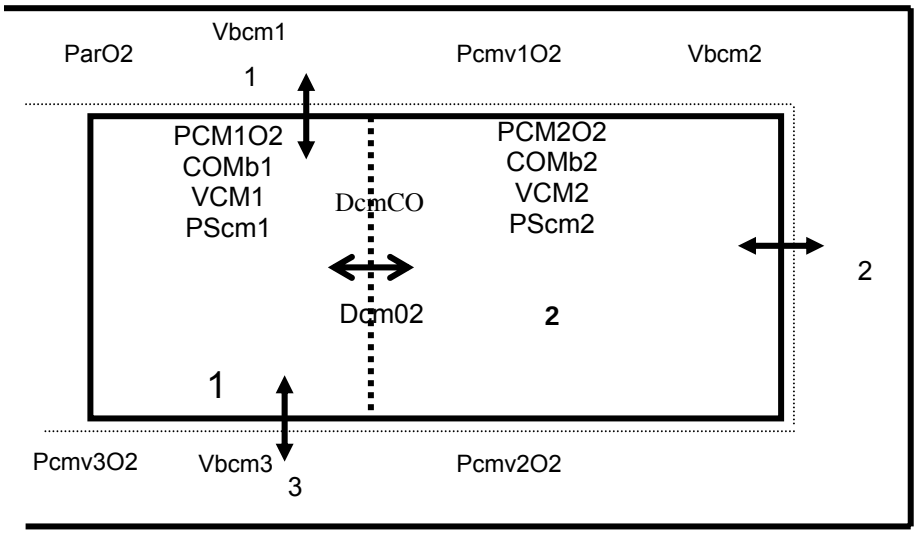

Figure 3.4 : Two Subcompartment Cardiac Tissue. *The figure shows the two cardiac tissue compartments -**1**, **2** and the three cardiac blood compartments -1, 2, and 3 surrounding the cardiac tissue.*

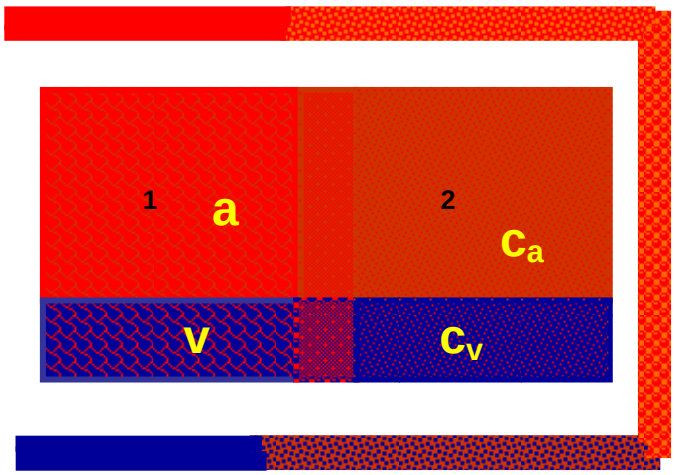

Figure 3.5: Vasculature of Cardiac Compartment. *The tissue compartment **1** is assumed to be perfused by small arterioles (a) and small venules (v), as well as by capillaries The tissue compartment 2, is perfused mostly by capillaries (Ca, Cv).*

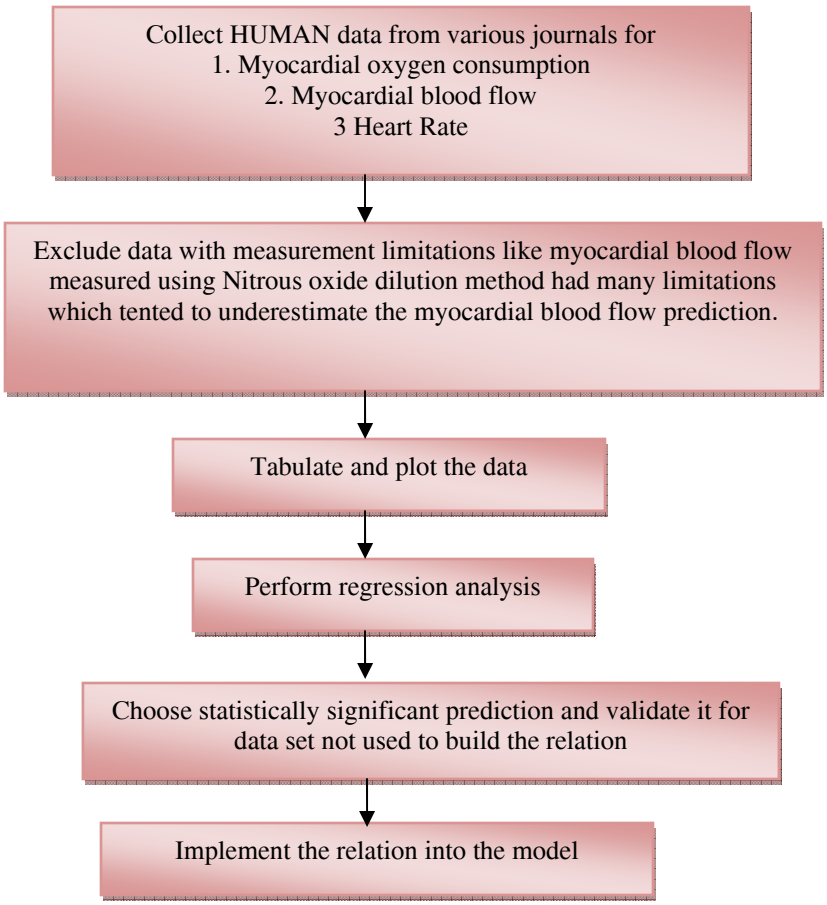

Figure 3.6: Strategy for Developing Prediction Equations for the Model

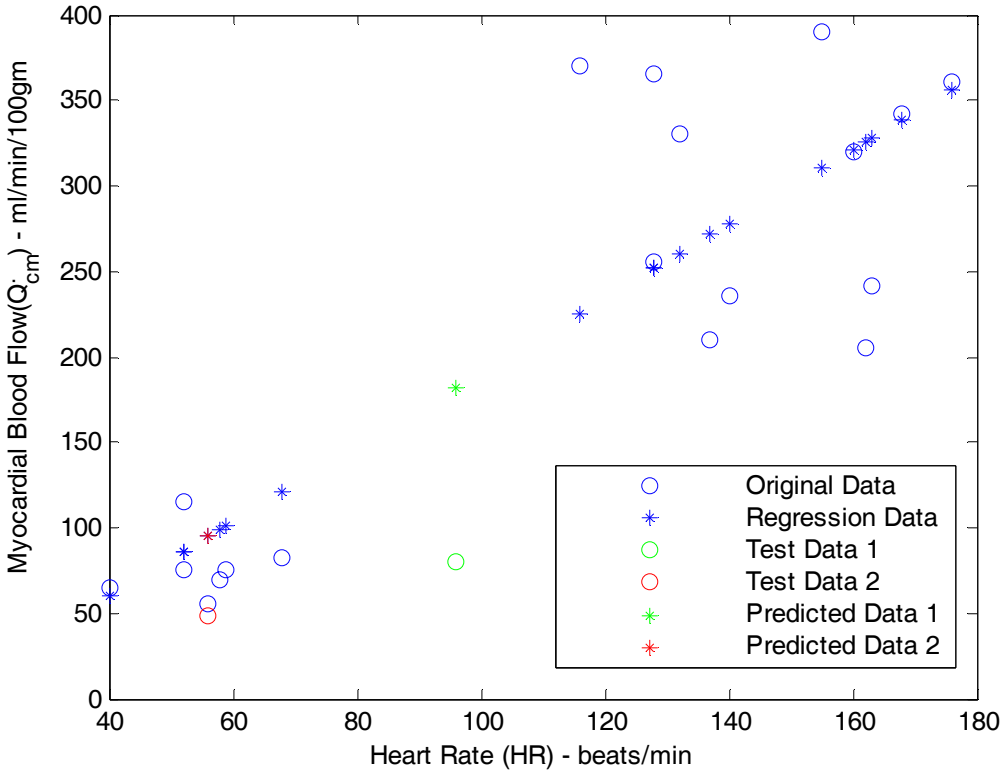

Figure 3.7: Heart Rate and Myocardial Blood Flow. Figure shows the plot of the data (o) used to build the relationship (79) and predicted data (*).The heart rate is plotted on the x-axis and the myocardial blood flow is plotted on the y-axis. Test data points (o,o) were considered from experiments whose data (161) were not included in building the relation to check with the values(*,*) obtained from the predictor equation.

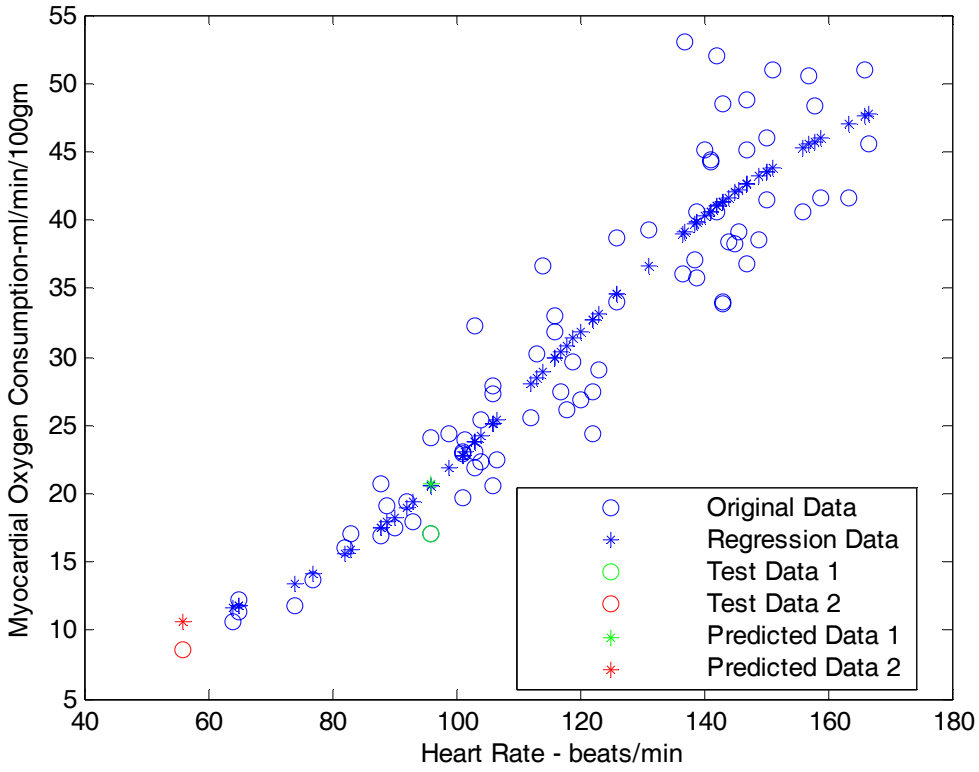

Figure 3.8: Heart Rate and Myocardial Oxygen Consumption. Figure shows the plot of the data (o) used to build the relationship (80-86) and predicted data (*).The heart rate is plotted on the x-axis and the myocardial oxygen consumption is plotted on the y-axis. Test data points (o,o) were considered from experiments whose data was not included in building the relation to check with the values(*,*) obtained from the predictor equation.

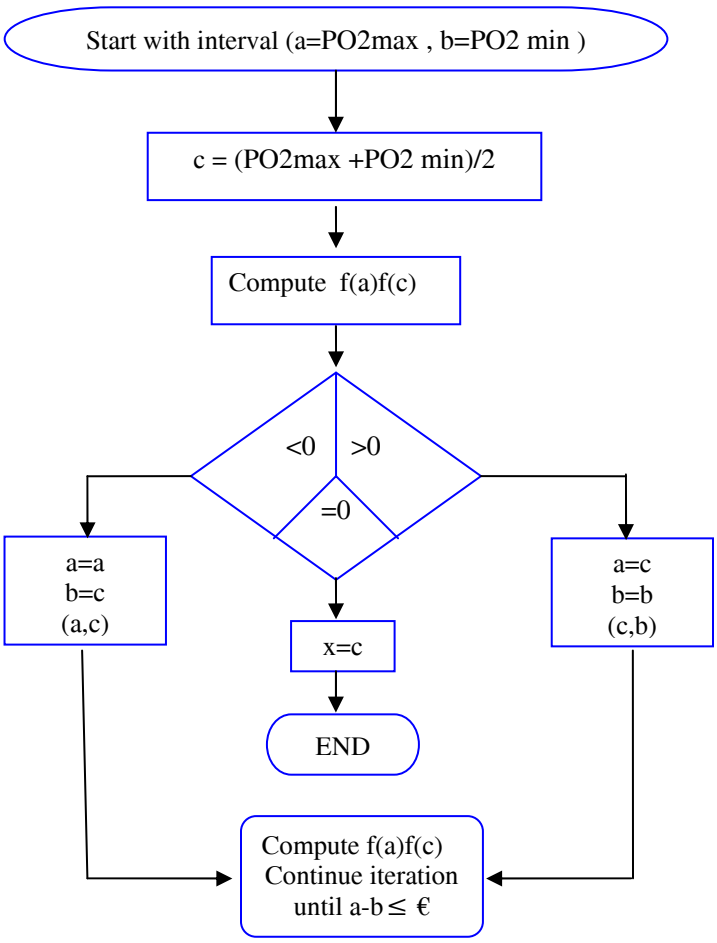

Figure 3.9: Flow chart for the Algorithm

CHAPTER 4

Results

Chapter 4 presents both the validation results for the cardiac compartment and model predictions of extravascular burden of *CO*, and the resulting PO_2 levels, for various simulations. This chapter describes the simulation conditions in detail like the inputs to the model, levels of *CO* exposures, time of *CO* exposure, type of treatment (room air or 100% O_2) and data source etc. Also in this chapter, model predictions are graphed and tabulated for various experimental conditions that were simulated using the developed model.

The final model (Figure 3.2) is used for validating the cardiac compartments and for all other simulations listed below. The validation protocol for the cardiac compartment has already been described in Section 3.7 of Chapter 3. Predictions from the model were compared with published observations on human subjects and animal data (Table 4.1). The model of the cardiac compartment is validated for conditions of hypoxia, exercise and hyperoxia.

4.1 Model Validation

Model predictions for the blood and tissue PO_2 were compared with experimentally measured values from various experiments reported in the literature (Table 4.1). These variables (myocardial tissue and blood PO_2) were evaluated for conditions of hypoxia, hyperoxia and exercise in the absence of *CO*. Most of the available experimental data are from anesthetized animal studies. Figure 4.1, Figure 4.2, and Figure 4.3 show the comparison of model predictions (myocardial tissue and coronary venous PO_2) with experimentally measured values. From Figure 4.1 it can be seen that the model predictions of coronary venous tend to overestimate the coronary venous PO_2 when compared to the experimental data reported in the literature. The model estimates are ~34.7% greater than the experimentally measured coronary venous PO_2 values. Figure 4.2 shows the comparison of model predictions of

myocardial tissue PO_2 in subcompartment 1 with experimentally measured myocardial tissue PO_2 (measurement sites close to arterioles or generally a large electrode or the average value of the upper half of PO_2 histograms was used). The model predictions of the first compartment tissue PO_2 match well with the experimentally measured values reported in the literature. However, at lower experimental PO_2 the model tends to slightly overestimate the predicted PO_2's. In Figure 4.3, comparison of model predictions of myocardial tissue PO_2 in subcompartment 2 with experimentally measured myocardial tissue PO_2 is shown. The experimental measurement made with electrodes whose size is comparable to that of a capillary and the average value of the lower half of PO_2 histograms was assumed to represent the tissue PO_2 in the second compartment. The predictions made by the model for myocardial tissue PO_2 of subcompartment 2 slightly underestimate the experimentally made measurements by 28.37%. At very low experimentally measured PO_2's, the model predicts negative tissue PO_2. Values of certain parameters like PS (permeability surface area product) and FVcm (volume distributing fraction of cardiac compartment) were determined to best fit the model predictions with the experimental data. Thus, model validation also helped to determine the values (Section 3.6) for some parameters.

4.2 Model Simulations

The major goal of the thesis was to predict myocardial *MbCO* levels and tissue PO_2 levels (extravascular burden) during *CO* exposures and treatment sessions. Estimating the extravascular burden of *CO* on the heart will aid in understanding the severity of myocardial tissue hypoxia during (or after) *CO* poisoning. The various simulations done below explain the data source, experiment protocol, relevance of simulation, inputs to the model available (provided by the investigators of the experiment), model parameters determined, and predictions of extravascular burden of *CO* on heart and coronary venous PO_2 (outputs). In all the simulations extravascular

(myocardial tissue PO_2 and *MbCO*) burden of *CO* on human heart is predicted. The following simulations have been analyzed in this thesis:

1. Simulation of short-high concentration *CO* exposure.
2. Simulation of long-low concentration *CO* exposure.
3. *CO* rebreathing during 100% O_2 administration.
4. *CO* exposure during Rest and Exercise Sessions

4.2.1 Short Duration-High Concentration CO Exposure:

Data Source for the Simulation: Subject 120, Reference 154. Benignus et.al exposed human subjects to high concentration of *CO* (6683 PPM) during room air breathing for 4-6 Minutes, followed by washout on air for 4-5 hrs.

Experiment Protocol:

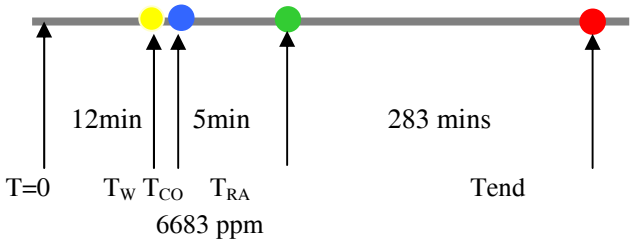

Tw = Time for the model to reach a steady state (12 min)

T_{CO}= Start time of CO exposure

T_{RA}= Start time for treatment with room air

Tend = End time of simulation

Simulation Relevance: This kind of simulation would find relevance when trapped for 5-10 mins in a house or a coal mine which is on fire, or in a car with its exhaust blocked.

Parameters Provided by Investigators: age, gender, height, body weight, concentration of *CO*, hemoglobin concentration in blood, barometric pressure, temperature, cardiac output , ventilation, volume of blood, exposure and treatment times, room air treatment, HbCO levels in radial artery and antecubital vein sampled every minute for the first 6 min, then intermittently thereafter.

Parameters Determined: Total body O_2 consumption (233 ml/min/Kg), heart rate (Section 3.5.3), ventilation adjusted, diffusion coefficient for *CO* (Bruce, Bruce and Erupaka), myocardial blood flow (Section 3.5.1), myocardial O_2 consumption (Section 3.5.1), increases in cardiac output (Section 3.2.4) and increases in heart rate (Section 3.5.3) with increases in blood *HbCO* levels. These parameters are the values determined from regression relationships or from the literature.

Model Predictions: Figure 4.4 shows the predicted *HbCO* levels in arterial blood, coronary venous partial pressure of O_2 ($PcvO_2$), oxygen tension in cardiac subcompartment 1 (Pcm_1O_2), *MbCO* levels in cardiac subcompartment 1 ($MbCOcm_1$), oxygen tension in cardiac subcompartment 2 (Pcm_2O_2) and *MbCO* levels in cardiac subcompartment 2 ($MbCOcm_2$). The values of the predicted variables are as shown below:

Variable	Values before begin of CO Exposure	Values at End of CO Exposure	Values at End of Treatment
% HbCO	0.73	14.17	6.19
$\%MbCOcm_1$,$\%MbCOcm_2$	0.25, 0.32	5.39, 7.38	2.34, 3.08
Pcm_1O_2, Pcm_2O_2(Torr)	36.52, 19.33	21.45, 13.26	36.01, 21.08
$PcvO_2$ (Torr)	19.06	12.84	16.46

As seen in Figure 4.4 *MbCO* levels in compartment 2 are higher than in compartment 1, resulting in a lower tissue *PO2* in compartment 2 after *CO* exposure. The *HbCO* level in arterial blood increases, resulting in increased cardiac output. Increase in cardiac output is achieved by increased myocardial O_2 consumption accompanied with increase in myocardial blood flow. More *CO* load is delivered to the tissues due to increase in blood flow to the tissue. Also, the myocardial O_2 consumption increases and the tissue PO_2 falls resulting in higher *MbCO* levels. Figure 4.5 shows comparison of the *MbCO* levels and tissue PO_2 of resting skeletal muscle and cardiac muscle tissues for the same *CO* exposure protocol. It can be seen from the Figure 4.5 that the *MbCO* levels are lower and the tissue PO_2 are greater in skeletal muscle than that of cardiac muscle. Lower MbCO levels in resting skeletal muscle are due to lower oxygen consumption, lower blood flow, less *CO* load delivered and higher PO_2 than that of cardiac muscle, which is a rigorously working muscle. The values for the resting skeletal muscle are as shown below

Variable	**Values before begin of CO Exposure**	**Values at End of CO Exposure**	**Values at End of Treatment**
% HbCO	6.19	0.73	14.17
%MbCOcm$_1$,%MbCOcm$_2$	1.99, 2.05	0.39, 0.48	2.3, 1.57
Pm$_1$O$_2$, Pm$_2$O$_2$ (Torr)	42.03, 27.75	35.9, 22.16	39.16, 25.09

4.2.2 Long Duration-Low Concentration CO Exposure

Data Source for the Simulation: The same parameters used in section 4.2.1 were used for this simulation. But the experiment protocol is different for this simulation. Subject 120 is exposed to 90 ppm of *CO* for a period of 8 hrs. There is no treatment in this protocol.

Simulation Relevance: This kind of simulation would find relevance when there is a faulty heater at work place or a faulty furnace at home.

Experiment Protocol:

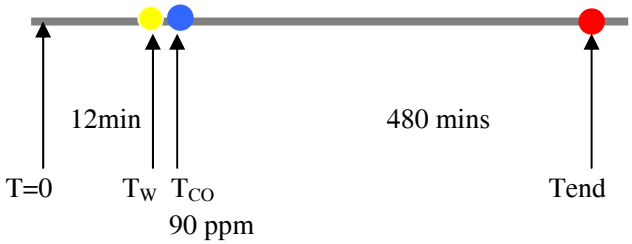

Model Predictions: Figure 4.6 shows the predicted *HbCO* levels, coronary venous *PO2, PcvO₂, MbCO* levels, $MbCOcm_1$ and $MbCOcm_2$ and myocardial oxygen tensions, Pcm_1O_2 and Pcm_2O_2,. The predicted values before *CO* exposure are similar to the values of the simulation above (Section 4.2.1). Simulating this experimental protocol would help to understand the impact of *CO* load on the heart for a greater length of time and its resulting effect on the myocardial O_2 tension. Concentration of *CO* exposure is lower in this simulation but is present for a greater length of time. The *HbCO* levels in blood reach ~9.6% resulting in *MbCO* levels of 3.84% and 5.24% in cardiac subcompartments 1 and 2. The tissue PO2 in the first subcompartment is 32 Torr, which is a reasonable PO_2 however, the tissue PO_2 is slightly lower in the subcompartment 2 (which is a major subcompartment of the heart model) for a long duration of time, resulting in tissue hypoxia. If the duration of *CO* exposure or concentration of *CO* would be increased, then the cardiac tissue would be O_2 impaired for longer duration of time resulting in imbalance of homeostasis of O_2 delivery and metabolism of heart. The values of the predicted variables are as follows:

Variable	**Values at End of CO Exposure**
% HbCO	9.5904
% MbCO	3.84, 5.24
Tissue PO2 (Torr)	32, 15.12
Cardiac Venous Po2 (Torr)	14.91

4.2.3 CO Rebreathing During 100% O_2 Administration

Data Source for the Simulation: Subject 1, Reference 155. Burge & Skinner had conducted *CO* rebreathing experiments in hyperoxia (100% O_2) to estimate the total blood volume. Subjects in this study rebreathed 60-70ml of *CO* for a period of 40 mins while breathing 100% oxygen.

Simulation Relevance: This method is a standard one used for determining total blood volume of a subject. Also, the closed breathing design of the experiment helps in estimating the blood-to-tissue diffusion coefficient of *CO* (35) because the slow decrease in %*HbCO* after 10 min is sensitive to this coefficient.

Experiment Protocol:

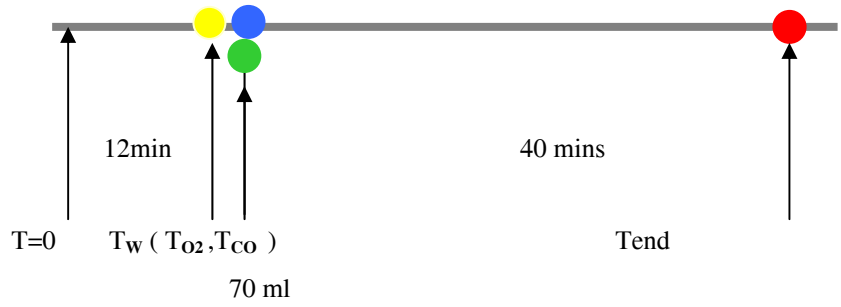

T_{O2}= Start time for treatment with 100% O2

Parameters Provided by Investigators: age, gender, height, body weight, injected volume of CO, barometric pressure, temperature, volume of blood, exposure and hyperoxia breathing times, and volume of the rebreathing circuit.

Parameters Determined: Total body O_2 consumption (233 ml/min/kg), cardiac output (Section 3.5.2), heart rate (Section 3.5.3), ventilation is assumed to be 0 during rebreathing, diffusion coefficient for *CO* (Bruce, Bruce and Erupaka), myocardial blood flow (Section 3.5.1), myocardial O2

consumption (Section 3.5.1), increases in cardiac output (Section 3.2.4) and increases in heart rate (Section 3.5.3) with increases in blood *HbCO* levels The parameters during 100% oxygen breathing are not known. Regression equations developed for determining parameters during normoxia were applied for predicting cardiac ouput, heart rate etc., during hyperoxia.

Model Predictions: Figure 4.7 shows the predicted *HbCO* and *MbCO* levels in arterial blood and tissue subcompartments, coronary venous partial pressure of O_2 ($PcvO_2$) and myocardial oxygen tensions. *MbCO* levels of subcompartment 1 are greater by 2% than the subcompartment 2 during the intial 5-6 mins of the experiment and then the *MbCO* levels in the two subcompartments reach equilibrium. The tissue PO_2 falls approximately by 46 Torr in the subcompartment 1 and 7 Torr in the subcompartment 2. However after the end of *CO* exposure, the tissue PO_2 of cm1 increases approximately to 92 (close to value before *CO* exposure) Torr, and the PO_2 of cm2 increases to 20.31 Torr. However the tissue PO_2 in cm2 does not increases as much as expected during 100% O_2 breathing. This could be due to errors in determining the parameters during treatment protocol. The values of the predicted variables are as follows:

Variable	Values before begin of CO Exposure	Values at End of CO Exposure
% HbCO	1.07	10.94
$\%MbCOcm_1$,$\%MbCOcm_2$	1.07, 0.92	3.96, 3.56
Pcm_1O_2, Pcm_2O_2(Torr)	96.4, 22.56	50, 17.3
$PcvO_2$ (Torr)	23.29	17.07

4.2.4 CO Exposure During Exercise

Data Source for the Simulation: Subject 21, Reference 69. Kizakevitch et al. conducted experiments where the subjects performed lower body

exercise using a treadmill. Subjects underwent air exposures at their base level *HbCO* (0-2%) and *CO* exposures to fours levels of *HbCO* (5%, 10%, 15%, 20%). At each level of *HbCO*, subjects underwent exercise sessions comprised of rest and three 5 min exercise periods (R, E1, E2, E3). The exercise intensity was increased in a step wise fashion and the experiment was conducted over two days.

Simulation Relevance: Working groups exposed to *CO* concentrations higher than the permissible levels are more susceptible to severe tissue hypoxia because increased work increases the oxygen demand in the tissue, but *CO* interferes with O_2 delivery by binding to hemoglobin. Myoglobin functionality is also impaired as *CO* binds to myoglobin, further impairing O_2 availability. Predicting tissue oxygenation and *MbCO* levels in the cardiac compartment during *CO* exposures will estimate the extent of tissue hypoxia in the heart.

Parameters Provided by Investigators: age, gender, height, body weight, concentration of *CO* in inspired air (1000 ppm for 5% *HbCO*, 3000 ppm for 10%, 15% and 20% *HbCO* levels. 27 ppm, 55ppm, 83ppm and 100 ppm were used to maintain *HbCO* concentrations at 5%, 10%, 15% and 20% respectively), total body metabolic rate, ventilation , cardiac output, heart rate, times for begin of exercise stages and time of 100% O_2 exposure.

Experiment Protocol:

The protocol the authors followed was as follows:

E = Exercise; R= Rest

Day 1: Baseline *HbCO* (R, E1, E2, E3) - 5% HbCO(R, E1, E2, E3) - 15% *HbCO* – (R, E1, E2, E3)- Administer 100% O2

Day 2: Baseline *HbCO* (R, E1, E2, E3) - 10% *HbCO*(R, E1, E2, E3) - 20% *HbCO* – (R, E1, E2, E3) - Administer 100% O2.

Parameters Determined: Diffusion coefficient for *CO* (2.5 ml/min/Torr), myocardial blood flow (Section 3.5.1), myocardial O_2 consumption (Section 3.5.1), blood volume, ventilation adjusted to maintain normoxic arterial PO_2, cardiac output (Section 3.5.2,3.5.3) and heart rate during O_2 administration .

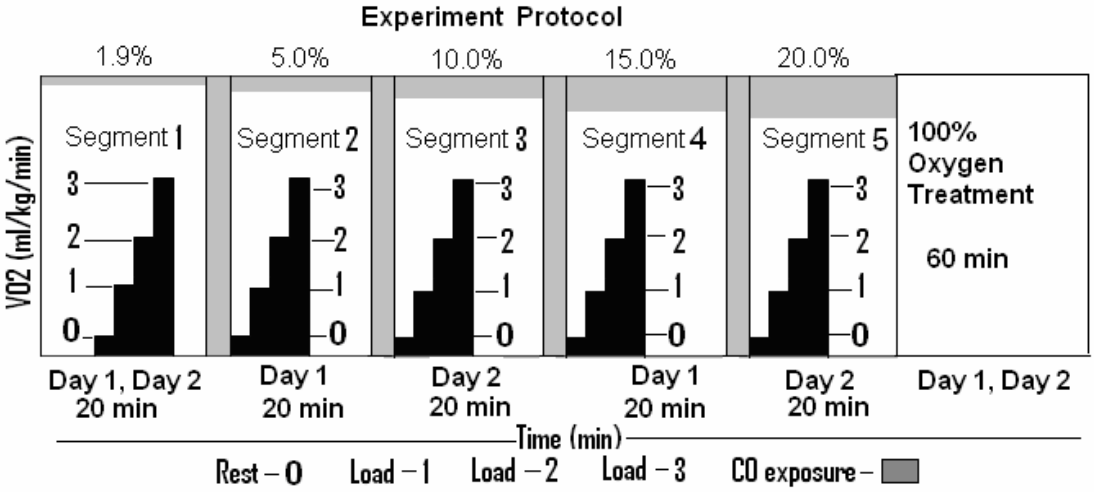

Model Predictions:

4.2.4.1 Baseline HbCO (1.9%) at Rest and Three Levels of Exercise: (Figure 4.8). Myocardial tissue and venous PO_2 decrease from rest in a stepwise fashion with exercise stages 1 and 2. At the beginning of exercise stage 3, the PO_2 in the myocardial tissue and blood subcompartments increase. The MbCO levels in the subcompartments increase but are insignificant. There is a significant decrease in tissue PO_2 (decreases by 10 Torr and 6 Torr, respectively) of cm1 and cm2 at the end of exercise stage 2. There is an increase in tissue oxygen tensions during exercise stage 3. With increased exercise load one would expect the tissue PO_2 to fall, but the tissue PO_2 increases because the cardiac output increases by 2.6 times the resting value. Increase in cardiac output results in increased blood flow to the heart and there is more O_2 available for delivery to the tissues. Also the *HbCO*

levels are minimal, resulting in noncompetitive binding of O_2 with hemoglobin, there by resulting in increased tissue PO_2. The values are

Variables	Rest	Exercise 1	Exercise 2	Exercise 3
% HbCO	1.9	1.9	1.9	1.9
% MbCO	0.68, 0.87	0.73, 0.98	0.86, 1.24	0.73, 0.95
Tissue PO_2 (Torr)	34.26, 18.66	28, 15.8	24.43, 12.36	32.5, 18.2
Cardiac Venous PO_2	20.9 Torr	17.8 Torr	15.09 Torr	19.54 Torr

4.2.4.2 HbCO (10%) at Rest and Three Levels of Exercise (Figure 4.9)

The subcompartment *MbCO* levels increase with stages of exercise, though the *HbCO* levels are maintained at 10%. The PO_2 (tissue and blood) in the cardiac subcompartments decrease and *MbCO* levels increase linearly till the constant *HbCO* levels of 10% are attained. There is a negligible increase noticed in *MbCO* levels during the 5 min rest period, followed by a steep increase during exercise stages 1 and 2 and then a linear increase during exercise stage 3.

Variables	Rest	Exercise1	Exercise 2	Exercise 3
% HbCO	9.94	10	9.97	10
% MbCO	3.76, 5.09	4.12, 5.62	4.05 , 5.51	4.8, 7.1
TissuePO2 (Torr)	32.03, 15.33	31.14, 14.15	31.22 , 14.17	25.15, 10.45
Cardiac Venous Po2	16.61 Torr	15.76 Torr	15.74 Torr	12.85 Torr

The tissue and blood PO_2's of heart decrease by 1-2 Torr initially during the rest session, then fall by few Torr and are maintained constant during stages 1 and 2 of exercise. There is a significant drop of PO_2 in tissue and blood subcompartments during exercise stage 3, especially in tissue subcompartment 2. The heart rate during stage 3 increases approximately by 98% due to exercise and increase in blood *HbCO* levels. Increased heart rate increases

myocardial O_2 consumption and myocardial blood flow. Also the cardiac ouput increases due to exercise and *CO* exposure. This results in more *CO* load being delivered to the heart, as *CO* has more affinity than O_2 to bind to hemoglobin. It results in higher *MbCO* levels and lower tissue PO_2 in the subcompartments of the heart.

4.2.4.3 HbCO (20%) at Rest and Three Levels of Exercise (Figure 4.10)

The subcompartment *MbCO* levels increase with stages of exercise, though the *HbCO* levels are maintained at 20%. After reaching constant *HbCO* level of 20%, there is a step wise decrease in PO_2's (of myocardial tissue and blood subcomparments) with exercise stages. There is a decrease of tissue and blood PO_2 in the cardiac subcompartments with linear increase of tissue *MbCO* levels. There is a significant large drop in the oxygen tensions of tissue subcompartment 2 during exercise stage 1 and exercise stage 2 compared to exercise stage 3. The cardiac output increases by 81%, 102% and 119% respectively compared to the rest session at 20% HbCO levels. Increasing metabolic demand of O2 with exercise stages and poor tissue oxygenation due to increased *CO* load (due to increasing blood flow) results in PO_2 of 3.7 Torr and 2.28 Torr. If these tissue PO_2 persists for longer time, then the metabolic oxygen demands may be met with anaerobic metabolism.

Variables	Rest	Exercise1	Exercise 2	Exercise 3
% HbCO	19.78	19.73	19.7	19.6
% MbCO	8.81, 12.74	11.07, 17.49	14.25, 25.25	18.75, 33.93
TissuePO2 (Torr)	23.8, 10.29	20.03, 6.66	14.55, 3.71	9.19, 1.92
Cardiac Venous Po2	11.91 Torr	8.8 Torr	5.6 Torr	2.28 Torr

4.2.4.4 HbCO (20%) at Rest and Three Levels of Exercise Followed with 100% O2 Treatment:

After the third stage of exercise, the subject breathed 100% O_2 for 60 mins (Figure 4.11). The model predictions at the end of 60 mins are as follows

Variables	Rest	End of therapy
% HbCO	1.9	13.78
% MbCO	0.68, 0.87	6.97, 8.38
TissuePO2 (Torr)	34.26, 18.66	108, 17
Cardiac Venous Po2	20.9 Torr	18.45 Torr

100 % O_2 breathing after *CO* exposure decreases the *HbCO* and *MbCO* levels in arterial blood and the cardiac tissue subcompartment (Figure 4.11). There is an increase in myocardial blood and tissue PO_2's with 100% O_2 breathing. A significant increase in the tissue PO_2 of cardiac subcompartment 1 is observed with 100% O_2 breathing. However, the PO_2 of tissue subcompartment 2 only increases to 17 Torr after 100% O_2 breathing. The *MbCO* levels in cm2 are 8.38% after breathing 100% O_2. The cardiac output for this session (breathing 100% O_2) was determined from the predictive equation considering the total body O_2 consumption at rest (during 20% *HbCO*). Making this assumption may have effected the prediction for second compartment myocardial tissue PO_2. The determined cardiac output may have been underestimated for the hyperoxia session which resulted in lower blood flow to the heart compartment. Also the *MbCO* levels were higher in the second compartment accompanied with lower blood flow during hyperoxia which resulted in lower tissue PO_2 in cm2 at end of therapy (recovery) session. Figure 4.12 compares the model predictions for extravascular burden of *CO* (PO_2 and *MbCO*) while breathing 100% O_2 vs Room air after *CO* exposure. It can be seen from the figure that breathing 100% O_2 after exposure shows higher tissue PO_2 and lower *MbCO* levels than breathing room air.

4.2.4.5 Baseline HbCO (1.9%) - HbCO (5%) - HbCO (15%) (Each session at Rest and Three Levels of Exercise) Followed with 100% O2 Treatment. Figure 4.13

There is a step wise decrease in PO_2's (of myocardial tissue and blood subcomparments) with exercise stages and increasing *HbCO* levels. There is an increase in myocardial blood and tissue PO_2's with 100% O_2 breathing. Also, the *HbCO* and *MbCO* levels in arterial blood and the cardiac tissue subcompartment decreases with 100 % O_2 breathing after *CO* exposure. The responses of decreases in PO_2 and increases in *MbCO* levels (of the cardiac subcompartments) are qualitatively similar to the exercise simulations discussed above for 10% and 20% *HbCO* levels but the values reach are quantitatively different as the current simulation involves lower *HbCO* levels of 5% and 15 % compared to 10% and 20%. Thus we can expect that with increasing *HbCO* levels, the quantitative values attained may be different but the same qualitative response pattern may be followed.

Table 4.1 : Validation of the Model.

R	Species	Exp. Par O_2	Model Par O_2	Exp. PcmvO_2	Model PcmvO_2	Exp. PtO_2	Model Pcm1 O_2	Model Pcm2 O_2	Qcm	Mr O_2cm
91	Human	99	98.98954	17.25	20.50	-	34.84992	19.69238	118	15
91	Human	42	43.66366	15.75	12.96	-	16.6563	13.77764	167	17
91	Human	36	36.9957	15	11.45	-	13.41558	12.40324	261	25
157	Dog	92	91.76348	18.8	25.39	19.9	48.66612	29.18559		
157	Dog	92	91.76348	26	25.39	-	48.66612	29.18559	90	6.6
45	Dog	32	32.05925	22	19.99286	-	23.1705	21.40628	160	9.79
45	Dog	27	27.79234	18	19.91647	-	21.8324	20.94568	210	6.7
96	Swine	103	103.4311	27.33	27.34	50	41.64232	27.36177	94	6.7
96	Swine	57	57.94478	22.77	30.84952	35	40.77736	33.06806	129.72	5.695
96	Swine	44	44.08298	19.75	27.27827	26	30.6389	27.93219	147.58	5.963
96	Swine	189	190.4437	31.8	24.08567	-	59.21405	27.35737	125	11.3
94	Swine	39	39.42103	21	17.97635	-	23.59683	19.52166	175	12.5
94	Swine	40	40.54051	17	20.95588	-	26.80393	22.58181	173	9.8
93	Dog	64.2	64.1	18.3	19.314	18.9	35.456	24.34		
93	Dog	326	325.36	-	20.93615	49/26	61.77243	23.12536	0.8	0.1

Table 4.1: Validation of the Model (Continued)										
R	**Species**	**Exp. Par O_2**	**Model Par O_2**	**Exp. PcmvO_2**	**Model PcmvO_2**	**Exp. PtO_2**	**Model Pcm1 O_2**	**Model Pcm2 O_2**	**Qcm**	**mrO_2cm**
93	Rat	99	100.1104	-	20.80742	40/20	42.32027	21.26861	4.5	0.54
93	Rat	89	88.34195	-	20.24898	15/35	38.95486	19.60096	4.5	0.54
94	swine	150	150.178	-	26.8742	30.3± 4.7	59.84115	30.68439	94	6.7
161	swine	150	150.178	-	26.8742	42±4	59.84115	30.68439	94	6.7
95	Rat	99	100.094	-	20.685	48/18	41.1873	21.41581	4	0.4
96	Dog	143	142.191	46	19.43323	42±7	47.515	21.56576	0.8	0.1
97	swine	359	358.476	-	29.10781	112± 8.48	77.4706	33.0111	94	6.7
98	swine	90	90.4641	23.25	24.90368	46±7. 5	47.8475	28.38637	94	6.7
99	Rat	99	100.1104	-	20.80742	10	42.32027	21.26861	4.5	0.54
44	swine	99	98.1135	-	25.2926	49±2	49.9177	28.86385	94	6.7
100	Rat	87		20		25			233.1	39.6

R= Reference, Exp.= Experimental, $ParO_2$ = Arterial PO_2, $PcmO_2$ = Coronary Venous PO_2, PtO_2 = Cardiac Tissue PO_2, $Pcm1O_2$ = Cardiac Subcompartment 1 PO_2, $Pcm1O_2$ = Cardiac Subcompartment 1 PO_2, Qcm= Myocardial Blood Flow, mrO_2cm = Myocardial Oxygen Consumption.

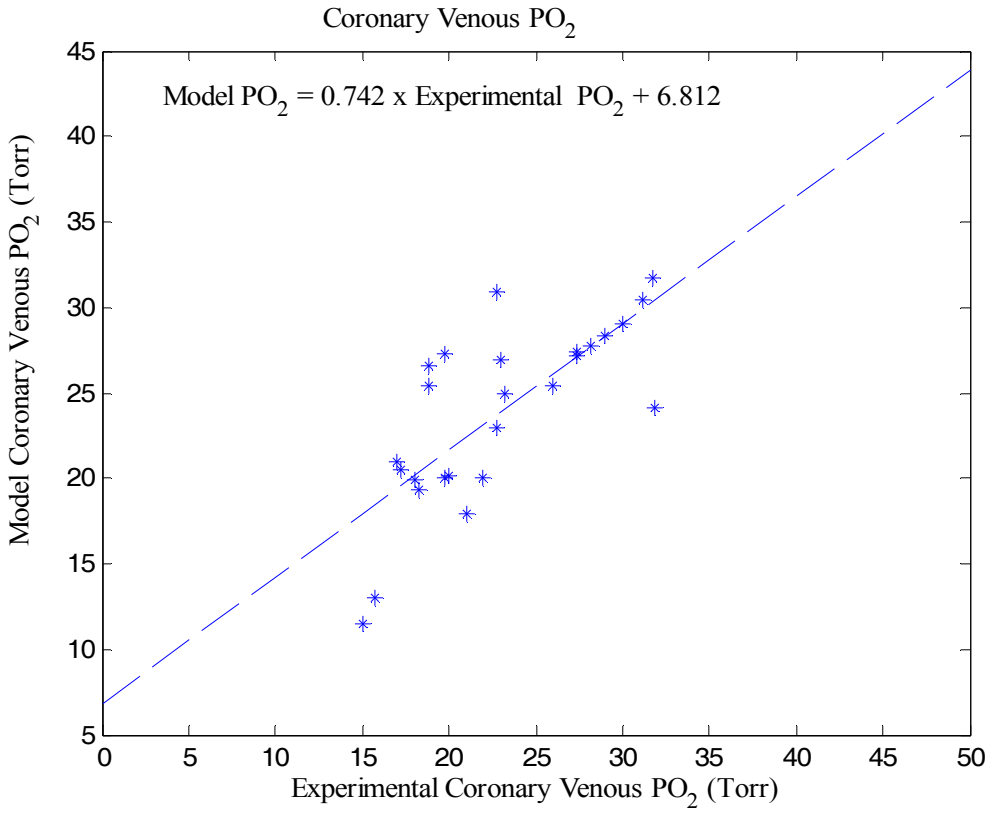

Figure 4.1: Comparison of Coronary Venous PO2. Comparison of model predictions of coronary venous PO_2 (y-axis) with experimentally measured coronary venous PO_2 (x-axis). (Table 4.1). The dashed line represents the regression equation.

Statistical Significance:

Model Coronary Venous PO_2 = 0.742 x Experimental Coronary Venous PO_2 + 6.812

Standard error of estimate: 3.566

Regression coefficient, R: 0.743

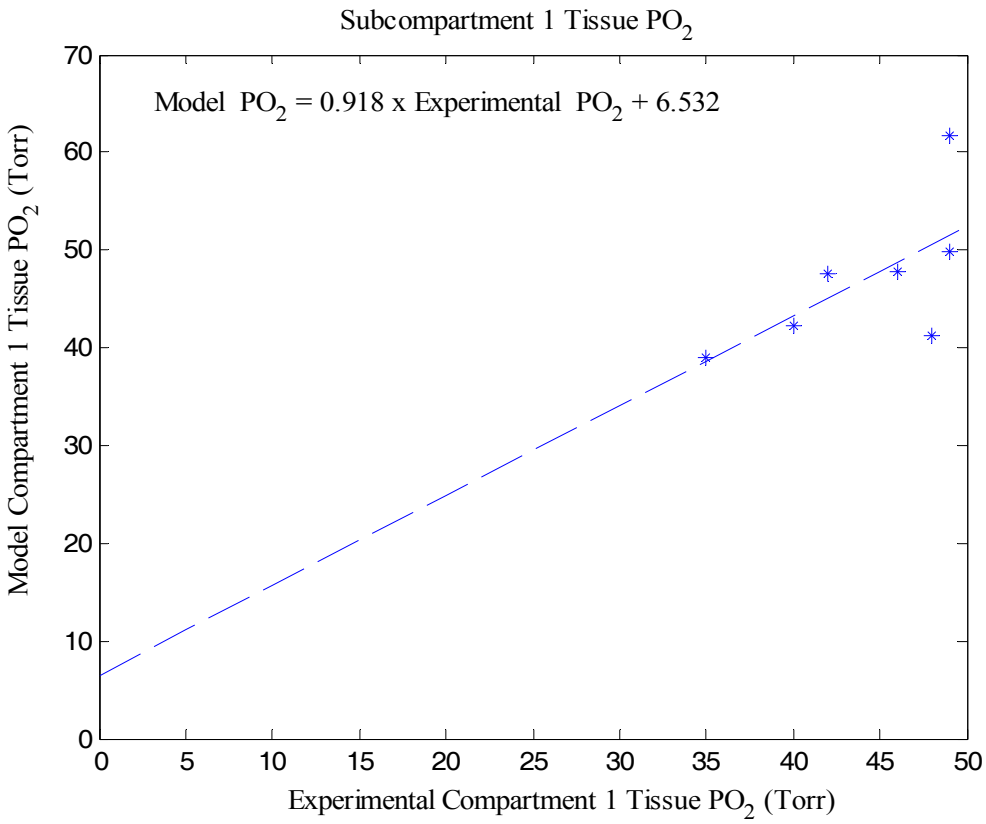

Figure 4.2 : Comparison of Myocardial Tissue PO_2 in Subcompartment 1. Comparison of model predictions of myocardial tissue PO_2 (y-axis) in subcompartment 1 with experimentally measured (x-axis) myocardial tissue PO_2 (measurement sites close to arterioles or generally large electrode was used). (Table 4.1). The dashed line represents the regression equation.

Statistical Significance:

Model Compartment 1 PO_2 = 0.918 x Experimental Compartment 1 PO_2 + 6.532

Standard error of estimate: 6.387

Regression coefficient , R: 0.643

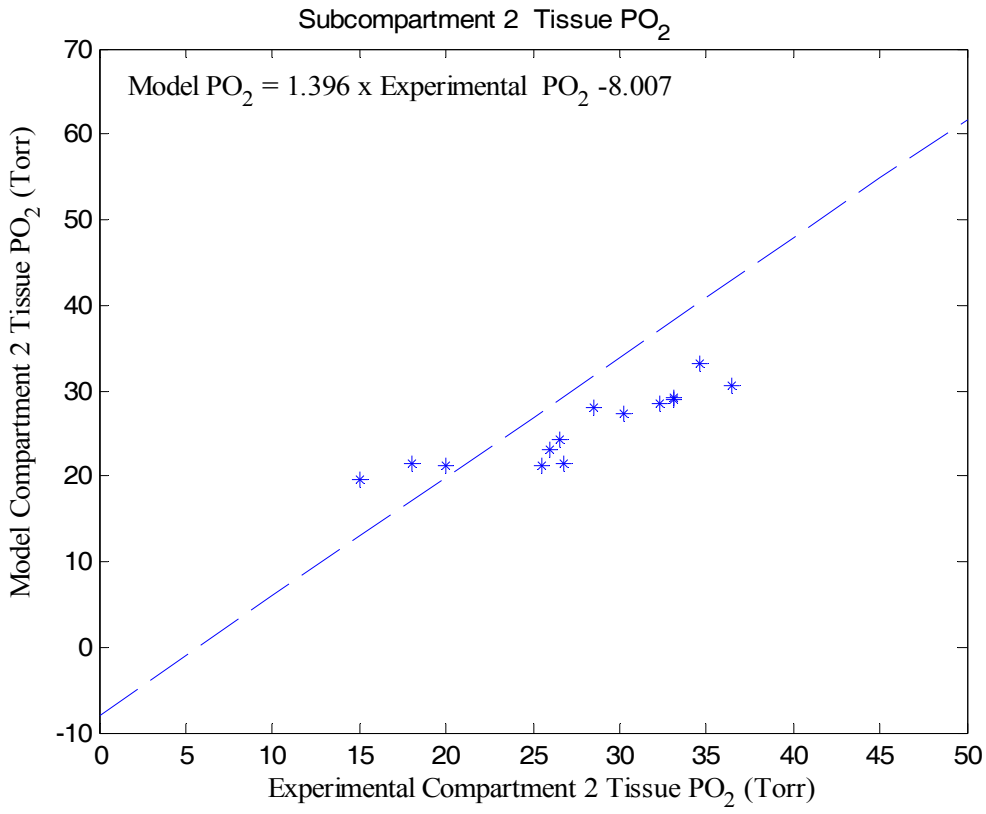

Figure 4.3: Comparison of Myocardial Tissue PO_2 in Subcompartment 2. Comparison of model predictions of myocardial tissue PO_2 (y-axis) in subcompartment 2 with experimentally measured (x-axis) myocardial tissue PO_2 (measurements made with electrodes whose size is comparable to that of size of a capillary). (Table 4.1). The dashed line represents the regression equation.

Statistical Significance:

Model Compartment 2 PO_2 = 1.396 x Experimental Compartment 2 PO_2 -8.007

Standard error of estimate: 2.803

Regression coefficient , R: 0.913

HbCO and MbCO Levels in Percentile PO_2 in Torr

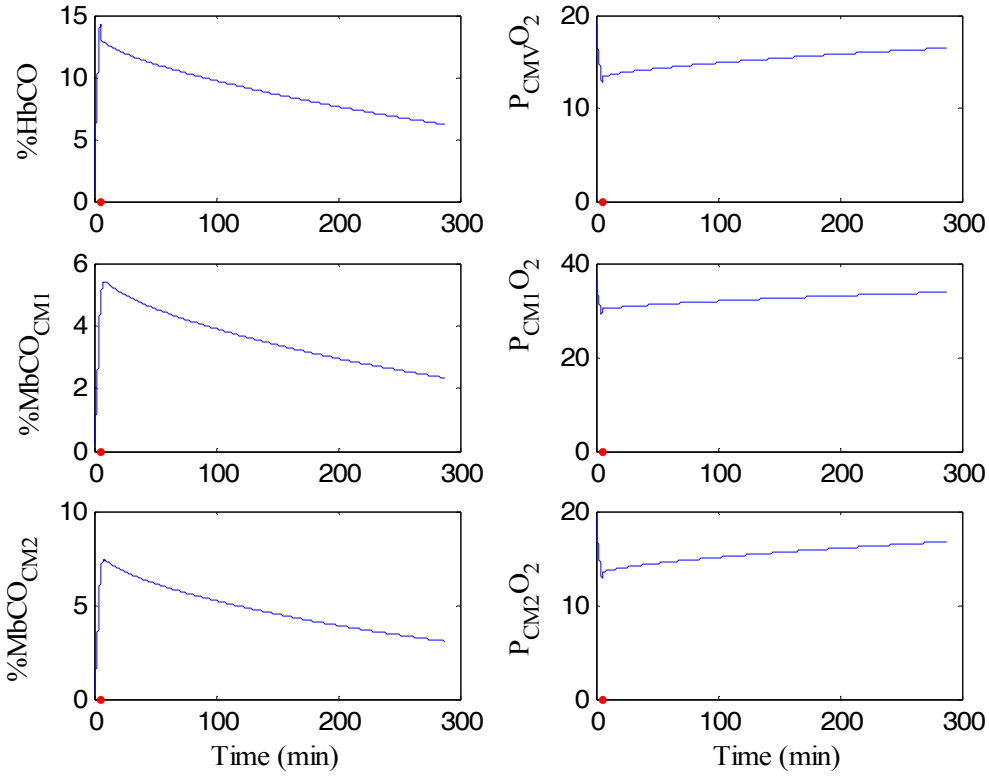

Figure 4.4: Prediction for Short Duration-High Concentration *CO* Exposure. Figure shows the predicted %HbCO levels in arterial blood, coronary venous partial pressure of O_2 ($PcmvO_2$), oxygen tension in cardiac subcompartment 1 (Pcm_1O_2), MbCO levels in cardiac subcompartment 1 ($\%MbCOcm_1$), oxygen tension in cardiac subcompartment 2 (Pcm_2O_2) and MbCO levels in cardiac subcompartment 2 ($\%MbCOcm_2$) for a short (5min) CO exposure (6683 ppm). The point (•) shows the start of therapy (room air administration) at t = 5 min, lasting for 283mins after CO exposure. Simulation time is plotted on the x-axis and the model predicted variables are plotted on the y-axis.

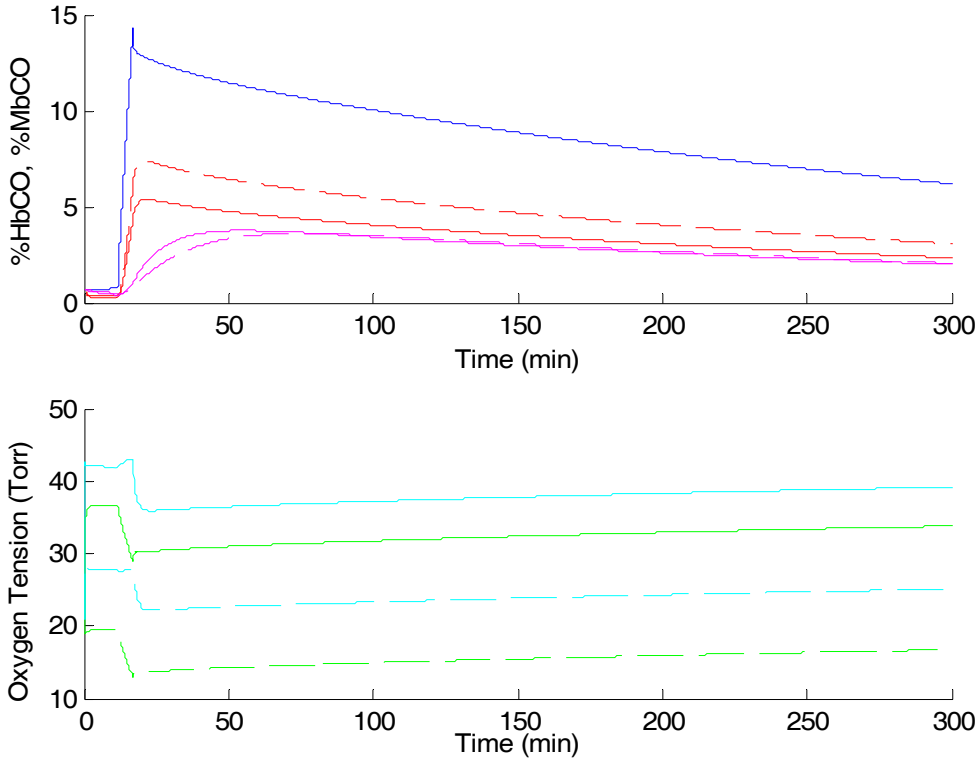

Figure 4.5: Prediction Summary for Short Duration-High Concentration *CO* Exposure. Figure shows the predicted %HbCO (blue) levels in arterial blood, % MbCO levels in cardiac subcompartment 1 (red solid) and cardiac subcompartment 2 (red dashed), oxygen tension in cardiac subcompartment 1 (green solid) and cardiac subcompartment 2 (green dashed); % MbCO levels in resting skeletal muscle subcompartment 1 (magenta solid) and resting skeletal muscle subcompartment 2 (magenta dashed), oxygen tension in skeletal muscle subcompartment 1 (cyan solid) and skeletal muscle subcompartment 2 (cyan dashed) for a short (5min) *CO* exposure (6683 ppm). Simulation time is plotted on the x-axis and the model predicted variables are plotted on the y-axis.

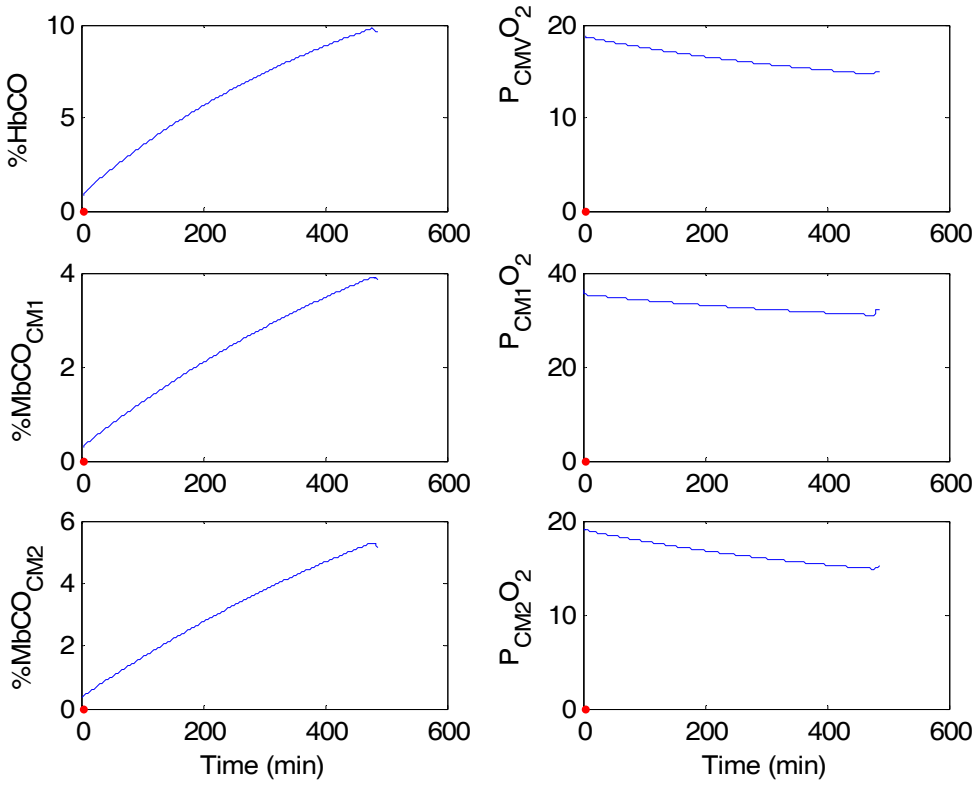

Figure 4.6 :Prediction for Long Duration-Low Concentration *CO* Exposure. Figure shows the predicted %HbCO levels in arterial blood, coronary venous partial pressure of O_2 ($PcmvO_2$), oxygen tension in cardiac subcompartment 1 (Pcm_1O_2), MbCO levels in cardiac subcompartment 1 ($\%MbCOcm_1$), oxygen tension in cardiac subcompartment 2 (Pcm_2O_2) and MbCO levels in cardiac subcompartment 2 ($\%MbCOcm_2$) for a long (480min) *CO* exposure (90 ppm). The point (•) shows the start time of *CO* exposure. Simulation time is plotted on the x-axis and the model predicted variables are plotted on the y-axis.

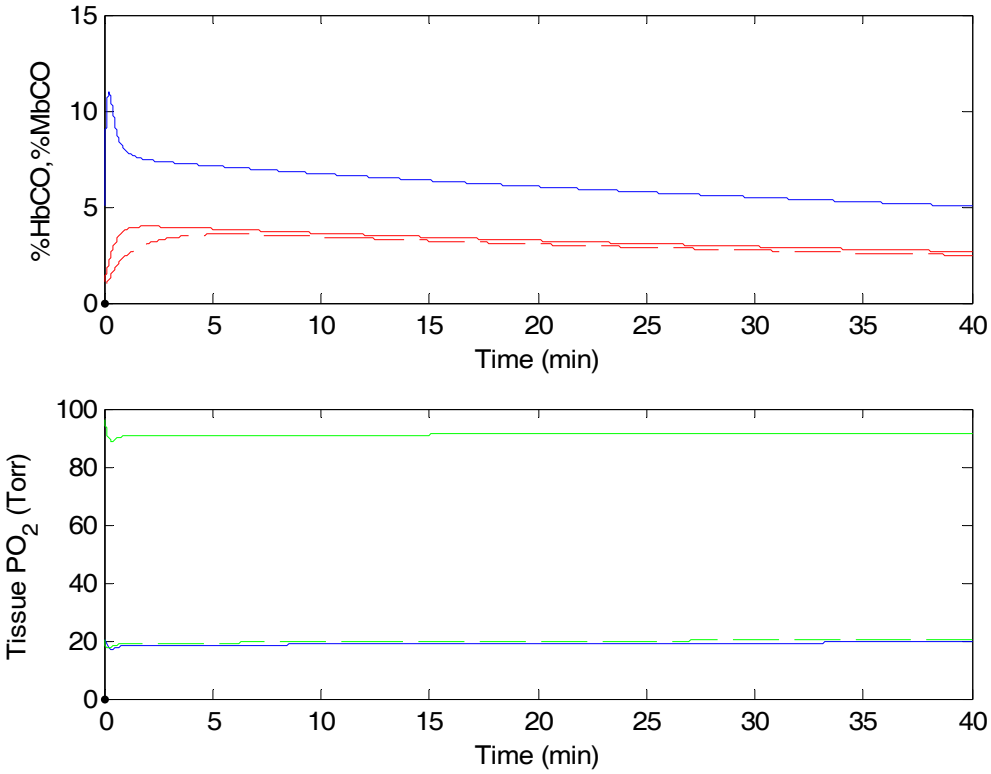

Figure 4.7: CO Rebreathing During 100% O_2 Administration. Figure shows the predicted %HbCO (blue) levels in arterial blood, % MbCO levels in cardiac subcompartment 1(red solid) and cardiac subcompartment 2 (red dashed), coronary venous PO_2 (blue solid) oxygen tension in cardiac subcompartment 1(green solid) and cardiac subcompartment 2(green dashed) for a period 480 mins with *CO* concentrations being 90ppm. The point (•) shows the start of *CO* exposure. Simulation time is plotted on the x-axis and the model predicted variables are plotted on the y-axis.

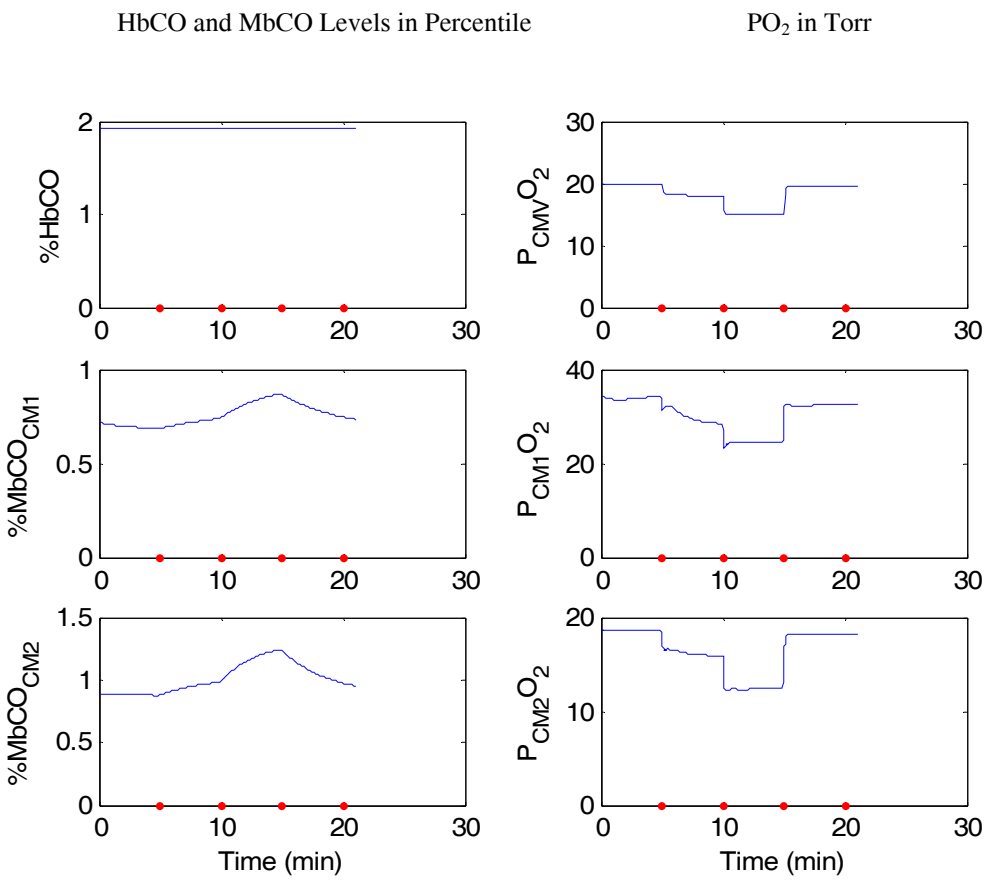

Figure 4.8: Baseline HbCO (1.9%) at Rest and Three Levels of Exercise. Figure shows the predicted %HbCO levels in arterial blood, coronary venous partial pressure of O2 ($PcmvO_2$), oxygen tension in cardiac subcompartment 1(Pcm_1O_2), MbCO levels in cardiac subcompartment 1($\%MbCOcm_1$), oxygen tension in cardiac subcompartment 2(Pcm_2O_2) and MbCO levels in cardiac subcompartment 2($\%MbCOcm_2$. The points (•) show the end times of 5 min sessions of rest, exercise 1, exercise 2 and exercise 3. The sessions are simulated at baseline HbCO levels of 1.9%. Simulation time is plotted on the x-axis and the model predicted variables are plotted on the y-axis.

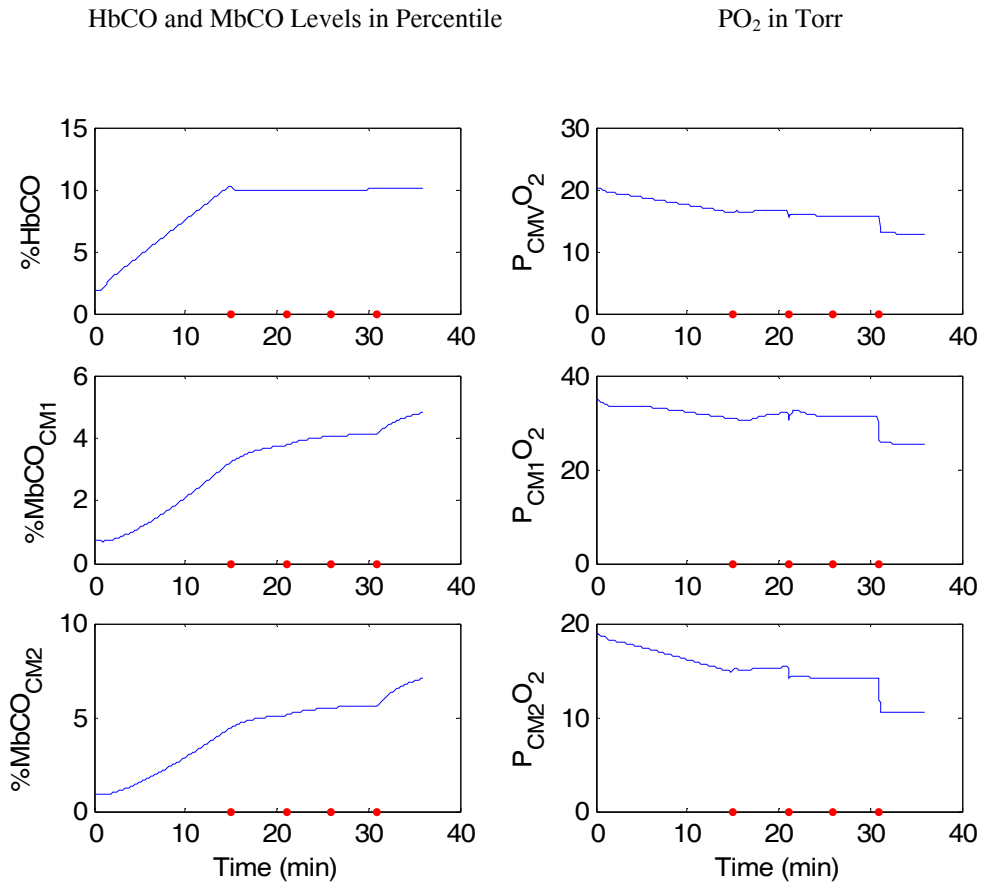

Figure 4.9 : HbCO (10%) at Rest and Three Levels of Exercise. Figure shows the predicted %HbCO levels in arterial blood, coronary venous partial pressure of O_2 ($PcmvO_2$), oxygen tension in cardiac subcompartment 1(Pcm_1O_2), MbCO levels in cardiac subcompartment 1(%$MbCOcm_1$), oxygen tension in cardiac subcompartment 2(Pcm_2O_2) and MbCO levels in cardiac subcompartment 2(%$MbCOcm_2$. The points (•) show the start times of 5 min sessions of rest, exercise 1, exercise 2 and exercise 3. The sessions are simulated at baseline HbCO levels of 10%. Simulation time is plotted on the x-axis and the model predicted variables are plotted on the y-axis.

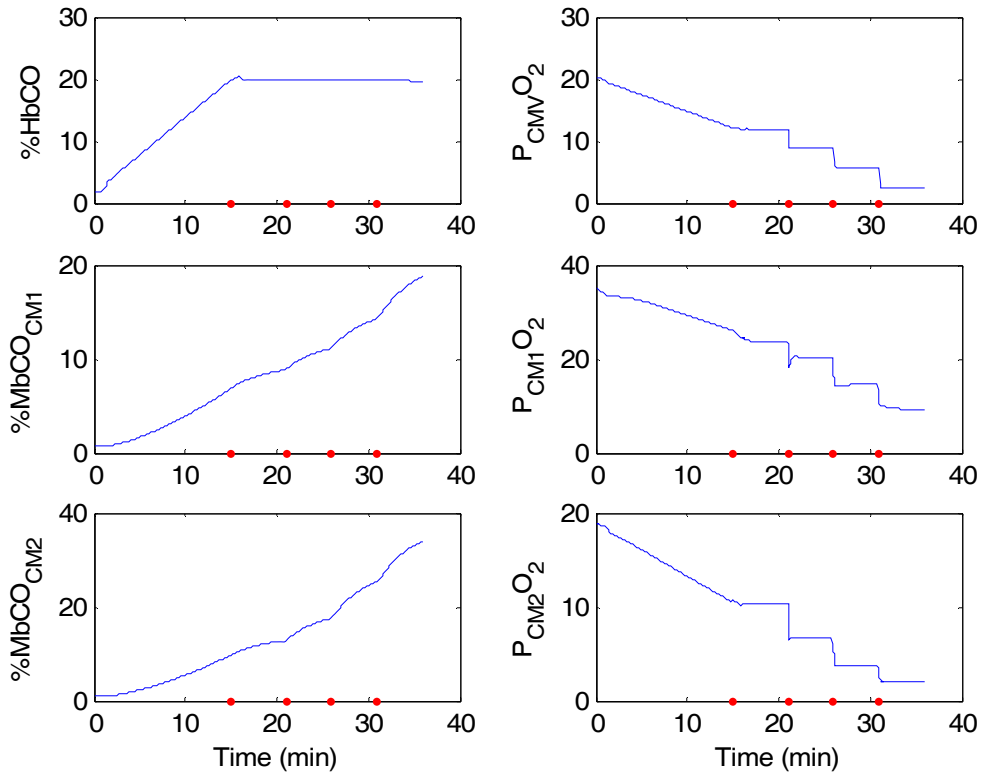

Figure 4.10 : HbCO (20%) at Rest and Three Levels of Exercise. Figure shows the predicted %HbCO levels in arterial blood, coronary venous partial pressure of O_2 ($PcmvO_2$), oxygen tension in cardiac subcompartment 1(Pcm_1O_2), MbCO levels in cardiac subcompartment 1(%$MbCOcm_1$), oxygen tension in cardiac subcompartment 2(Pcm_2O_2) and MbCO levels in cardiac subcompartment 2 (%$MbCOcm_2$).The points (•) show the start times of 5 min sessions of rest, exercise 1, exercise 2 and exercise 3. The sessions are simulated at baseline HbCO levels of 20%. Simulation time is plotted on the x-axis and the model predicted variables are plotted on the y-axis.

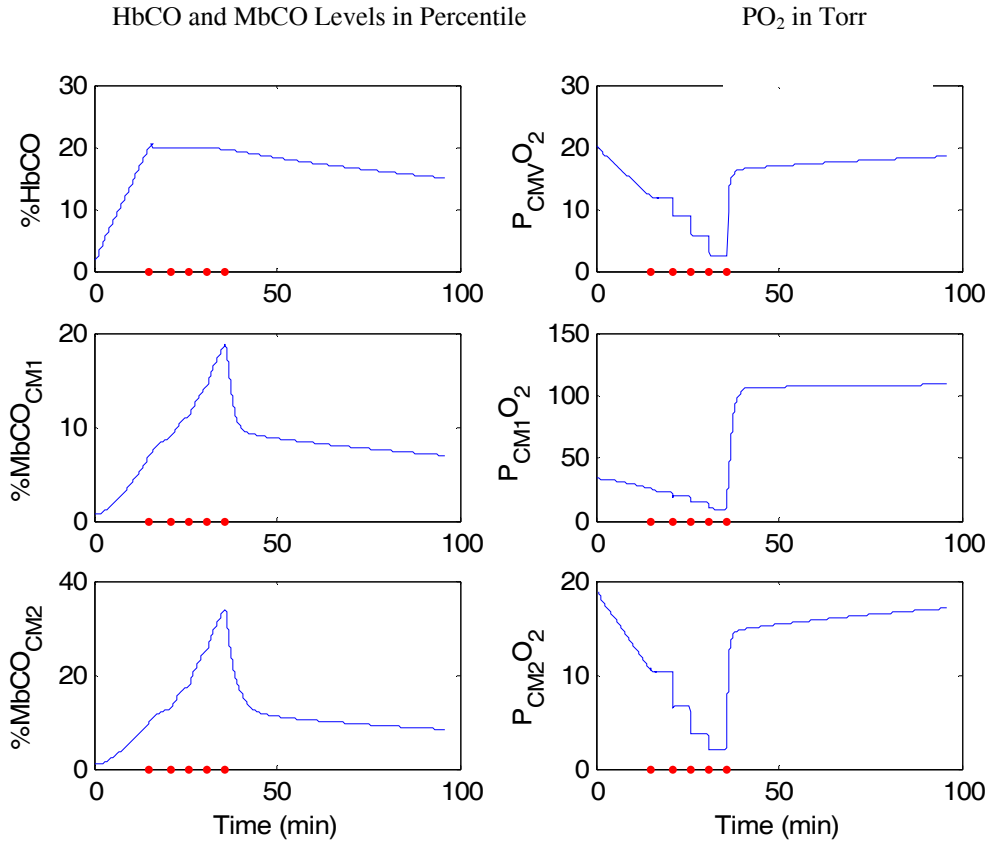

Figure 4.11: HbCO (20%) at Rest and Three Levels of Exercise Followed with 100% O_2 Treatment. Figure shows the predicted %HbCO levels in arterial blood, coronary venous partial pressure of O_2 ($PcmvO_2$), oxygen tension in cardiac subcompartment 1(Pcm_1O_2), MbCO levels in cardiac subcompartment 1(%$MbCOcm_1$), oxygen tension in cardiac subcompartment 2(Pcm_2O_2) and MbCO levels in cardiac subcompartment 2(%$MbCOcm_2$).The points (•) show the end times of 5 min sessions of rest, exercise 1, exercise 2, exercise 3 and start time of 100% O2 breathing for period of 60 mins. The sessions are simulated at baseline HbCO levels of 20%. Simulation time is plotted on the x-axis and the model predicted variables are plotted on the y-axis.

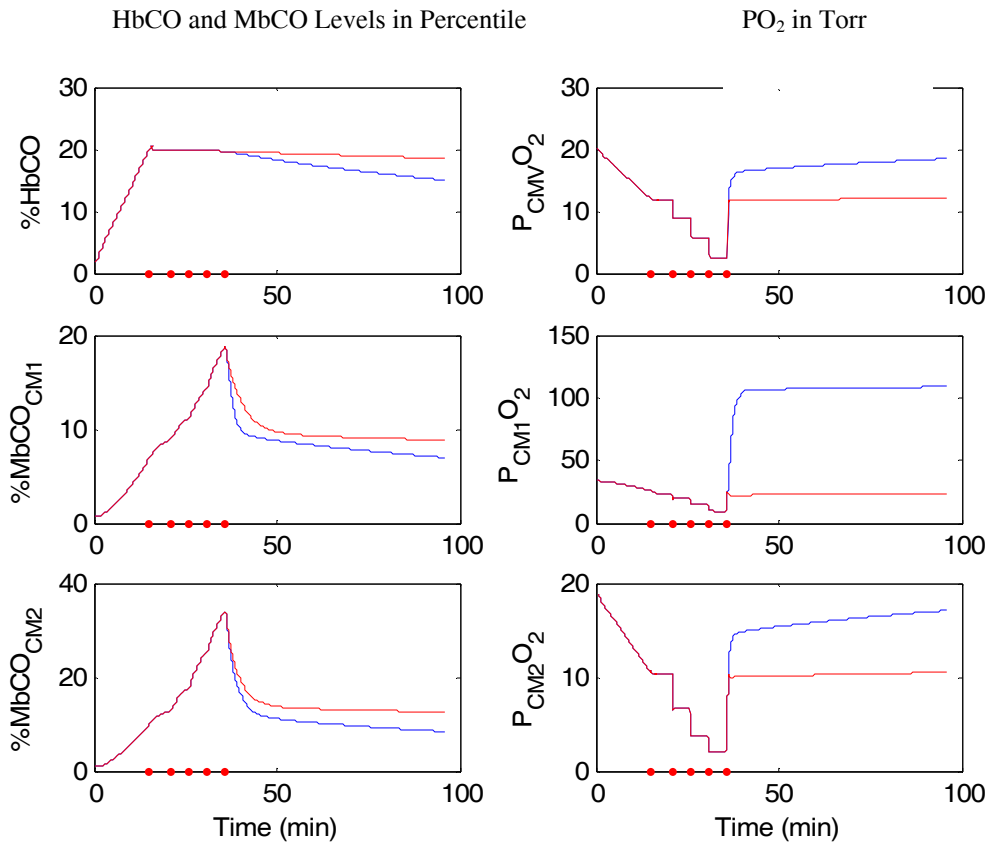

Figure 4.12: Comparison of 100% O2 and Room Air breathing after *CO* exposure. Comparison of 100% O2 VS. Room Air Treatment During 20% HbCO at Rest and Three Levels of Exercise: Figure shows the predicted %HbCO levels in arterial blood, coronary venous partial pressure of O_2 ($PcmvO_2$), oxygen tension in cardiac subcompartment 1(Pcm_1O_2), MbCO levels in cardiac subcompartment 1(%$MbCOcm_1$), oxygen tension in cardiac subcompartment 2(Pcm_2O_2) and MbCO levels in cardiac subcompartment 2(%$MbCOcm_2$).The points (•) show the start times of 5 min sessions of rest, exercise 1, exercise 2, exercise 3 and start time of 100% O_2 (blue) or room air (red) breathing for period of 60 mins. The sessions are simulated at baseline HbCO levels of 20%. Simulation time is plotted on the x-axis and the model predicted variables are plotted on the y-axis.

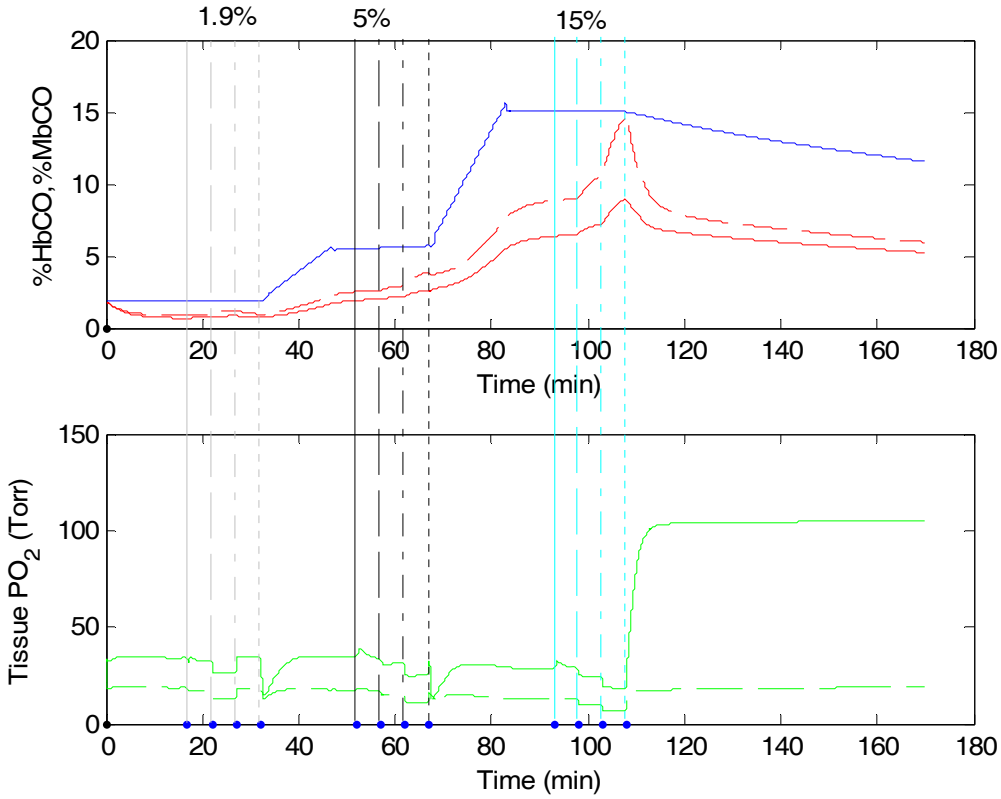

Figure 4.13: Baseline HbCO (1.9%) - HbCO (5%) - HbCO (15%) (Each session at Rest and Three Levels of Exercise) Followed with 100% O2 Treatment. Figure shows the predicted %HbCO (blue) levels in arterial blood, % MbCO levels in cardiac subcompartment 1(red solid) and cardiac subcompartment 2 (red dashed), oxygen tension in cardiac subcompartment 1 (green solid) and cardiac subcompartment 2 (green dashed). The point (•) shows the 5 min end time session of rest (-), exercise 1(--), exercise 2 (-.-.-) and exercise 3 (….). The HbCO level attained are **1.9%**, **5%** and **15%**. Simulation time is plotted on the x-axis and the model predicted variables are plotted on the y-axis.

CHAPTER 5
Discussion

This chapter summarizes the modifications made to the selected primary model (Figure 2.1), and discusses the limitations of the current model, issues related to parameter estimations, and concerns regarding the model validation and results.

The most essential step in modeling is to determine the exact need for the model. In this thesis we need the model to predict the amount of *CO* entering the blood and the cardiac tissues and to determine the effects of *CO* on tissue oxygenation ($PcmO_2$, tissue PO_2 of the cardiac compartment). Uptake of *CO* by blood can be determined by measuring the *COHb* levels in the venous blood. But it is difficult to measure *MbCO* (carboxymyoglobin) levels and tissue PO_2 in the human heart noninvasively. It is not expected from the model that the predictions be literally true but one can insist that the models provide useful approximations and their usefulness is measured against the value of the proposed objectives.

5.1 Model Modifications

The following modifications were made to enhance the model predictions:

5.1.1 Implementing O_2 Mass Balance Equations

The primary model (35) has been enhanced and modified in many aspects. *CO* impairs O_2 delivery to the tissues, so the primary issue is to predict impairment of O_2 delivery in the presence of *CO* and its effect on tissue PO_2. At the same time, the extravascular burden of *CO* depends on the O_2 levels of the tissue. That is, the *CO* - O_2 interaction involves a feedback loop, making it difficult to calculate the deliveries of O_2 and *CO* unless the O_2 mass balance equations are included. Thus to predict the *CO* load delivered, it is important to understand O_2 availability (PO_2) in the tissue. Hence mass balance equations for O_2 were added for all compartments of the model. In the initial model O_2 parameters were passed as constants, while in the current

model all O_2 parameters are calculated within the model. They are determined by solving simultaneous algebraic equations for oxyhemoglobin dissociation curves, and integrating the differential mass balance equations as described in Section 3.8 of chapter 3. We know that impaired O_2 delivery (*CO* hypoxia, hypoxic hypoxia, increased demand for oxygen while performing high stress exercise), and insufficient O_2 availability (coronary artery diseases, occlusion and ischemia) can disturb the homeostasis of energy metabolism (ATP production), blood flow and O_2 pressure gradients. Incorporating O_2 mass balance equations into the model has enhanced the ability of the model to predict O_2 tensions (which are difficult to measure experimentally) in the cardiac compartment and extended its application to simulate hypoxia, exercise and other conditions resulting in O_2 insufficiency.

5.1.2 Model Architecture and Flow Design

Modifying the model design to incorporate two subcompartments instead of a single compartment to represent the heart and the skeletal muscle helped in addressing the limitations related to O_2/*CO* diffusion and arterio-venous shunting, and the well-known fact that PO_2 is not the same throughout a tissue. Maintaining the balance of the O_2 supply and demand is very important in determining tissue oxygen tension. Attributing the skeletal muscle with regional flow and metabolic demand has allowed a better prediction of O_2 tension and *CO* load. Blood to tissue oxygen flux equations (Section 2.1.3, chapter 1) were modified by estimating them as a function of pressure gradients and the diffusion coefficient of O_2 (Section 3.2.2, chapter 3) instead of making an assumption of equality between O_2 flux and metabolic demand of the compartment (35). Also, in the current model, the nonlinear changes in O_2 and *CO* are being better accounted for due to improved algorithms (Section 3.8, chapter 3). I also implemented a new algorithm to solve the simultaneous algebraic equations to calculate the partial pressure of O_2 corresponding to the concentration of oxygen halfway between the inlet and outlet of the vascular subcompartment of the tissue (Section 3.8, chapter 3).

Adding a Cardiac Compartment to the Model: A two-subcompartment cardiac compartment was added to the model which is one of the main goals of the thesis.

The skeletal and cardiac muscle exhibit major differences in anatomy, blood flow, and O_2 demand. Unlike skeletal muscle, cardiac muscle works constantly to pump blood and it would, therefore, be inappropriate to lump the cardiac muscle with the resting skeletal muscle. Implementing a cardiac compartment made noninvasive predictions of *MbCO* levels and oxygen tension in the tissues possible. These values are difficult to measure experimentally (noninvasivly) in the human heart.

5.1.3 Physiological Relevance

Regulation of cardiac output with respect to increased blood *HbCO* (carboxyhemoglobin) levels was implemented into the model by means of a predictive equation (68, 69, 70). Blood volume was estimated for individual subjects by means of a regression equation reported in the literature (78). Estimating myocardial O_2 consumption and myocardial blood flow as a function of heart rate (increases in heart rate would increase the work load of the heart resulting in higher O_2 demand and increased O_2 supply to meet the increased O_2 demand) helps in calculating estimates close to physiological values with increased heart rate. Permeability surface area product increases linearly with increases in blood flow, contributing to efficient diffusion of O_2 in times of O_2 impairment; this phenomenon was also added to the model.

Model application: Applying these modifications has enhanced the capability of the model to make predictions of tissue oxygen tension in the human heart during hypoxic hypoxia, exercise, higher altitude and other O_2 insufficiency conditions.

5.2 Model Limitations

The foremost limitation of the model is that it has lumped component parameters causing aggregation errors. This results in loss of anatomic resolution and functional representation of the organ, such as in the case of cardiac component layers of the heart (epicardium, midmyocardium, endocardium) and chambers of the heart (atria and ventricles) which display varied heterogeneity in blood flow, O_2 consumption, capillary density and tissue volume. But if one had to model the cardiac

muscle tissue for the purpose of this thesis, the best choice to model would be the region of left ventricular mid myocardium, as this region is especially susceptible to injury during *CO* exposure due to its high O_2 demand and the fact that *CO* interferences cause impairment of O_2 delivery. The heart is a dual pump, the left and right sides of the heart pump blood separately, but simultaneously, into the systemic and pulmonary systems. In order to pump blood efficiently, it is required for the right and left atria to contract first followed immediately by contraction of the right or left ventricle, respectively. Spreading of action potentials from one myocyte to other and depolarization of the plasma membrane triggers contraction of the cardiac muscle. Thus, mismatch of O_2 supply and demand in the most susceptible left ventricular myocardial region may cause alterations in myocyte functionality (spreading of action potential) in this region, resulting in disruption of synchronous functionality (sequence of excitation) of the heart leading to arrhythmia. Thus, most of the predictive equations for determining the blood flow and O_2 consumption were built for the left ventricular region (left ventricle and intraventricular septum) of the heart. When the model was tested using experimentally measured values of regional myocardial blood flow and O_2 consumption as inputs, model predictions of experimental coronary venous PO_2 were able to match the experimental values obtained as seen from Figure 4.1 of chapter 4. However, limitations due to diffusion and capillary heterogeneity were overcome to an extent by implementing two subcompartments. This allowed intertissue diffusion of O_2 and *CO*. Also, using two subcompartments allowed indirect arterio-venous O_2 and *CO* shunting within the tissue. However, the design for incorporating two subcompartments instead of a single compartment raises issues regarding the maximum number of subcompartments that can be implemented. This concern must be considered in relation to the thesis objective of predicting injury to the heart due to *CO* exposure. Our main concern here is to model the *CO* uptake by the blood and the cardiac tissue. We are basically predicting the average *MbCO* and PO_2 levels of the tissue by means of the model. Thus by distributing cardiac muscle into two compartments, we assume that the first compartment is the tissue perfused with small arterioles and small venules, as well as by capillaries, and the second compartment is perfused by

capillaries. By making this assumption, we are making an attempt to understand the behavior of tissue with respect to its distance from a capillary, arteriole or venule during *CO* hypoxia. The *MbCO* levels and tissue PO_2 in the first compartment would reflect experimental measurements of values made near an arteriole while the second compartment predictions would be comparable to measurements made in the tissue close to a capillary. Also, one has to make a trade off between computational expense and achieved numerical accuracy in model predictions. Thus, considering all these issues, the two subcompartment cardiac model seems to be a reasonable compromise.

Another limitation of the model is that it does not incorporate details of metabolic pathways (change from aerobic to anaerobic metabolism), coupling with electro-physiological events (action potential due to K^+, Na^+ Ca^{2+} channels) regulating coronary venous PO_2 (156) and biochemical events (*Pcr, pH*). The human heart, being a complex system, has many other backup regulation modules to restore homeostasis during conditions of diminished O_2 availability such as *CO* exposure or increase in O_2 demand as in exercise. Regulation of cardiac output and heart rate was implemented into the model by adding predictive equations to estimate variations in both cardiac output and heart rate as functions of blood *HbCO* levels. The effect of vasodilatation and capillary recruitment on blood-tissue gas exchange was implemented by increasing the permeability surface area product (*PScm*) as a linear function of increases in blood flow to the heart. Apart from increases in cardiac output, HR and vasodilatation which are implemented into the model, there are other functional mechanisms taking place like the change of metabolic pathways from aerobic cycle to anaerobic cycle due to diminished O_2 levels in tissue, variation in blood pressure, etc. Also, the role of myoglobin facilitated diffusion and cytochrome C oxidase interactions with *CO* is not clear (130,150). Gutierrez (1986), Waller et al., (1988), Forster (1970), Holland (1970), Roughton (1964), Sharan et al., (1990) , Corpes et al., (1989) have shown the dependence of rate of *CO* uptake by blood on a series of chemical reactions of O_2 and *CO* in the blood (association and dissociation rate coefficients of O_2 and *CO* with Hb), *pH* and PO_2. Representation of kinetics of O_2 and *CO* with hemoglobin (Hb) in modeling O_2 and *CO* transport in the blood flowing through pulmonary and systemic circulation is difficult as the order of

magnitude of association and dissociation rate coefficients of O_2 and CO with Hb are unknown (Sharan et al.,1989). pH was found to have second order effect on CO uptake. The effects of PO_2 were considered in models built by Benignus et al., Bruce et al. and also in the present model (by solving for the oxyhemoglobin dissociation curves for Hb and Mb (myoglobin), Haldane equation and blood to tissue O_2 flux equations).

5.3 Parameter Estimation Concerns

Estimating the parameters for a model is a crucial issue. Models have several parameters, some of which may greatly impact the model behavior while other parameters may not affect the model behavior at all. The impact of the parameters on the model behavior becomes important when there is scarce or no data available for the parameters. In such cases sensitivity analysis is conducted for the parameters to determine their impact on model behavior. For the cardiac compartment in the model, average values from experimental data were considered for most of the parameters. Predictive equations were developed for estimating myocardial blood flow and oxygen consumption.

Prediction formulas were also used to estimate cardiac output and heart rate when actual values were not available. Subject variability is one major concern in using average values or prediction equations to estimate parameters. The estimates made for the parameters using predictive formulas would be valid for a specific group (age, ethnicity, gender, geographical area being at higher altitudes or below sea level, method of measurement) from which they were developed. Appling a prediction equation or an average value obtained from a specific subject group to a varied population set may tend to underestimate or overestimate the model predictions. However, after developing these formulas, their statistical significance and validity were tested for data which were not used for developing the relationships (Section 3.5, chapter 3). For predicting the myocardial O_2 consumption and myocardial blood flow, a more reliable prediction could have been made by calculating the estimates from heart rate-blood pressure product. But blood pressure was unavailable for many databases we planned to simulate although heart rate was a parameter which was

readily available and can also be calculated from total body metabolic rate. But no such relationship could be applied to estimate blood pressure as it is a greatly varying physiological parameter. Predicting myocardial O_2 consumption and blood flow as functions of cardiac output seems to be an alternative estimation approach, but information supporting functional relations between cardiac output, myocardial O_2 consumption and blood flow is currently unavailable in the literature.

Estimating a value for resting permeability surface area product for the two cardiac subcompartments was very difficult due to unavailability of data. The initial guess values were obtained from models from Beard and Bassinghwaite and then the resting values were scaled to match the size of the tissue, type of the tissue, and the species. The permeability surface area products increased as a linear function of blood flow. This was to indirectly implement coronary vasodilatation and capillary recruitment into the model.

The values for distribution of volume in each of the compartments (Fvcm) and for the fraction of venous cardiac blood compartment 3 perfusing the tissue compartment 1 was estimated by analyzing data available on vascular distribution in heart, coronary physiology, and statistics on density of arterioles, capillaries and venules in the heart (103,104). The sensitivity analysis of these parameters is shown in table 3.8 of chapter 3, so that one can estimate the deviations in the predicted model values for variation in the parameters (to which model predictions are sensitive).

5.4 Model Validation Concerns

The major concern in validating the model was unavailability of human data for testing the model predictions. Animal data, however, were available for model validation. Data are shown in table 4.1. One can see from the table the extent of variability and heterogeneity in the data available. Though data for dogs, swine and rats were available, the experimental values obtained from experiments involving swine were emphasized due to the similarity with human coronary anatomy and vasculature. Also, most of the data available are from anesthetized animals. Type of anesthesia used in the experiment can have a significant effect on the experimental

values measured (96). Another issue related to the experimental data available is the method of measurement. Most of the methods available for measuring myocardial tissue O_2 tension are invasive. Reported values may have 10- 15% error due to the measurement electrodes consuming O_2, errors due to diffusion of oxygen from blood or tissue to the electrode, shift in electrode position due to beating of the heart etc. Also insertion of the some electrodes (like needle electrodes) causes damage to tissue and cells and bleeding, thereby possibly contaminating the measured values. From the Figures 4.1-4.3 shown in chapter 4, it can be seen that coronary venous PO_2 and compartmental tissue PO_2 model predictions are close to the experimental values. Also, the predicted myocardial tissue PO_2's are in agreement with other models (95, 101,104) that utilized a single heart compartment or a distributed (finite-element) model.

5.5 Concerns Related to Simulated Experiments

In this model heart rate is required to estimate myocardial O_2 consumption and blood flow. In the experimental data provided by Benignus et. al and Burge & Skinner, heart rate information is unavailable. Heart rate might have been estimated by using the regression equation described in Section 3.5.3 of chapter 3, where heart rate is calculated as a function of total body O_2 consumption. But total body O_2 consumption was not measured by the investigators (Benignus et. al and Burge & Skinner), thus heart rate for simulations in Section 4.2.1- 4.2.3 was estimated using an average metabolic rate of 0.0032 ml/gm/min. Total body O_2 consumption, heart rate, myocardial O_2 consumption and blood flow estimated in the model may differ from actual values at the time of experiments. Errors in estimation of the above parameters, especially heart rate, may have significant effects on the model predictions. For simulations having exercise sessions (Section 4.2.4), *CO* diffusion coefficient of lungs (*DLCO*), shunt fraction SF are assumed to be constants. Zavorsky et al. (2004), Demirjian (1980) and Paoletti (1985) have reported age dependent changes in *DLCO* with varying exercise intensity. Also the shunt fraction is reported to increase with increases in exercise intensity (159, 160).

5.6 Simulation Findings

In all the simulations of Section 4.2, except for the simulation in Section 4.2.3 (where the subject rebreathes *CO* during 100% O_2), the *MbCO* levels of cardiac subcompartment 2 ($MbCOcm_2$) are higher than the *MbCO* levels in subcompartment 1 ($MbCOcm_1$). Higher *MbCO* levels in subcompartment 2 may be explained as follows: when *CO* is inhaled, it diffuses through the lung and binds with *Hb* in blood, resulting in elevated *HbCO* levels. *CO* then leaves blood and diffuses into the cardiac subcompartment 1, resulting in increased *MbCO* levels in the compartment initially. *CO* then diffuses into subcompartment 2 from the blood subcompartment 2 and also from the tissue subcompartment 1, thereby resulting in higher *MbCO* levels in subcompartment 2. Also, with increase in blood *HbCO* levels the cardiac output increases. Increased cardiac output would result in increased myocardial O_2 consumption and myocardial blood flow. This means that *CO* delivery to the heart increases with increase in cardiac blood flow, resulting in increased myocardial O_2 consumption and fall in tissue PO_2, facilitating an increase in *MbCO*. This effect is more significant in the subcompartment 2 as the amount of *CO* delivered, blood flow and metabolic rate of this subcompartment is greater than subcompartment 1 resulting in lower tissue PO_2 and higher *MbCO* levels. In the case of the simulation of *CO* rebreathing during 100% O_2, the *MbCO* levels in the two subcompartments reach equilibrium after few minutes as seen in Figure 4.7 of chapter 4. The *HbCO* and *MbCO* levels are 10% and 4.5%, respectively, and the PO_2 in the cardiac subcompartments decreases by ~1-2 Torr from base line. The reason for the heart compartments not being hypoxic during *CO* rebreathing is that the subject is breathing 100% O_2. During hyperoxia, dissolved O_2 plays a major role in tissue oxygenation. At the end of the simulation although the subject breaths 100% O_2, a significant increase in PO_2 of cardiac subcompartment 2 is not seen.

Another interesting observation in all the simulations discussed in Section 4.4.4 is that the *MbCO* levels of the two tissue subcompartments increase with exercise, though the *HbCO* levels are maintained constant. This means that increase in exercise increases the *CO* load on heart due to increased blood flow. Also, increased intensity of exercise causes a rise in O_2 consumption, requiring higher O_2 demand, thus

resulting in tissue hypoxia. This observation also supports the reported observations of a higher risk of cardiac injury in a working population exposed to *CO*.

The developed model is capable of predicting myocardial tissue and blood PO_2 during all transients (different exercise sessions at different *HbCO* levels, long and short *CO* exposures etc) in the simulations. However, tissue PO_2 in cardiac subcompartment 2 being maintained at 19 torr during hyperoxia (administration of 100% O_2 after 3 graded levels of exercise with 20% HbCO) after 60 min of breathing 100% O_2 seems to be a concern. Prediction of lower PO_2 during hyperoxia may be due to the following reason: insufficient treatment time (simulation can be done by increasing the treatment time from 60 mins to 300-400 mins and see if the PO_2 in subcompartment 2 increases), or due to errors in model parameters in the treatment protocol (as parameters were not measured by the investigators).

Decreases in coronary venous PO_2 with increased exercise intensity have been reported (156). The cardiac compartment venous PO_2 decreases with exercise as seen from Figure 4.5. However changes in coronary venous PO_2 during combined exercise and *CO* exposure have not been reported in human or swine in the current literature. Thus validating the simulation results becomes difficult. Tissue PO_2 of 6-7 Torr have been reported in mild exercising skeletal muscle tissue of humans whose steady state resting values at baseline *HbCO* levels are 35 Torr (158). An average myocardial tissue PO_2 of 3.36 Torr at the end of third stage of moderate exercise (E3) at 20% HbCO levels seems reasonable. Prediction of tissue PO_2 by the model in the range of 0.5-1 Torr for a time span of 8-9 mins may be considered lethal (75,130,132,133). The model can be validated further if experimentally measured data for myocardial blood and tissue PO_2 would be available in humans or swine during *CO* exposures at rest, exercise, hyperoxia and O_2 hypoxia.

As seen in Figure 4.5 there is a sharp increase in the *MbCO* levels of the cardiac compartments with increase in *HbCO* levels of the blood, whereas the *MbCO* levels of the skeletal muscle increase gradually after the *HbCO* blood levels decrease. This sharp immediate increase in *MbCO* levels suggest that the *CO* released from hemoglobin binds to the myoglobin present in the cardiac muscle. Also the cardiac

tissue PO_2 decreases with increases in *HbCO* and *MbCO* levels, suggesting greater risk of injury than skeletal muscle. The cardiac muscle has higher O_2 consumption, blood flow and capillary density than that of resting skeletal muscle and unavailability of O_2 store would result in greater degree of hypoxia. As seen in Figure 4.6, during long-low *CO* exposure the *MbCO* levels of the cardiac compartment increase with increase in *HbCO* levels and after a certain amount of time exceed *HbCO* levels in the blood, suggesting that myocardial tissue hypoxia is the combination of impaired O_2 carrying capacity of blood and impaired O_2 storage in myoglobin. Thus one can confirm that the response of various tissue to *CO* exposure is different, based on their functionality and oxygen consumption. Thus it would not be valid to apply the same response to all the tissues.

The hypothesis tested for the thesis was that during *CO* exposures and subsequent therapies, the temporal changes of *%MbCO* in the heart differ from those of *%HbCO* was tested. From the various simulations, it was found that *HbCO* and *MbCO* levels in the heart greatly depend on the type of *CO* exposure. In the case of short-high *CO* exposures, the *MbCO* levels positively correlate with *HbCO*, while in long-low *CO* exposures, the *MbCO* levels increase with increasing *HbCO* initially but later increase to levels higher than blood *HbCO* levels. During exercise though the *HbCO* levels are constant, the *MbCO* levels increase resulting in decreased tissue oxygen tensions. Thus, the results obtained support the hypothesis made. The *CO* load is related to both *%HbCO* in arterial blood perfusing the heart and *%MbCO* in cardiac tissue. In long-low *CO* exposures myocardial hypoxia occurs due to impaired O_2 transport (decrease in $\%HbO_2$) and unavailability of O_2 storage ($\%MbO_2$) where as in short-high *CO* exposures, tissue hypoxia is mainly due to impaired O_2 transport and in exercise protocols the cardiac hypoxia is mainly due to unavailability of O_2 storage (*%MbCO*). Thus basing the treatment on the currently-used clinical indicator of potential injury (i.e., *%HbCO*) will be inaccurate and possibly misleading. Thus, determining the total *CO* load on the cardiac cells (or its effect on tissue PO_2) is likely to be a better predictor of injury.

Overall, the developed model proves to be an excellent tool for predicting extravascular burden (*MbCO* levels and tissue PO_2) of *CO* on human heart.

CHAPTER 6
Conclusion

Noninvasive measurement of myocardial tissue PtO_2 and *MbCO* levels during or after *CO* exposure is difficult. The main goal of the thesis was to develop a model that is capable of predicting extravascular burden of *CO* in the human heart and its effects on tissue oxygenation. A multi compartment model was developed consisting of six major compartments: 1.The arterial blood, 2. The Lungs, 3. Skeletal Muscle with two subcompartments, 4. Non-muscle tissue, 5. Cardiac Muscle with two subcompartments and 6. Mixed venous blood compartments. Mass balance equations are written for O_2 and *CO* for each of these compartments. In each blood compartment, to determine PO_2, *PCO* and O_2 flux we solve three simultaneous algebraic equations: the oxyhemoglobin dissociation curve, Haldane's equation, and the blood-to-tissue flux equation for oxygen. Myocardial blood flow and oxygen consumption are estimated from regression equations developed for the thesis. The model is simulated on a Windows XP system using *ACSL*™ software which is capable of solving nonlinear differential equations. Sensitivity analysis is performed and the myocardial tissue PO_2 (P_tO_2) is shown to be sensitive to myocardial blood flow, myocardial oxygen consumption, volume distribution fraction of the tissue, diffusion coefficient of O_2 and the permeability surface area product. The developed model was used for the simulations to test the validity of the predicted variables of the cardiac compartment with published observations on human subjects and anesthetized animals. The model was validated for conditions of normoxic rest, hypoxic rest, hypoxic exercise and hyperoxia with regard to its predictions of coronary venous PO_2 and tissue PO_2. Simulation of short-high concentration *CO* exposure, long-low concentration *CO* exposure, *CO* rebreathing during 100% O_2 administration and *CO* exposure during rest and exercise sessions for different levels of *HbCO* have been analyzed. In short-high concentration exposures, the tissue *MbCO* levels increase sharply unlike in long-low concentration exposures where the *MbCO* levels increase gradually. The tissue PO_2 levels seem to be correlated more with %*HbCO* levels than with %*MbCO* levels in short-high *CO* exposures. This

would suggest that there is impaired O_2 delivery to tissues due to impaired O_2 transport. During long-low CO exposures, the tissue PO_2 correlates with MbCO levels i.e., it decreases with increase in *MbCO*. In the simulation where subject rebreathes *CO* during 100% O_2 administration, the tissue PO_2's correlate with %*HbCO* levels and %*MbCO* levels increase with corresponding decreases in %*HbCO* levels suggesting that during hyperoxia, *CO* dislodged from hemoglobin is taken up by myoglobin. During exercise, the tissue PO_2's are strongly correlated with *MbCO* levels, suggesting that myocardial tissue hypoxia occurs during elevated levels of *MbCO*. Also, during room air treatment the *MbCO* and *HbCO* levels fall slowly compared to treatment with 100% O_2, indicating that 100% O_2 can be an effective treatment for CO hypoxia in cardiac muscle. The hypothesis that *CO* load *(%HbCO*, *%MbCO*) delivered to the heart impairs oxygen delivery further affecting the tissue oxygen tension (PtO_2). Thus during *CO* exposures and therapies, the temporal changes of %*MbCO* in the heart differ from those of %*HbCO* depending on the type of exposure. %*MbCO* levels can increase when %*HbCO* is maintained constant (during exercise) or is decreasing (in case of hyperoxia treatment). This *CO* load is related to both *%HbCO* in arterial blood perfusing the heart and *%MbCO* in cardiac tissue. The correlation of *%HbCO, %MbCO* and tissue PO_2 should be clearly understood for different types of *CO* exposure to consider them as clinical indicators of potential injury. The decreasing tissue PO_2 in the cardiac muscle during short-high *CO* exposure correlates with increasing %*HbCO* levels while the %MbCO of skeletal muscle shows a correlation with %*HbCO* after a delay. The %*MbCO* levels of the cardiac compartment show sharp increases unlike gradual increases as seen in skeletal muscle. This is a very important observation as it emphasizes the fact that cardiac muscle is at higher risk than resting skeletal muscle. During elevated %*MbCO* levels, the PO_2 stores may diminish resulting in the tissue being further hypoxic.

The cardiac muscle is a rigorously working muscle with high metabolic demands for oxygen. Myoglobin provides the storage site for O_2 in times of increased O_2 demand. During *CO* exposure the storage site of O_2 is lost as *CO* binds to myoglobin, resulting in increased %*MbCO* levels and tissue oxygen deprivation, thus resulting in severe hypoxia. A tissue PO_2 in the range of 0.5 to 1 Torr is assumed to be indicative

of injury. O_2 is needed for the heart to maintain its functions and lack of O_2 supply can cause severe injury to the tissue. Thus the risk of injury would be greater when someone is exercising and is exposed to *CO*. Also in a patient population with congestive heart failure or coronary artery disease where myocardial perfusion is not normal, exercise or exposure to *CO* may be fatal to the myocardial tissue.

Thus, determining the *CO* load on the cardiac tissue seems to be an important predictor of injury. The model proves to be an effective tool for noninvasive determination of the *MbCO* levels and oxygen tensions in a human heart during and after *CO* exposure.

CHAPTER 7

Future Work

1) Compare *CO* dose to myocardium with occurrence of abnormal features in ECG (ElectroCardioGram). Myocardial hypoxia during *CO* exposures has been reported to produce changes in ECG (S-T segment elevation, QT dispersion, T wave changes). The extent to which the *CO* load (*HbCO* and *MbCO* levels) contributes to ECG alterations seen in *CO* poisoning victims is unknown. Assesing the correlations between the occurrence of predicted peak *MbCO* and *HbCO* levels with occurrence of abnormalities in ECG will aid in understanding the *CO* poisoning related increased risk of cardiac injury.
2) Investigate effects of *DcmCO* (diffusion coefficient of *CO* for cardiac muscle) in exercise. Determination of *DcmCO* is difficult. The time for blood-tissue equilibrium of partial pressure of *CO* is dependent on *DcmCO*. The rate of exchange of *CO* between tissues and blood is determined by the value of *DcmCO*, thus determining the values for this parameter is important. If a large value of *DcmCO* better explains data, it would imply that the equilibrium between tissue and blood occurs at a faster rate, but if a smaller value for *DcmCO* would better fit the data, then it would support the concept of slow equilibration between tissue and blood. Understanding the effects of *DcmCO* during exercise will result in further understanding the value for *DcmCO*.
3) Prediction of the extravascular burden for all subjects of references 69,154,155. Applying the model to predict extravasuclar burden and assessing the produced response for different types of *CO* exposure conditions and population will help in improving the validation of the model. Also, if the same kind of response is displayed by the subject population, then the result can be better trusted. By fitting the model to a number of individuals, we can determine the mean as well as the range of responses in the normal population.
4) Implement changes in *DLCO* (diffusion coefficient of *CO* in lungs) and *SF* (shunt fraction) with exercise. Adding effects of changing *DLCO* and SF into the model

as function of exercise intensity, age, gender etc. will further enhance the accuracy of model predictions.

5) Predict *CO* burden on different regions (epicardium, endocardium) and chambers of the heart. Knowing that the heart displays heterogeneity in blood flow, capillary density, oxygen consumption etc., it would be interesting to predict cardiac injury in various regions to determine the region at higher risk for injury with *CO* exposure.
6) Conduct experiments in swine to measure myocardial O_2 consumption, myocardial blood flow, heart rate, blood lactate levels, weight of the heart, multiple measurements of myocardial tissue PO_2 in various regions of the heart, coronary venous PO_2, myocardial arterial PO_2 during rest, graded levels of exercise, hypoxic hypoxia and *CO* hypoxia in order to validate the model. There is scarce data available in the literature for efficiently validating the model. Thus, if one conducts an experiment and measures all the above parameters, then the model can be better validated and also determination of parameters like permeability surface area product etc., will be more reasonable.
7) Design effective treatment protocols. As seen from the results, the *CO* load would differ with type (short-high, long-low or during exercise) of *CO* exposure, thus it would not be advisable to treat all the *CO* - poisoned victims with the same protocol. Using the model to simulate different treatment protocols that may include mixed session of room air, 100% O_2 breathing or hyperbaric treatment to improve tissue oxygenation will be a effective approach for efficient treatment strategies. The model may use the *CO* victim's parameters and simulate different treatment protocols, which would be quick and easy to accomplish unlike conducting clinical trials.
8) Estimate concentration and duration of *CO* exposure after the fact. Knowing the concentration and time for which the victim was subjected to *CO* would better determine the load of *CO* on organs at high risk like heart and brain during exposure and treatment. If it is a short *CO* exposure at high concentrations, then myocardial hypoxia would be produced due to impaired O_2 capacity of blood unlike in long-low *CO* concentration *CO* exposures, where tissue hypoxia is

produced due to impaired O_2 transport accompanied with impaired O_2 storage as hemoglobin as well as myoglobin are bound to *CO*. Thus, estimating concentration and duration of *CO* exposure would be very crucial in designing an effective treatment protocol. .

9) Implement equations for CO_2 in to the model. During both exercise and hypoxic hypoxia, the tissue PO_2 are dependent on the partial pressure of *CO*.. Thus implementing equation for CO_2 into the model will enhance the model to better predict the tissue PO_2 and also conditions of hypoxic hypoxia can be better predicted. Also the effects of *pH* can be implemented into the model. These additions will result in enhanced model predictions as the oxygen dissociation curve which is solved to determine tissue PO_2 and *PCO* would be dependent on CO_2 and *pH*.
10) Modify the model to predict myocardial oxygen tension in patient population with coronary artery diseases etc. The model can also be used to predict myocardial O_2 tensions apart from using it for predicting *MbCO* and *HbCO* levels. Generally in patients with coronary artery diseases, there is decreased blood flow to the heart due to narrowed or blocked arteries. Thus the blood flow to the myocardium can be reduced depending on the degree of blockage and myocardial oxygen tensions can be predicted. Also, conditions of exercise can be simulated for this population and the predicted myocardial tissue PO_2's can be correlated with abnormalities in ECG.
11) The model can also be modified for predicting outcomes of hyperbaric O_2 treatment. It is often debated if hyperbaric (breathing 100% O_2 at 2-3 ATA) treatment would have better treatment outcomes than hyperoxia treatment (breathing 100% O_2).
12) Implementing metabolic pathways into the model may be suggested to understand the effects on model prediction with changes in metabolic cycles from aerobic to anerobic during exercise, hypoxia or ischemia.
13) Introduce interactions of cytochrome c oxidase with *CO*. Cytochrome c oxidase is also known to bind irreversibly with *CO*. Understanding the contribution of this protein will further enhance the knowledge database for *CO* toxicity.

Appendix

Skeletal muscle mass distributed to trunk muscle, leg muscle and arm muscle:

Oxygen consumption for the skeletal muscle was found to be 250% of total body oxygen consumption at rest when calculated in the simulated model. According to the following books;

1. An introduction to cardiovascular physiology by J.Rodney Levick
2. Medical physiology by Philip Bard

Muscle metabolic rate (MRO_2m) should be 20% of the total body oxygen consumption (MRO_2). It is known that metabolic rates of leg, arm and trunk muscles are different. Thus, to incorporate different metabolic rates of muscle in various regions we distributed the skeletal mass into three muscle volume compartments namely leg muscle volume, arm muscle volume and trunk muscle volume. Distributions of skeletal mass were calculated from the references 105-115. From the papers we had data for lean mass of trunk, arms, legs, upper legs, upper arms and also total skeletal mass. Data were entered only from normal men and women. The abbreviations used are as follows:

%asm: percent arm skeletal mass

%tsm: percent trunk skeletal mass

%lsm: percent leg skeletal mass

The final result obtained after taking average of data obtained :

MEN: WOMEN:

%lsm	*%asm*	*%tsm*	%lsm	%asm	%tsm
46.63981	*15.66698*	*37.76795*	49.52738	13.96499	36.50763

Validation for the relationship obtained was done by selecting a random subject record from the database and calculating the values using the obtained relationship and comparing them with the measured values. The differences in the values can be explained as follows:

1. Total lean soft tissue included muscle as well as soft tissue
2. Reference involved study on Japanese subjects in the age group of 19-24yrs. We know that muscle mass is effected with age and also ethnicity.

3. Also one can consider errors due to averaging, pooling data from various sources which have different methods of measurement, varying number of subjects, different age population, ethnicity etc.

gender	Men (total lean soft tissue= 57.8kg)			Women (total lean soft tissue= 40kg)		
parameter	lsm	asm	tsm	lsm	asm	tsm
measured	20.9	8.7	28.2	14.8	4.9	20.3
calculated	26.9	9.05	21.82	19.8	5.58	14.6

Prediction equation for cardiac output:

Equation to predict the cardiac output in the initial model was based on gender and body weight. $Q^{\cdot} = (54.1 + 7.9G).BW + 1400 - 200.G$

But after modifying the model, we intended to simulate experiments that involved exercise, CO exposure etc. It was clear that cardiac output $Q^{\cdot}$ changed with exercise, postural changes and age. Thus to implement variation of cardiac output, we implemented the following prediction equation,

$Q^{\cdot}$ =3.186+7.346* (MRO_2)-0.535*(MRO_2)^2

Where, cardiac output $Q^{\cdot}$ is calculated as a quadratic expression function of total body metabolic rate (MRO_2). Also this equation was very helpful in predicting the cardiac output when experimental data did not provide the value. Literature survey established the fact that cardiac output can best be predicted as a function of total body oxygen consumption (references). Thus, to work on this idea, various journals were searched for data from humans at rest and exercise for cardiac output and total body oxygen consumption (MRO_2).The inclusive criterion for the data was that it was considered from healthy, non smoking untrained individual subjects. The method of measurement for MRO_2 was either Fick's method or the Douglas bag method. Cardiac output was calculated from dye dilution method, Fick's method etc. Though the measurement techniques were different, the values obtained for cardiac output for specific oxygen body consumption did not vary significantly. Data from references 137-144 were used to implement the relationship. The reason for building a quadratic expression was to have a

regression relation with strong statistical significance and also cardiac output is known to reach a plateau as maximal body oxygen consumption is reached.

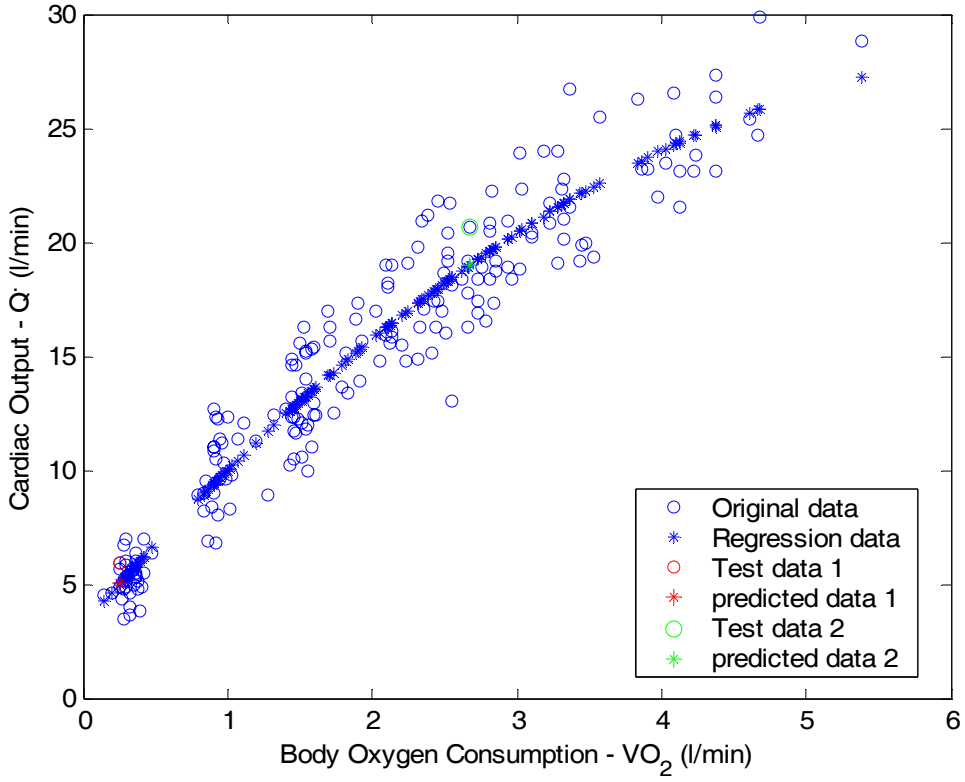

Figure above shows the plot of the data (o) used to build the relationship and predicted data (*). On the X-axis we have the myocardial O_2 consumption and on the Y-axis is the cardiac output. Test data points (o,o) were considered from experiments whose data were not included in building the relation to check with the values(*,*) obtained from the predictor equation. Cardiac output ($\dot{Q}$) and myocardial oxygen consumption (MRO_2) are specified and calculated in the unit of liter/min. When implemented into the model they are converted into milliliter. MRO2 is in STPD and is converted to BTPS in the model.

Order of relation	Regression coefficient	Error of estimate
$\dot{Q} = b.MRO_2 + c$	0.907	1.949
$\dot{Q} = a.(MRO_2)^2 + b.MRO2 + c$	**0.962**	**1.75**

Prediction equations for Heart rate: In most of the experiments, heart rate was mentioned. But in the case of data where information regarding heart rate was missing, it

was estimated from the following equation: Heart Rate (HR) =42.819+68.884*(MRO2)-8.26* $(MRO_2)^2$

The main purpose for developing a prediction equation for heart rate was to estimate the myocardial blood flow and myocardial oxygen consumption for the cardiac compartment discussed in Chapter 3. Heart rate is often considered to be a predictor of extent of myocardial activity. Heart rate and blood pressure product would have been a better predictor of myocardial parameters like myocardial blood flow and oxygen consumption than just heart rate. But it was difficult to predict blood pressure from body oxygen consumption or cardiac output due to unavailability of sufficient data. Thus, heart rate was expressed as a function of MRO2. The following references (68-70), were considered to obtain a relationship between heart rate (HR) and body oxygen consumption (MRO2).

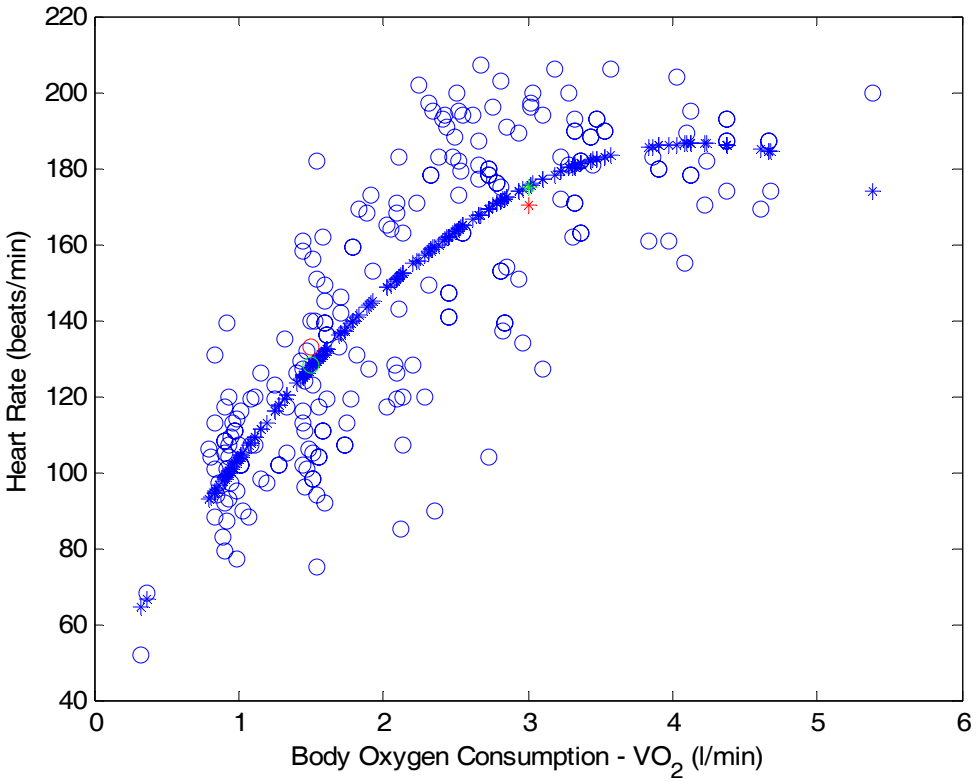

Figure above shows the plot of the data (o) used to build the relationship and predicted data (*). On the X-axis we have the myocardial O2 consumption and on the Y-axis is the Heart rate. Test data points (o,o) were considered from experiments whose data was not

used to estimate the above regression relation to check with the values(*,*) obtained from the predictor equation.

Order of relation	Regression coefficient	Error of estimate
HR = b.MRO_2 +c	0.592	23.678
HR = a.$(MRO_2)^2$+b.MRO2+ c	**0.664**	**21.5**

Predicting percent increases in cardiac output ($\dot{Q}$) and heart rate (HR) as functions of percent carboxyhemoglobin (%Δ COHb) levels in blood:

There is a reported increase in cardiac output and heart rate with increase in carboxyhemoglobin levels in blood (68, 69). While simulating experiments involving carbon monoxide (CO) exposures, increased cardiac output and heart rate due to increased carboxyhemoglobin levels in the blood had to be taken into account. These increases were implemented by introducing the following equations

$$\%\Delta\dot{Q} = 0.572 \times (\%\Delta COHb)$$

$$\%\Delta HR = 0.012 \times (\%\Delta COHb)^2 + 0.26 \times (\%\Delta COHb)$$

The cardiac output $\dot{Q}$ and heart rate (HR) were increased by %ΔQ and %ΔHR, respectively, calculated from the above equations in the discrete section of the program.

Data for cardiac output, heart rate and carboxyhemoglobin (up to 50%) were tabulated from references 68,69.

Linear regression was performed on the data. Outliers of the data were removed. Statistical significance of the relationships was tested and the best relation was chosen and implemented into the model to incorporate the changing effects in cardiac output and heart rate with increasing CO levels in the body.

Cardiac output and Carboxyhemoglobin levels in blood:

Order of relation	Regression coefficient	Error estimate
$\%\Delta\dot{Q} = a(\%\Delta COHb) + c$	0.377	15.155
$\%\Delta\dot{Q} = a(\%\Delta COHb)^2 + b(\%\Delta COHb) + c$	0.178	15.184
$\%\Delta\dot{Q} = a(\%\Delta COHb)$	**0.713**	**12.483**

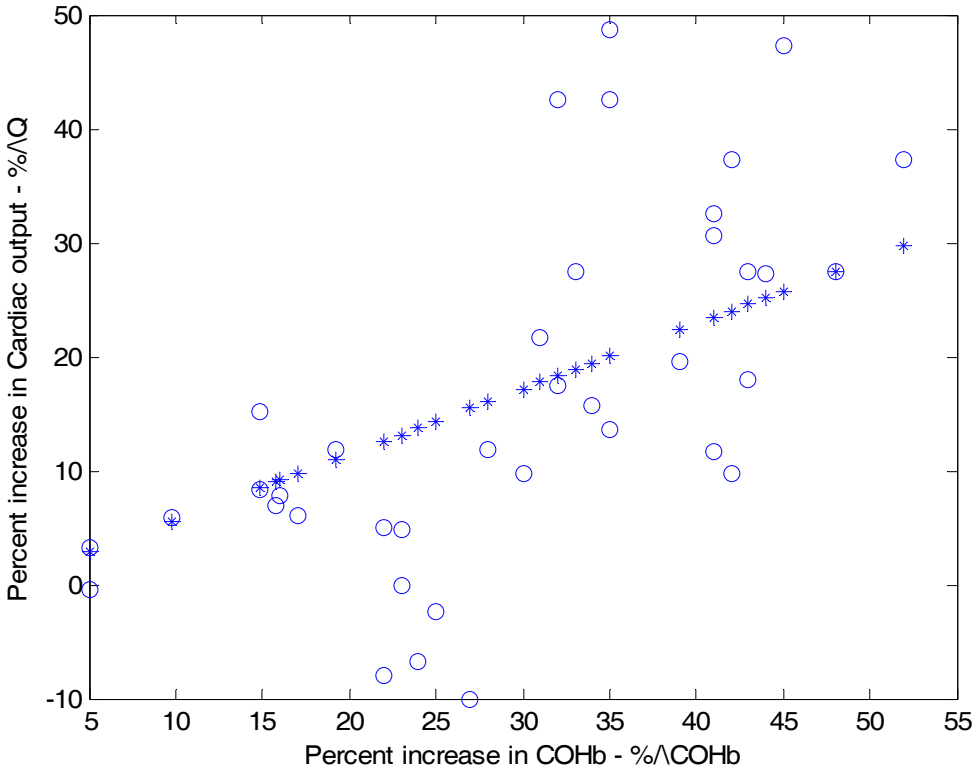

Figure above shows the plot of the data (o) used to build the relationship and predicted data (*). On the X-axis we have the percent increase in carboxyhemoglobin levels of blood, %ΔCOHb and on the Y-axis is the percent increase in cardiac output, %ΔQ˙.

Cardiac output and Carboxyhemoglobin levels in blood:

Figure below shows the plot of the data (o) used to build the relationship and predicted data (*). On the X-axis we have the percent increase in carboxyhemoglobin levels of blood, %ΔCOHb and on the Y-axis is the percent increase in cardiac output, %ΔHR.

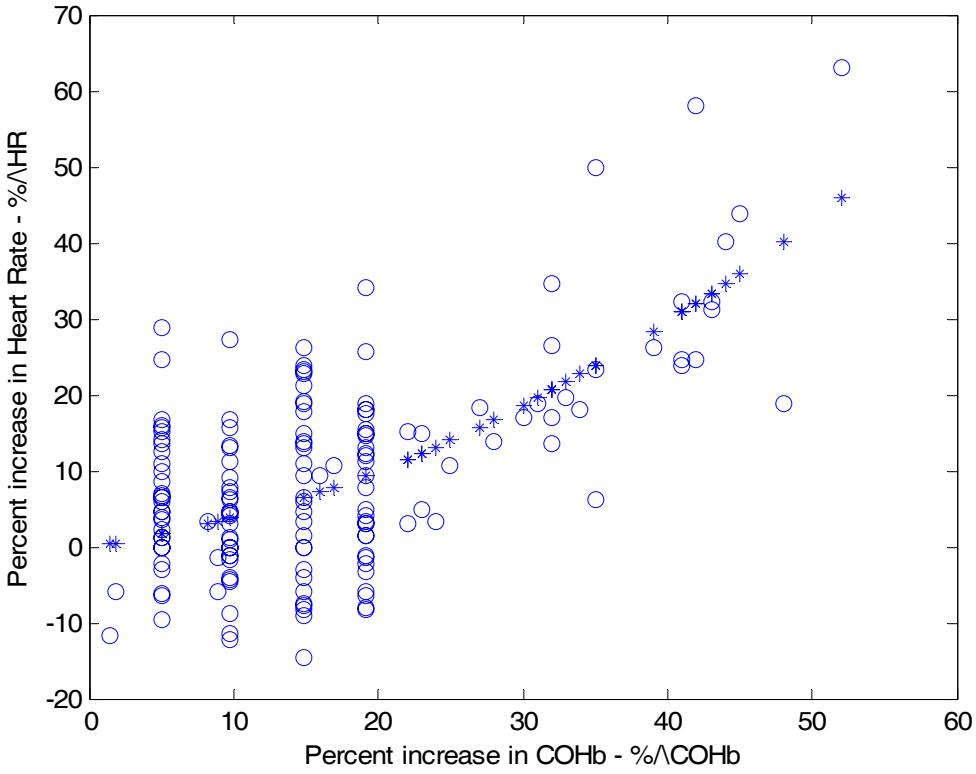

Order of relation	Regression coefficient	Error estimate
$\%\Delta HR=a(\%\Delta COHb)^2+b(\%\Delta COHb)+c$	0.422	9.962
$\%\Delta HR=a(\%\Delta COHb)^2+c$	0.422	9.961
$\%\Delta HR=a(\%\Delta COHb)^2+b(\%\Delta COHb)$	**0.612**	**9.958**

References

1. James A. Raub., Robert S. Chapman., Air Quality Criteria for Carbon Monoxide., National Center for Environmental Assessment., US Environmental Protection Agency, October 1999.

2. Environmental Health Criteria For Carbon Monoxide, Environamental Health Criteria 13, Carbon Monoxide, World Health Organization, 1979.

3. Study: Unintentional Non-Fire-Related Carbon Monoxide Exposures — United States, 2001–2003.

4. M Tucker, B Eichold, MD, Carbon Monoxide Poisonings After Two Major Hurricanes --- Alabama and Texas, August-October 2005.

5. MF&RS Headquarters, [online] 12 Oct 2007, < http://www.merseyfire.gov.uk />

6. David Penney., "Carbon Monoxide HQ", [online] 12 May 2004, <http://www.coheadquarters.com/>

7. Vander, Sherman, Luciano's Human Physiology, The Mechanisms of Body Function, Mc Graw Hill Higher Education, 2004.

8. King, C.E., S. L. Dodd and S. M. Cain, O2 delivery to contracting muscle during hypoxic or CO hypoxia, Journal of Applied Physiology, Vol 63, Issue 2 726-732, 1987.

9. Jim D. Adams, Howard H. Erickson, and Hubert L. Stone, Myocardial metabolism during exposure to carbon monoxide in the conscious dog, Journal of Applied Physiology, Vol. 34, No. 2, February 1973.

10. Naihong Zhu., Harvey R. Weiss, Myocardial Venous O_2 Saturation Becomes More Heterogeneous during Hypoxic and Carbon Monoxide Hypoxia, Microvascular Research 49, 253-267, 1995.

11. Naihong Zhu., Harvey R. Weiss, Effect of hypoxic and carbon monoxide-induced hypoxia on regional myocardial segment work and O_2 consumption, Research in Experimental Medicine, Volume 194, December 1994.

12. Stewart RD, Peterson JE, Fisher TN, Hosko MJ, Baretta ED, Dodd HC, Herrmann AA. Experimental human exposure to high concentrations of carbon monoxide. Arch Environ Health. 1973 Jan;26(1):1–7.

13. K Luomanmaki and RF Coburn, Effects of metabolism and distribution of carbon monoxide on blood and body stores. American Journal of Physiology -- Legacy Content, Vol. 217, Issue 2, 354-363, August 1, 1969.

14. Hemma Resch, Claudia Zawinka, Günther Weigert, Leopold Schmetterer, and Gerhard Garhöfer, Inhaled Carbon Monoxide Increases Retinal and Choroidal Blood Flow in Healthy Humans, Investigative Ophthalmology and Visual Science. 2005;46:4275-4280.

15. J. P. Chalmers, P. I. Korner, and S. W. White, Distribution of peripheral blood flow in primary tissue hypoxia induced by inhalation of carbon monoxide, J Physiol. 1967 September; 192(2): 549–559.

16. D G Penney, Hemodynamic response to carbon monoxide, Environmental Health Perspectives, Vol 77, pp 121-130, 1988.

17. Richard D. Stewart, The effect of carbonmonoxide on humans, Dept of Environmental Medicine, 1999.

18. Aberg Anna-Maja, Hultin Magnus, Abrahamsson Pernilla, Larsson Jan Erik, Circulatory effects and kinetics following acute administration of carbon monoxide in a porcine model, Life Sciences 75 (2004), 1029-1039.

19. Armin Ernst, and Joseph D. Zibrak, Carbon Monoxide Poisoning, Volume 339:1603-1608, 1998.

20. Hampson NB, Little CE., Hyperbaric treatment of patients with carbon monoxide poisoning in the United States, 2005 Jan-Feb;32(1):21-6.

21. Lindell K. Weaver, Ramona O. Hopkins, Karen J. Chan, Susan Churchill, N.P., C. Gregory Elliott, Terry P. Clemmer, James F. Orme, Jr., Frank O. Thomas, M.D., and Alan H. Morris, Hyperbaric Oxygen for Acute Carbon Monoxide Poisoning., New England Journal of Medicine, October, 2002.

22. Tibbles PM, Perrotta PL. Treatment of carbon monoxide poisoning: a critical review of human outcome studies comparing normobaric oxygen with hyperbaric oxygen. Ann Emerg Med 1994; 24: 269-276[Medline].

23. Scheinkestel CD, Bailey M, Myles PS, Jones K, Cooper DJ, Millar IL, et al. Hyperbaric or normobaric oxygen for acute carbon monoxide poisoning: a randomized controlled clinical trial. Med J Australia 1999; 170: 203-210[Medline].

24. A. Dueñas-Laita, G. Burillo Puzte, S. Nogué Xarau, M. Ruiz Mambrilla., Cardiovascular Manifestations of Carbon Monoxide Poisoning., Journal of the American College of Cardiology, Volume 47, Issue 3, Pages 690-691.

25. Koskela RS. Cardiovascular diseases among foundry workers exposed to carbon monoxide. Scand J Work Environ Health. 1994;20:286–293[Medline]

26. Stern FB, Lemen RA, Curtis RA. Exposure of motor vehicle examiners to carbon monoxide: a historical prospective mortality study. Arch Environ Health. 1981;36:59–65[Medline]

27. Youngran Chung, Shih-Jwo Huang, Alan Glabe, and Thomas Jue., Implication of CO inactivation on myoglobin function, American Journal Physiology Cell Physiol 290: C1616-C1624, 2006.

28. Lin PC, Kreutzer U, Jue T., Myoglobin translational diffusion in rat myocardium and its implication on intracellular oxygen transport, Journal of Physilogy 2007 Jan 15;578(Pt 2):595-603.

29. Glabe A, Chung Y, Xu D, Jue T., Carbon monoxide inhibition of regulatory pathways in myocardium, American Journal Physiology, 1998 Jun;274(6 Pt 2):H2143-51.

30. Christopher R. Henry, Daniel Satran, Cheryl D. Adkinson, Caren I. Chaney and Timothy D. Henry., Myocardial Injury Associated with Carbon Monoxide Poisoning Predicts Long-term Mortality., Acad Emerg Med Volume 11, Issue5 469.

31. Shoshana Zevin, Sandra Saunders, Steven G. Gourlay, Peyton Jacob, and Neal L. Benowitz, Cardiovascular effects of carbon monoxide and cigarette smoking, Journal of American Coll Cardiol, 2001; 38:1633-1638.

32. V. Fineschi, E. Agricola, G. Baroldi, G. Bruni, D. Cerretani, S. Mondillo, M. Parolini, E. Turillazzi, Myocardial findings in fatal carbon monoxide poisoning: a human and experimental morphometric study, International Journal of Legal Medicine, Volume 113, August 2000.

33. Massahiro Endo, Tsunekazu Hino, Toshinari Itaoka, Hisae Hayashi and Juro Wada., Continuous Measurement of Human Myocardial Tissue Oxygen Tension.

34. Bjerrum JT, Perko MJ, Beck B., Myocardial oxygen tension during surgical revascularization. A clinical comparison between blood cardioplegia and crystalloid cardioplegia. Eur J Cardiothorac Surg. 2006 Feb;29(2):181-5. Epub 2006 Jan 4.

35. Eugene N. Bruce and Margaret C. Bruce., A multicompartment model of carboxyhemoglobin and carboxymyoglobin responses to inhalation of carbon monoxide., Journal of Applied Physiology 95: 1235-1247, 2003.

36. S. Selvakumar, Maithili Sharan and M. P. Singh, Mathematical model for the exchange of gases in the lungs with special reference to carbon monoxide, Volume 30, Number 5 / September, 1992.

37. A. Jonathan Kaye, Shaojie Wang, The Interactive Oxyhemoglobin Dissociation Curve, Department of Medicine, June 2001.

38. Schenkman KA, Marble DR, Burns DH, and Feigl EO, Myoglobin oxygen dissociation by multi wavelength spectroscopy. J Appl Physiol 82: 86–92, 1997.

39. Jian-Wei Gu, Megan Shparago , Wei Tan , Amelia Bailey, Tissue Endostatin Correlates Inversely with Capillary Network in Rat Heart and Skeletal Muscles, Angiogenesis. 2006 Jun 22 : 16791708.

40. Marcus JT, DeWaal LK, Gotte MJ, van der Geest RJ, Heethaar RM, and Van Rossum AC. MRI-derived left ventricular function parameters and mass in healthy young adults relation with gender and body size. International Journal Card Imaging 15: 411–419, 1999.

41. Lee RC, Wang Z, Heo M, Ross R, Janssen I, and Heymsfield SB. Total-body skeletal muscle mass: development and cross validation of anthropometric prediction models. American Journal Nutr 72: 796–803, 2000.

42. Xhonneux R,Schaper W (1969) The PO_2 in the coronary sinus: Correlation studies with other circulatory and respiratory parameters based on a population of 500 dogs. Prog Respir Res 3:89 –93

43. A. Deussen, M. Brand, A. Pexa and J. Weichsel, Metabolic coronary flow regulation-Current concepts, Volume 101, Number 6 / November, 2006.

44. P. Gonschior, G. M. Gonschior, P. F. Conzen, J. Hobbhahn, A. E. Goetz, K. Peter and W. Brendel, Myocardial oxygenation and transmural lactate metabolism during experimental acute coronary stenosis in pigs, Basic Res Cardiol 87: 27-37 (1992).

45. Naihong Zhu and Harvey R. Weiss, Effect of hypoxic and carbon monoxide-induced hypoxia on regional myocardial segment work and O_2 consumption, Volume 194, Number 1 December, 1994.

46. KR Walley, RM Collins, DJ Cooper and CB Warriner, Myocardial anaerobic metabolism occurs at a critical coronary venous PO2 in pigs, Am. J. Respir. Crit. Care Med., Vol 155, No. 1, Jan 1997, 222-228.

47. Eiji Takahashi and Katsuhiko DOI, Impact of Diffusional Oxygen Transport on Oxidative Metabolism in the Heart, Japanese Journal of Physilogy, 48, 243-252, 1998.

48. Van Beekvelt MC, Van Engelen BG, Wevers RA, Colier WN, In vivo quantitative near-infrared spectroscopy in skeletal muscle during incremental isometric handgrip exercise, Clin Physiol Funct Imaging. 2002 May;22(3):210-7.

49. Girardis M, Rinaldi L, Busani S, Flore I, Mauro S, Pasetto A., Muscle perfusion and oxygen consumption by near-infrared spectroscopy in septic-shock and non-septic-shock patients, Intensive Care Med. 2003 Jul;29(7):1173-6. Epub 2003 May 28.

50. Mizuno M, Kitamura Y, Iwakawa T, Oda K, Ishii K, Ishiwata K, Nakamura Y, Muraoka I., Regional differences in blood volume and blood transit time in resting skeletal muscle., Jpn J Physiol. 2003 Dec;53(6):467-70.

51. Tune JD, Yeh C, Setty S, Zong P, Downey HF., Coronary blood flow control is impaired at rest and during exercise in conscious diabetic dogs., Basic Res Cardiol. 2002 May;97(3):248-57.

52. Haraoka S, Saito D, Kusachi S, Sogo T, Yamada N, Nishiyama O, Yasuhara K., Effect of graded coronary constriction on the flow reserve in regional myocardium in dog, Jpn Heart J. 1979 Mar;20(2):207-17.

53. Sun KT, Yeatman LA, Buxton DB, Chen K, Johnson JA, Huang SC, Kofoed KF, Weismueller S, Czernin J, Phelps ME, Schelbert HR, Simultaneous measurement of myocardial oxygen consumption and blood flow using [1-carbon-11]acetate, J Nucl Med. 1998 Feb;39(2):272-80.

54. Porenta G, Schima H, Pentaris A, Tsangaris S, Moertl D, Probst P, Maurer G, Baumgartner H, Assessment of coronary stenoses by Doppler wires: a validation study using in vitro modeling and computer simulations., Ultrasound Med Biol. 1999 Jun;25(5):793-801.

55. King RB, Bassingthwaighte JB, Hales JR, Rowell LB, Stability of heterogeneity of myocardial blood flow in normal awake baboons, Circ Res. 1985 Aug;57(2):285-95.

56. Gold FL, Bache RJ, Transmural right ventricular blood flow during acute pulmonary artery hypertension in the sedated dog. Evidence for subendocardial ischemia despite residual vasodilator reserve, Circ Res. 1982 Aug;51(2):196-204.

57. Deussen A, Local myocardial glucose uptake is proportional to, but not dependent on blood flow, Pflugers Arch. 1997 Feb;433(4):488-96.

58. Eliasen P, Amtorp O, Tøndevold E, Haunsø S, Regional blood flow, microvascular blood content and tissue haematocrit in canine myocardium, Cardiovasc Res. 1982 Oct;16(10):593-598.

59. Franzen D, Conway RS, Zhang H, Sonnenblick EH, Eng C, Spatial heterogeneity of local blood flow and metabolite content in dog hearts, Am J Physiol. 1988 Feb;254(2 Pt 2):H344-53.

60. Laaksonen MS, Kalliokoski KK, Luotolahti M, Kemppainen J, Teräs M, Kyröläinen H, Nuutila P, Knuuti J, Myocardial perfusion during exercise in endurance-trained and untrained humans, Am J Physiol Regul Integr Comp Physiol. 2007 Aug;293(2):R837-43. Epub 2007 May 23.

61. Tuunanen H, Kuusisto J, Toikka J, Jääskeläinen P, Marjamäki P, Peuhkurinen K, Viljanen T, Sipola P, Stolen KQ, Hannukainen J, Nuutila P, Laakso M, Knuuti J, Myocardial perfusion, oxidative metabolism, and free fatty acid uptake in patients with hypertrophic cardiomyopathy attributable to the Asp175 Asn mutation in the alpha-tropomyosin gene: a positron emission tomography study, J Nucl Cardiol. 2007 May-Jun;14(3):354-65. Epub 2007 May 10.

62. Elia M, Kurpad A, What is the blood flow to resting human muscle, Clin Sci (Lond). 1993 May;84(5):559-63.

63. Raitakari M, Nuutila P, Ruotsalainen U, Teräs M, Eronen E, Laine H, Raitakari OT, Iida H, Knuuti MJ, Yki-Järvinen H, Relationship between limb and muscle blood flow in man, J Physiol. 1996 Oct 15;496 (Pt 2):543-9.

64. Van Beekvelt MC, Borghuis MS, van Engelen BG, Wevers RA, Colier WN, Adipose tissue thickness affects in vivo quantitative near-IR spectroscopy in human skeletal muscle, Clin Sci (Lond). 2001 Jul;101(1):21-8.

65. Mattson K, Niiranen A, Ruotsalainen T, Maasilta P, Halme M, Pyrhönen S, Kajanti M, Mäntylä M, Tamminen K, Jekunen A, Sarna S, Cantell K, Interferon

maintenance therapy for small cell lung cancer: improvement in long-term survival, J Interferon Cytokine Res. 1997 Feb;17(2):103-5.

66. Raitakari M, Nuutila P, Knuuti J, Raitakari OT, Laine H, Ruotsalainen U, Kirvelä O, Takala TO, Iida H, Yki-Järvinen H, Effects of insulin on blood flow and volume in skeletal muscle of patients with IDDM: studies using [15O]H2O, [15O]CO, and positron emission tomography, Diabetes. 1997 Dec;46(12):2017-21.

67. Kotzerke J, van den Hoff J, Burchert W, Wagner TF, Emter M, Hundeshagen H, A compartmental model for alveolar clearance of pertechnegas, J Nucl Med. 1996 Dec;37(12):2066-71.

68. H. Chiodi, D. B. Dill, F. Consolazio, and S. M. Horvath, Respiratory and circulatory responses to acute carbon monoxide poisioning, American Journal of Physilogy 134: 683-693, 1941.

69. Paul N. Kizakevich, Michael L. McCartney, Milan J. Hazucha, linda H. Sleet., Noninvasive Ambulatory Assessment of Cardiac Function and Myocardial Ischemia in Healthy Subjects Exposed to Carbon Monoxide during upper and Lower body Exercise, Am Journal of Applied Physiology (2000) 83: 7-16.

70. Vogel JA, Gleser MA, Effect of carbon monoxide on oxygen transport during exercise, J Appl Physiol. 1972 Feb;32(2):234-9.

71. Bell, Hales, King and Fawcett, Exercise, Heat Stress, And Blood Distribution.

72. I. Kuwahira, N. C. Gonzalez, N. Heisler and J. Piiper, Changes in regional blood flow distribution and oxygen supply during hypoxia in conscious rats, J Appl Physiol 74: 211-214, 1993;

73 Reiner L, Mazzoleni A, Rodriguez FL, Freudenthal RR, The weight of the human heart. Normal cases, AMA Arch Pathol. 1959 Jul;68(1):58-73.

74. Rakusan K, Flanagan MF, Geva T, Southern J, Van Praagh R, Morphometry of human coronary capillaries during normal growth and the effect of age in left ventricular pressure-overload hypertrophy, 1992 Jul;86(1):38-46.

75. Eiji Takahashi, Katsuhiko Doi, Visulization of oxygen level inside a single cardiac myocyte, Am. J. Physiol. 268 (Heart Circ. Physiol. 37): H2561- H2568,1995.

76. Steven B Heymsfield, Timothy G Lohman, Zimian Wang. Human Body Composition.

77. McGuire BJ and Secomb TW. A theoretical model for oxygen transport in skeletal muscle under conditions of high oxygen demand. J Appl Physiol 91: 2255–2265, 2001.

78. Harry J.M.Lemmens, Donald P. Bernstein, Jay B Brodskymodern, Estimating blood volume in obese and morbidly obese patients, surgery obesity surgery,16,773-776

79. Marko S. Laaksonen, Kari K. Kalliokoski, Matti Luotolahti, Jukka Kemppainen, Mike Teras, Juhani Knutti., Myocardial perfusion during exercise in endurance-trained and untrained humans.

80. Richard R. Nelson.; Fredarick L. Gobel; Charles R. Jorgensen; Kyuhyun Wang; Yang Wang; Henry L. Taylor , Hemodynamic Predictors of Myocardial Oxygen Consumption During Static and Dynamic Exercise, Circulation. 1974;50:1179.

81. Charles R. Jorgensen, Kazuto Kitamura, Fredarick L. Gobel, Henry L. Taylor, and Yang Wang, Long-term precision of the N,O method for coronary flow during heavy upright exercise, Journal of Applied Physiology, Vol. 30, No. 3,March 1971.

82. Kazuto Kitamura, Charles R. Jorgensen, Fredarick L. Gobel, Henry L. Taylor, AND Yang Wang, Hemodynamic correlates of myocardial oxygen consumption during upright exercise, Journal of Applied Physics, Vol. 32, No. 4, April 1972.

83. Charles R. Jorgensen, Kyuhyun Wang**,** Yang Wang; Fredarick L. Gobel; RICHARD R. Nelson; Henry L. Taylor; Frank R. Gams Jr.; John E. Vilandre., Effect of Propranolol on Myocardial Oxygen Consumption and Its Hemodynamic Correlates during Upright Exercise, Circulation. 1973;48:1173.

84. Walter T. Goodale, Donald B. Hackel, Measurement of Coronary Blood Flow in Dogs and Man from Rate of Myocardial Nitrous Oxide Desaturation, Circulation Research. 1953;1:502.

85. Seymour S. Ketty, Carl F. Schmidt, The Determination of cerebral Blood Flow in Man by the use of Nitrous Oxide in Low Concentrations.

86. Timothy J. Regan, Gerald Timmis, Murray Gray, Kenan Binak,‡ and Harper K. Hellems, Myocardial Oxygen Consumption During Exercise in Fasting and Lipemic Subjects, J Clin Invest. 1961 April; 40(4): 624–630.

87. Leo A. Sapirstein, Eric Ogden, Theoretic Limitations of the Nitrous Oxide Method for the Determination of regional Blood Flow,. Circ. Res. 1956;4;245-249.

88. Philip Bard., Louis J. Cizek, Jean M. Marshall., Medical Physiology., 1961.

89. Gerard J. Tortora, Principles of Anatomy & Physilogy, Tenth Edition, 2003.

90. James H. Caldwell, Gary V. Martin, Gary M. Raymond, and James B. Bassingthwaighte, Regional myocardial flow and capillary permeability surface area products are nearly proportional, 1993.

91. Edlund A, Sollevi A., Theophylline increases coronary vascular tone in humans : evidence for a role of endogenous adenosine in flow regulation., Acta Physiol Scand 1995, 155, 303-311.

92. Helmut Habazett, Peter F. Conzen, Hans Baier, Michael Christ, Epicardial Oxygen Tensions During Changes in Arterial PO_2 in Pigs., 1990.

93. T. E. Gayeski and C. R. Honig, Intracellular PO2 in individual cardiac myocytes in dogs, cats, rabbits, ferrets, and rats, Am J Physiol Heart Circ Physiol 260: H522-H531, 1991;

94. Georg Horstick, Axel Heimann, Otto Gotze, Gerd Hafner, Oliver Berg, Peter Boehmer, Phillip Becker, Harald Darius, Hans-Jurgen Rupprecht, Michael Loos, Sucharit Bhakdi, MD; Jurgen Meyer, Oliver Kempski, Intracoronary Application of C1 Esterase Inhibitor Improves Cardiac Function and Reduces Myocardial Necrosis in an Experimental Model of Ischemia and Reperfusion, 1997;95:701-708.

95. Z. Turek, K. Rakusan, J. Olders, L. Hoofd and F. Kreuzer, Computed myocardial PO2 histograms: effects of various geometrical and functional conditions, J Appl Physiol 70: 1845-1853, 1991;

96. Hoffman, W. E, Albrecht, R. F, Jonjev, Z. S., Myocardial tissue oxygen during coronary artery constriction and hypotension in dogs, Acta Anaesthesiologica Scandinavica, Volume 46, Number 6, July 2002 , pp. 707-712(6).

97. S. Faithfull, M. Fennema, W. Erdmann, M. Dhasmana and G. Eilers., The effects of Acute Ischaemta on Intramyocardial Oxygen Tensions, Advances in Experimental Medicine and Biology.

98. Jonny Hobbhahn, Peter F.M. Conez, Alwin Goetz, Gabriele Seidl, Peter Gonschior., Myocardial Surface PO_2 – an indicator of myocardial tissue oxygenation

99. Tokunaga, Chiho; Bateman, Ryon M.; Boyd, John; Wang, Yingjin BSc; Russell, James A.; Walley, Keith R., Albumin resuscitation improves ventricular contractility and myocardial tissue oxygenation in rat endotoxemia.

100. W.A Grunewald, W. Sowa, Distribution of the Myocardial Tissue PO_2 in the Tar and the Inhomogenity of the Coronary Bed, Pflugers Arch. 374, 57-66 (1978).

101. Beard DA, Bassingthwaighte JB., Modeling advection and diffusion of oxygen in complex vascular networks, Annals of Biomedical Engineering, Vol 29, pp. 298-310, 2001.

102. C. R. Honig, C. L. Odoroff and J. L. Frierson, Capillary recruitment in exercise: rate, extent, uniformity, and relation to blood flow, Am J Physiol Heart Circ Physiol 238: H31-H42, 1980;

103. Ananda R. Jayaweera, Kevin Wei, Matthew Coggins, Jiang Ping Bin, Craig Goodman, and Sanjiv Kaul, Role of capillaries in determining CBF reserve: new insights using myocardial contrast echocardiography, Am J Physiol Heart Circ Physiol 277: H2363-H2372, 1999.

104. Daniel A. Beard, James B. Bassingthwaighte, Advection and diffusion of substances in biological tissues with complex vascular networks, Annals of Biomedical Engineering, Vol 28, pp. 253-268, 2000.

105. T. Abe, C F Kearns, T Fukunaga. Sex differences in whole body skeletal muscle mass measured by magnetic resonance imaging and its distribution in young Japanese adults. Br J Sports Med 37: 436–440, 2003.

106. Ian Janssen, Steven B. Heymsfield, ZiMian Wang, and Robert Ross. Skeletal muscle mass and distribution in 468 men and women aged 18-88 yr. J Appl Physiol 89: 81-88, 2000.

107. Gallagher D; Visser M.; DeMeersman R.E.; Sepulveda D. ; Baumgartner R. N.; Pierson R. N. ; Harris T.; Heymsfeild S. B.; Appendicular skeletal muscle mass : effects of age, gender, and ethnicity ; J. Appl. Physiol.,, vol. 83,(1), pp. 229-239,1997.

108. Nuala M Byrne, Roland L Weinsier, Gary R Hunter, Renee Desmond, Mindy A Patterson, Betty E Darnell, Paul A Zuckerman. Influence of distribution of lean body mass on resting metabolic rate after weight loss and weight regain: comparison of responses in white and black women. Am J Clin Nutr 2003; 77:1368–73.

109. Bernardo Lio Wajchenerg, Adriana Bosco, Marilla Martins, Shlomo Levin, Manoel Rocha, Antonio Carlos Lerkio, Marcia Nery,Jay-Me Goldman, and Bernardo Liberman. Estimation of Body Fat and Lean Tissue Distribution by Dual Energy X-Ray Absorptiometry and Abdominal Body Fat Evaluation by Computed Tomography in Cushing ’s disease. J Clin Endocrinol Metab 80: 2791-2794, 1995.

110. Marieke B. Snijder, Jacqueline M. Dekker, P. Marjolien Visser. Trunk Fat and Leg Fat Have Independent and Opposite Associations With Fasting and Postload Glucose Levels. Diabetes Care 27:372–377, 2004.

111. Barbara A. Gower and Lara Nyman. Associations among Oral Estrogen Use, FreeTestosterone Concentration, and Lean Body Mass among Postmenopausal Women. (J Clin Endocrinol Metab 85: 4476–4480,2000.

112. Isabel Ferreira, Marieke B. Snijder, Jos W. R. Twisk, Willem Van Mechlen, HanC. G. Kemper, Jacob C. Seidell, and Coen D. A. Stehouwer. Central Fat Mass Versus Peripheral Fat and Lean Mass:Opposite (Adverse Versus Favorable) Associations with Arterial Stiffness? The Amsterdam Growth and Health Longitudinal Study. J Clin Endo-crinol Metab 89: 2632–2639, 2004.

113. Raymond D Starling, Philip A Ades, Eric T Poehlman. Physical activity, protein intake, and appendicular skeletal muscle mass in older men . Am J ClinNutr 1999;70:91–96.

114. Mariëlle PKJ Engelen, Annemie MWJ Schols, Joan D Does, Emiel FM Wouters. Skeletal muscle weakness is associated with wasting of extremity fat-free mass but

not with airflow obstruction in patients with chronic obstructive pulmonary disease. Am J Clin Nutr 2000; 71:733–8.

115. Noriko Ishiguro, Hiroaki Kanehisa, Masae Miyatani, Yoshihisa Masuo, and Tetsuo Fukunaga. Applicability of segmental bioelectrical impedance analysis for predicting trunk skeletal muscle volume. J Appl Physiol 100: 572–578, 2006.

116. Kiichi Ishiwata, Yoshio Nakamura and Isao Muraoka Masaki Mizuno, Yuichi Kimura, Takashi Iwakawa, Keiichi Oda, Kenji Ishii. Regional differences in blood flow and oxygen, during recovery from exhaustive exercise consumption in resting muscle and their relationship. *J Appl Physiol*95:2204-2210, 2003.

117. Francesco Zurlo, Karen Larson, Clifton Bogardus, and Eric Ravussin. Skeletal Muscle Metabolism Is a Major Determinant of Resting Energy Expenditure. J. Clin. Invest. 1990. 86:1423-1427.

118. Mireille C. P. Van Beekvelt, Willy N. J. M. Colier, Ron A. Wevers, and Baziel G. Performance of near-infrared spectroscopy in measuring local O2 consumption and blood flow in skeletal muscle. J Appl *Physiol* 90: 511–519, 2001.

119. Massimo G., Laura R., Stefano B., Ivana F. ,Stefano M., Alberto P. , Muscle perfusion and oxygen consumption by near-infrared spectroscopy in septic-shock and non-septic-shock patients. Intensive Care Med (2003)29:1173-1176.

120. Scott Lyons, Mark Richardson, Phillip Bishop, Joe Smith, Hank Heath, Judy Giesen. Excess post-exercise oxygen consumption in untrained males: effects of intermittent durations of arm ergometry. Appl. Physiol. Nutr. Metab. 31: 196–201 (2006).

121. Robert Zelis, John Longhurst, Robert J. Capone, Dean T. Mason. A Comparison of Regional Blood Flow and Oxygen Utilization During Dynamic Forearm Exercise

in normal Subjects and Patients with congestive heart Failure. Circulation, Volume 50, July 1974.

122. Lennart Jorfeldt, Anders Juhlin-Dannfelt, and Jan Karlsson. Lactate release in relation to tissue lactate in human skeletal muscle during exercise. J. Appl. Physiol. Respirat, Environ. Exercise Physiol. 44(3): 350-352, 1978.

123. Robert Boushel, Henning Langberg, Jens Olesen, Markus Nowak, Lene Simonsen, Jens Bulow, and Michaeal Kjaer . Regional blood flow during exercise in humans measured by near-infrared spectroscopy and indocyanine green. *J Appl Physiol* 89: 1868-1878, 2000.

124. Timothy J. Regan, Gerald Timmis,† Murray Gray, Kenan Binak,‡ and Harper K. Hellems, Myocardial Oxygen Consumption During Exercise in Fasting and Lipemic Subjects, J Clin Invest. 1961 April; 40(4): 624–630.

125. Leo A. Sapirstein, Eric Ogden, Theoretic Limitations of the Nitrous Oxide Method for the Determination of regional Blood Flow,. Circ. Res. 1956;4;245-249.

126. Porenta G, Cherry S, Czernin J, Brunken R, Kuhle W, Hashimoto T, Schelbert HR, Noninvasive determination of myocardial blood flow, oxygen consumption and efficiency in normal humans by carbon-11 acetate positron emission tomography imaging, Eur J Nucl Med. 1999 Nov;26(11):1465-74.

127**.** Bradley C. Nindl, Charles R. Scoville, Kathleen M. Sheehan, Cara D. Leone, Robert P. Mello. Gender differences in regional body composition and somatotrophic influences of IGF-I and leptin. J Appl Physiol 92: 1611-1618, 2002.

128. Tune JD, Richmond KN, Gorman MW, Feigl EO, Role of nitric oxide and adenosine in control of coronary blood flow in exercising dogs, Circulation. 2000 Jun 27;101(25):2942-8.

129. Seymour S. Ketty, Carl F. Schmidt, The Determination of cerebral Blood Flow in Man by the use of Nitrous Oxide in Low Concentrations

130. Katz IR, Wittenberg JB, Wittenberg BA , Monoamine oxidase, an intracellular probe of oxygen pressure in isolated cardiac myocytes. J Biol Chem. 1984 Jun 25;259(12):7504-9.

131. Andrew D. Shaw, Natarajan Aravindan, Zheng Li, Bernhard J.C.J. Riedel: Temporal Variation In Tissue Oxygen Tension And Perfusion Response To Hypoxia And Ischaemia: The Importance Of Local Control Of The Microcirculation. The Internet Journal of Emergency and Intensive Care Medicine. 2003. Volume 7 Number 1.

132.Kindig CA, Stary CM, Hogan MC.,Effect of dissociating cytosolic calcium and metabolic rate on intracellular PO2 kinetics in single frog myocytes.,J Physiol. 2005 Jan 15;562(Pt 2):527-34

133. Arai AE, Kasserra CE, Territo PR, Gandjbakhche AH, Balaban RS.,Myocardial oxygenation in vivo: optical spectroscopy of cytoplasmic myoglobin and mitochondrial cytochromes. Am J Physiol. 1999 Aug;277(2 Pt 2):H683-97

134. Charles R. Jorgensen, Kazuto Kitamura, Fredarick L. Gobel, Henry L. Taylor, andYang Wang, Long-term precision of the N,O method for coronary flow during heavy upright exercise, Journal of Applied Physiology, Vol. 30, No. 3,March 1971.

135. Rolf Nordlander, S. Kenneth Pehrsson, Hans Astrom (1989) The Reliability of Rate-Pressure Product as an Index of Myocardial Oxygen Consumption in Atrial Synchronized Versus Fixed Rate Ventricular Pacing Pacing and Clinical Electrophysiology 12 (6), 917–921.

136. E. Braunwald, S. J. Sarnoff, R. B. Case, W. N. Stainsby and G, H. Welch, Hemodynamic Determinants of Coronary Flow: Effect of Changes in Aortic Pressure

and Cardiac Output on the Relationship Between Myocardial Oxygen Consumption and Coronary Flow, November, 1956.

137. A. Crisafulli, F. Melis, F. Tocco, U. M. Santoboni, F. Frongia, C. Carta, M. Caddeo and A. Concu, Anaerobic threshold and the oxygen consumption–cardiac output relationship during exercise, Sport Sciences for Heart, Volume 1, Number 2 / July, 2005.

138. Rebecca C. Barker, Susan R. Hopkins, Nancy Kellogg, I. Mark Olfert, Tom D. Brutsaert, Timothy P. Gavin, Pauline L. Entin, Anthony J. Rice, and Peter D. Wagner, Measurement of cardiac output during exercise by open-circuit acetylene uptake, Journal of Applied Physiology, 88; 1650-1658, 2000.

139. L. Hermansen, B. Ekblom, and B. Saltin, Cardiac output during submaximal and maximal treadmill and bicycle exercise, J Appl Physiol 29: 82-86, 1970;

140. Per-Olof Åstrand, T. Edward Cuddy , Bengt Saltin, and Jesper Stenberg,. Cardiac output during submaximal and maximal work, J Appl Physiol 19: 268-274, 1964;

141. Bjorn Ekblom, Perolof Astrand, Bengt Saltin, Jesper Stenberg, and Brittmari Wallstorm, Effect of training on circulatory response to exercise, Journal of Applied Physiology Vol. 24;No. 4, April 1968.

142. Kenneth C. Beck, Lakesha N. Randolph, Kent R. Bailey, Christina M. Wood, Eric M. Snyder, and Bruce D. Johnson, Relationship between cardiac output and oxygen consumption during upright cycle exercise in healthy humans, J Appl Physiol 101: 1474-1480, 2006. First published July 27, 2006;

143. J. Roca, A. G. Agusti, A. Alonso, D. C. Poole, C. Viegas, J. A. Barbera, R. Rodriguez-Roisin, A. Ferrer and P. D. Wagner, Effects of training on muscle O2 transport at VO2max, Journal of Applied Physiology, Vol 73, Issue 3 1067-1076.

144. Craig A. Harms, Thomas J. Wetter, Steven R. McClaran, David F. Pegelow, Glenn A. Nickele, William B. Nelson, Peter Hanson, and Jerome A. Dempsey, Effects of respiratory muscle work on cardiac output and its distribution during maximal exercise, J Appl Physiol 85: 609-618, 1998;

145. Wisel S, Chacko SM, Kuppusamy ML, Pandian RP, Khan M, Kutala VK, Burry RW, Sun B, Kwiatkowski P, Kuppusamy P., Labeling of skeletal myoblasts with a novel oxygen-sensing spin probe for noninvasive monitoring of in situ oxygenation and cell therapy in heart, Am J Physiol Heart Circ Physiol. 2007 Mar;292(3):H1254-61. Epub 2006 Dec 1.

146. Skolasinska K, Harbig K, Lübbers DW, Wodick R., PO_2 and microflow histograms of the beating heart in response to changes in arterial pO2, Basic Res Cardiol. 1978 May-Jun;73(3):307-19.

147. Zhao Y, Jiao J, Shan Z, Fan Q, Hu J, Zhang Q, Zhu X., Effective management of main bronchial rupture in patients with chest trauma, Thorac Cardiovasc Surg. 2007 Oct;55(7):447-9.

148. Carrier M, Pellerin M, Dagenais F, Perrault LP, Petitclerc R, Pelletier LC., Videoassisted thrombectomy of mechanical prosthetic heart valves, J Heart Valve Dis. 1999 Jul;8(4):404-6.

149. Tanizaki Y, Kitani H, Okazaki M, Mifune T, Mitsunobu F, Kotoh N, Tada S, Takahashi K, Kitamura I, Asthma classification by score calculated from clinical findings and examinations. Comparison between, clinical diagnosis and score diagnosis, Arerugi. 1992 Apr;41(4):489-96.

150. Brantigan JW, Perna AM, Gardner TJ, Gott VL, Intramyocardial gas tensions in the canine heart during anoxic cardiac arrest, Surg Gynecol Obstet. 1972 Jan;134(1):67-72.

151. Gonschior P, Gonschior GM, Conzen PF, Hobbhahn J, Goetz AE, Peter K, Brendel W, Myocardial oxygenation and transmural lactate metabolism during experimental acute coronary stenosis in pigs, Basic Res Cardiol. 1992 Jan-Feb; 87(1):27-37.

152. Mendler N, Schuchhardt S, Sebening F, Measurement of intramyocardial oxygen tension during cardiac surgery in man, Res Exp Med (Berl). 1973 Jan 25;159(3):231-8.

153. Gardner TJ, Brantigan JW, Perna AM, Bender HW, Brawley RK, Gott VL, Intramyocardial gas tensions in the human heart during coronary artery-saphenous vein bypass, J Thorac Cardiovasc Surg. 1971 Dec;62(6):844-50.

154. Benignus VA, Hazucha ML, Smith MV, and Bromberg, PA.Prediction of carboxyhemoglobin formation due to transient exposure to carbon monoxide. J Appl Physiol 76: 1739–1745, 1994.

155. Burge CM and Skinner SL., Determination of hemoglobin mass and blood volume with CO: evaluation and application of a method. J Appl Physiol 79: 623–31, 1995.

156. Duncker DJ, Merkus D., Exercise hyperaemia in the heart: the search for the dilator mechanism. J Physiol. 2007 Sep 15;583(Pt 3):847-54.

157. Lösse B, Schuchhardt S, Niederle N., The oxygen pressure histogram in the left ventricular myocardium of the dog. Pflugers Arch. 1975 Apr 29;356(2):121-32.

158. R. S. Richardson,E. A. Noyszewski, B. Saltin and J. Gonzalezalonso, Effect of mild carboxy-hemoglobin on exercising skeletal muscle: intravascular and intracellular evidence. Am J Physiol Regul Integr Comp Physiol 283: R1131–R1139, 2002.

159. Stickland M. K., Lovering A. T., Eldridge M. W., Exercise-induced arteriovenous intrapulmonary shunting in dogs. American J. Respir. Crit. Care Med. 2007 Aug 1;176(3):300-5.

160. Lovering AT, Stickland MK, Eldridge MW., Intrapulmonary shunt during normoxic and hypoxic exercise in healthy humans. Adv Exp Med Biol. 2006;588:31-45.161.

161. Matschke K, Gerk U, Mrowietz C, Park JW, Jung F.,Influence of radiographic contrast media on myocardial oxygen tension: a randomized, NaCl-controlled comparative study of iodixanol versus iomeprol in pigs. Acta Radiol. 2007 Apr;48(3):292-9.

VITA

Date and place of birth:

- 02-09-1982, Hyderabad, INDIA

Educational institutions attended and degrees already awarded:

- B. E., Bachelors in Biomedical Engineering, Jawaharlal Nehru Technological University, AP,INDIA
- Post Graduate Diploma in Information Technology, AP, INDIA

Professional positions held:

- Biomedical Engineer , Apollo Hospitals, Hyderabad, India
- Research Assistant, Computational Physiology Laboratory, U of KY

Professional publications:

- Prediction of the Rate of Uptake of Carbon Monoxide From Blood by Extravascular Tissues, Bruce, Bruce and Erupaka (In preparation)

Typed name of student on final copy

- Kinnera Erupaka